GENERALIZED FINITE DIFFERENCE METHOD IN ELASTODYNAMICS
USING PERFECTLY MATCHED LAYER

A THESIS SUBMITTED TO
THE GRADUATE SCHOOL OF NATURAL AND APPLIED SCIENCES
OF
MIDDLE EAST TECHNICAL UNIVERSITY

BY

FUAT KORKUT

IN PARTIAL FULFILLMENT OF THE REQUIREMENTS
FOR
THE DEGREE OF DOCTOR OF PHILOSOPHY
IN
ENGINEERING SCIENCES

JULY 2012

Approval of the thesis

GENERALIZED FINITE DIFFERENCE METHOD IN ELASTODYNAMICS USING PERFECTLY MATCHED LAYER

submitted by **FUAT KORKUT** in partial fulfillment of the requirements for the degree of **Doctor of Philosophy in Engineering Sciences Department, Middle East Technical University** by,

Prof. Dr. Canan ÖZGEN   _____
Dean, Graduate School of **Natural and Applied Sciences**

Prof. Dr. Murat DİCLELİ   _____
Head of Department, **Engineering Sciences**

Prof. Dr. Turgut TOKDEMİR   _____
Supervisor, **Engineering Sciences Dept., METU**

Examining Committee Members :

Prof. Dr. Ahmet YAKUT   _____
Civil Engineering Dept., METU

Prof. Dr. Turgut TOKDEMİR   _____
Engineering Sciences Dept., METU

Assoc. Prof. Dr. Zafer EVİS   _____
Engineering Sciences Dept., METU

Assist. Prof. Dr. M. Tolga YILMAZ   _____
Engineering Sciences Dept., METU

Assist. Prof. Dr. Ö. Fatih YALÇIN   _____
Civil Engineering Dept., İstanbul University

                                          Date   **:** 16:07:2012

I hereby declare that all information in this document has been obtained and presented in accordance with academic rules and ethical conduct. I also declare that, as required by these rules and conduct, I have fully cited and referenced all material and results that are not original to this work.

Name, Surname: Fuat KORKUT

Signature:

ABSTRACT

GENERALIZED FINITE DIFFERENCE METHOD IN ELASTODYNAMICS USING PERFECTLY MATCHED LAYER

KORKUT, Fuat

Ph.D., Engineering Sciences Department

Supervisor: Prof. Dr. Turgut TOKDEMİR

July 2012, 162 Pages

This study deals with the use of the generalized finite difference method (GFDM) in perfectly matched layer (PML) analysis of the problems in wave mechanics, in particular, in elastodynamics. It is known that PML plays the role of an absorbing layer, for an unbounded domain, eliminating reflections of waves for all directions of incidence and frequencies. The study is initiated for purpose of detecting any possible advantages of using GFDM in PML analysis: GFDM is a meshless method suitable for any geometry of the domain, handling the boundary conditions properly and having an easy implementation for PML analysis. In the study, first, a bounded 2D fictitious plane strain problem is solved by GFDM to determine its appropriate parameters (weighting function, radius of influence, etc.). Then, a 1D semi-infinite rod on elastic foundation is considered to estimate PML parameters for GFDM. Finally, the proposed procedure, that is, the use of GFDM in PML analysis, is assessed by considering the compliance functions (in frequency domain) of surface and embedded rigid strip foundations. The surface foundation is assumed to be supported by three types of soil medium: rigid strip

foundation on half space (HS), on soil layer overlying rigid bedrock, and on soil layer overlying HS. For the embedded rigid strip foundation, the supporting soil medium is taken as HS. In addition of frequency space analyses stated above, the direct time domain analysis is also performed for the reaction forces of rigid strip foundation over HS. The results of GFDM for both frequency and time spaces are compared with those of finite element method (FEM) with PML and boundary element method (BEM), when possible, also with those of other studies. The excellent matches observed in the results show the reliability of the proposed procedure in PML analysis (that is, of using GFDM in PML analysis).

ÖZ

ELASTODAYNAMİKTE GENELLEŞTİRİLMİŞ SONLU FARKLAR METODUNUN MÜKEMMEL UYUMLU TABAKAYLA KULLANILMASI

KORKUT, Fuat

Doktora, Mühendislik Bilimleri Bölümü

Tez Danışmanı: Prof. Dr. Turgut Tokdemir

Temmuz 2012, 162 Sayfa

Bu çalışma, dalga mekaniği problemlerinde özellikle elastodinamikte mükemmel uyumlu tabaka (MUT) kullanan genelleştirilmiş sonlu farklar metodu (GSFM) ile ilgilidir. MUT sınırsız etki alanına sahip problemlerde sönümleyici tabaka olarak görev alır ve tüm yönler ve frekanslardaki gelen dalgaların yansımalarını elimine eder. Bu çalışma ile MUT analizlerinde GSFM'nin avantajları ortaya konulmuştur. Bir ağsız metod olan GSFM'nin başlıca avantajları, herhangi bir geometiriye sahip problemin çözümünde kullanılabilmesi, sınır şartlarını uygun biçimde sağlaması ve MUT analizlerine kolay uygulanabilmesidir. Bu çalışmada öncelikle, GSFM için uygun parametrelerin (ağırlık fonksiyonları ve etki yarıçapı, vb.) belirlenmesi amacıyla iki boyutlu sınırlı bir düzlem birim deformasyon problemi çözülmüştür. Daha sonra, bir boyutlu yarı sonsuz elastik temele oturmuş çubuğun analizi yapılarak MUT parametreleri GSFM için belirlenmiştir. Son olarak, GSFM'nin MUT analizlerinde uygulanması için önerilen yöntem, yüzeysel ve gömülü şerit temellerin esneklik fonksiyonlarının (frekans uzayında) belirlenmesinde kullanılmıştır. Bu analizlerde, yüzeysel temelin yarım uzay (YU)

üzerinde, zemin tabakasının rijit kaya üzerinde ve zemin tabakası YU üzerinde olması durumları ele alınarak üç farklı zemin ortamı tarafından desteklendiği farz edilmiştir. Gömülü temellerde sadece YU zemin ortamı tarafından desteklendiği durum ele alınmıştır. Yukarıda belirtilen frekans uzayı analizlerine ek olarak sadece YU oturan rijit şerit temelin tepki kuvvetleri için doğrudan zaman etki alanı analizleri gerçekleştirilmiştir. Frekans ve zaman uzayında elde edilen sonuçlar MUT'lu sonlu elemanlar metodu ve sınır elemanlar metodu ve mümkün olan durumlarda başka yöntemlerden elde edilen sonuçlarla karşılaştırılmıştır. Sonuçlarda gözlenen mükemmel uyum önerilen yöntemin MUT analizlerinde GSFM kullanımının güvenilir olduğunu göstermektedir.

Anahtar Kelimeler: genelleştirilmiş sonlu farklar metodu, mükemmel uyumlu tabaka, esneklik fonksiyonu,rijit şerit temel

To my parents

ACKNOWLEDGEMENTS

TABLE OF CONTENTS

LIST OF FIGURES

FIGURES

xvii

LIST OF TABLES

TABLES

LIST OF ABBREVIATIONS

a_0	: nondimensional frequency
A	: cross-sectional area and amplitude of wave
ABC	: artificial boundary condition
b	: half-length of foundation and characteristic length
BC	: boundary condition
BEM	: boundary element method
c	: imaginary part of impedance function, dashpot or viscous coefficient
c_{ijmn}	: fourth order elasticity tensor
D	: plane strain stiffness matrix
d	: distance
dnodes	: distance between to successive point for regular mesh
dm	: radius of influence
E	: Young's modulus
f^e	: attenuation function for evanescent wave
f^p	: attenuation function for propagating wave
f_0	: strength of attenuation function
F_{VV}, F_{HH}, F_{RR}	: vertical horizontal and rocking compliance
F	: compliance matrix
FDM	: finite difference method
FEM	: finite element method
G	: shear modulus
GFDM	: generalized finite difference method
h	: depth of layer
H	: depth of embedment
i	: imaginary number
Im	: imaginary part of complex number

K	: impedance function
k	: real part of impedance function, spring or stiffness coefficient
L	: computational length
L_{PML}	: thickness of PML
M	: mass matrix
N_{nod}	: number of node
P_V, P_H, P_R,	: vertical, horizontal force and rocking moment
PML	: perfectly matched layer
R	: reflection coefficient
r_0	: characteristic length of rod
u	: horizontal displacement component
v	: vertical displacement component
w	: weighting function
λ	: stretching function
ζ	: damping ratio
ρ	: mass density
υ	: Poisson ratio
μ	: shear modulus
ω	: natural frequency
ε	: strain
σ	: normal stress
τ	: shear stress

CHAPTER 1

INTRODUCTION

1.1 GENERAL DESCRIPTION

Many fields of engineering and physical sciences are interested in the propagation of wave in unbounded domain problems. Soil-structure interaction and fluid-structure interaction problems are typical examples of this type of problems in wave mechanics. In addition, propagation of wave in unbounded domain is also significant concept in fields of acoustic, electromagnetism, and geophysics. Analytical, semi analytical and discrete methods are used to analyze such unbounded domain problems. The artificial boundary conditions (ABCs) are generally preferred in the analyses of unbounded domain problems using discrete methods. The truncation of unbounded domain by some surfaces (called artificial boundaries) and performing the analysis in the truncated finite domain by using ABCs is needed in the analysis of these problems by discrete methods such as; finite element method (FEM) and finite difference method (FDM). ABC's can minimize the reflections on artificial boundaries, however, they are not capable to eliminate them completely. Therefore, a method based on putting a perfectly matched layer (PML) around truncated domain is proposed to cure this shortcoming of ABC's. In this method, a reflectionless artificial layer which absorbs incident waves for all directions of incidence and frequencies is placed to the truncation boundary (interface). This study deals with the use of a meshfree method called generalized finite difference method (GFDM) in PML analysis of the problems in wave mechanics, in particular, in elastodynamics. The advantages of using GFDM in PML analysis are summarized as: GFDM is a meshless method suitable for any geometry of the domain, handling the boundary conditions

properly and having an easy implementation for PML analysis. In this thesis work, GFDM formulation in PML analysis at the elastodynamics problems is presented. The proper choice at the parameters appearing in GFDM and PML is made through the use of parametric studies carried out for some benchmark problems. The proposed formulation is appraised by applying it to the compliance of surface foundation and embedded rigid strip footing supported by a soil foundation. The surface foundation is considered having various configurations: uniform HS, soil layer on rigid bedrock and soil layer on uniform HS. The embedded foundation is considered only when the supporting soil medium is HS. Direct time domain analyses are also performed only for a surface rigid strip foundation on uniform HS.

1.2 RESEARCH OBJECTIVES AND SCOPE

The aim of this study is to demonstrate the effective use of a meshfree method called GFDM in PML to simulate the elastodynamics problems. For this end, theoretical formulation of the proposed method is given first. The main objectives of this thesis study are;

i. To determine the proper weighting function and radius of influence for GFDM algorithm.

ii. To define the appropriate PML parameters which enable to reduce numerical reflections and computational cost for GFDM in PML analysis.

iii. To propose a formulation to assess the compliance of surface foundation and embedded rigid strip footing supported by a soil foundation

iv. To propose a formulation to perform direct time domain analyses of a surface rigid strip foundation on uniform HS using GFDM in PML.

2

1.3 RESEARCH OUTLINE

The presented thesis study composed of four main parts. The outline of this thesis study is summarized as follows;

i. In the first part of this thesis study, an extensive literature review is conducted on artificial boundary conditions commonly used to represent unbounded domains. Then, a literature review is conducted on GFDM. Next, the information acquired from the literature about the determination of a compliance function of rigid strip foundation.

ii. In the second part of the research study, a bounded two dimensional fictitious plane strain problem is solved to determine the proper weighting function and radius of influence for GFDM algorithm.

iii. In the third part of the thesis study, a one dimensional semi-infinite rod on elastic foundation problem is solved to determine the appropriate PML parameters.

iv. Then, the analyses of the all cases of rigid strip foundation considered in the scope of this thesis study are conducted to obtain compliance functions of this type of foundation.

v. Furthermore, the direct time domain solution of reaction forces of rigid strip foundation are estimated for surface foundation over half space using GFDM in PML.

vi. The results of GFDM in PML analysis for both in frequency and time spaces are compared with those of FEM in PML and boundary element method (BEM), when possible, also with those of other studies.

1.4 LITERATURE REVIEW

1.4.1 UNBOUNDED DOMAINS AND ARTIFICIAL BOUNDARY CONDITION

During the analyses of unbounded domain problems by using discrete method, the unbounded domain should be truncated by some surfaces (artificial boundaries). This enables performing the analysis of unbounded domain problem in the truncated finite domain using some ABCs. Implementation of absorbing boundary conditions in the unbounded domain problem makes the problem solution applicable on computer (Lehmann, 2007). Two different procedures are generally used to truncate the boundaries in unbounded domain problems. ABC at truncation interface is introduced to truncate the unbounded domain or, an absorbing layer is located at the truncation domain. Tsynkov (1998) prepared a review for numerical solution of problems on unbounded domains. The researcher investigated all types of absorbing boundary conditions and divided them into three main groups: local boundary, non-local boundary and absorbing layer methods (PML). The local boundaries are easy to apply to non-homogenous systems and efficient both in time and frequency domain. In addition, local boundary conditions may be good energy absorbers, however, they are not sufficient to eliminate spurious wave along the boundary. Lysmer and Kuhlemeyer (1969) simulated radiation with simple local boundaries and developed viscous boundary condition which use viscous damper with constant properties connected to boundary. White and Valliappan (1977) added the effect of Poisson ratio in viscous boundary condition and so called 'unified boundary condition' which yields results more accurate than that of standard viscous boundary condition. Engquist and Majda (1977) and Clayton and Engquist (1977) developed a paraxial approximation. This approximation is used as boundary condition which derived for numerical wave simulation that minimizes spurious reflection. In addition, this method is computationally inexpensive and simple to apply.

Non-local boundaries create perfect absorbers of any type of waves so that the model can be reduced to minimum size, but they are properly defined only in frequency domain. They cannot be used for problems involving material nonlinear effects except through the approximate iterative scheme (Kausel and Tassoulas, 1981). Waas (1972) described first non-local (consistent) boundary for layered strata over rigid rock in frequency domain. Givoli and Keller (1989) developed a non-local exact absorbing boundary condition for some problem in elasticity and Laplace equations. Givoli (1992) improved Dirichlet-to-Neumann maps (DtN) boundary conditions to allow for time dependent problems.

The last type of ABCs is absorbing layer. Absorbing layer surrounds area of interest by a finite thickness and attenuates incidence wave from the computational domain. The boundary between the computational domain and the layer causes minimal and ideally zero reflection. This absorbing layer is called Perfectly Matched Layer (PML).

Berenger (1994) developed PML for electromagnetic waves in 2D medium. Berenger (1994) used finite difference time domain (FDTD) techniques in Cartesian coordinates. The field variables of the PML are split into nonphysical components to eliminate plane wave reflection for an arbitrary angle of incidence. This formulation has proved to be extremely efficient and has become popular. Chew and Weedon (1994) reformulated Berenger's PML and introduced complex coordinate stretching for 3D medium. They implemented a code for the PML algorithm using the FDTD technique. Sacks et al. (1995) performed an application of FEM in PML in frequency domain. Kuzuoğlu and Mittra (1997) applied Sacks' 'anisotropic' PML to cylindrical coordinates. Collino and Monk (1996) developed PML in curvilinear coordinates. Maloney et al. (1997) developed PML in cylindrical coordinates for electromagnetic waves. Teixeira and Chew (1997) used complex coordinate stretching method for develop PML in the problems having cylindrical and spherical domain.

The PML method was extended to elasticity problems. Chew and Liu (1996) and Hasting (1996) presented the PML method to elastic waves with FDTD technique independently. Hasting (1996) performed a research study on 2D elastic medium velocity stress finite difference formulation for PML. Chew and Liu (1996) first developed a method in elastodynamics half-space which used PML. They used complex-valued coordinate stretching to obtain the equations governing the PML. In addition, the same problem is also formulated by using FDTD with split field. Liu (1999) developed a new approach to PML used it in elastic waves having cylindrical and spherical coordinates for the split and unsplit FDTD. Collino and Tsogka (2001) presented and analyzed PML model for the velocity-stress formulation of elastodynamics. Zeng et al. (2001) applied the split PML to wave propagation in poroelastic media using finite difference method. Zheng and Huang (2002) developed new numerical anisotropic PML for elastic wave in curvilinear coordinates. The new PML are easy to implement for both isotropic and anisotropic solid media. Komatitsch and Tromp (2003) developed a second order PML system in velocity and stress for seismic wave equation. Festa and Nielsen (2003) used three-dimensional finite difference scheme for PML in elastodynamics. Basu and Chopra (2002, 2003, 2004) and Basu (2004, 2008) performed a study to develop direct time and frequency domain formulations for FEM. These formulae were used to elastic and transient waves in 1D, 2D and 3D finite element scheme. They also obtained compliance function for rigid strip foundation using FEM with unsplit PML. Küçükçoban (2010) and Kang (2010) used mixed FEM with unsplit PML for inverse and forward problems in elastic media.

1.4.2 GENERALIZED FINITE DIFFERENCE METHOD

In many problems of computational mechanics such as crack propagation, large deformations etc., the geometry of domain changes continuously. Accordingly, the analysis of such problems using classical FEM and FDM are difficult, time consuming and expensive task. Therefore, meshless methods can be an alternative technique for the analysis of such problems. The basic concept in meshless

6

methods is to eliminate the difficulties which arise from the meshes. Two main approximations for meshless methods are available: smooth particle hydrodynamics (SPH) and moving least square (MLS). SPH approximation was first used by Lucy (1977) to model astrophysical phenomena without boundaries. Nayroles et al. (1992) used to MLS approximation in a Galerkin method called diffuse element method (DEM). Element-free Galerkin (EFG) method is a modified version of the DEM (Belytschko et al., 1994). The other path of meshless method is GFDM which was developed by Liszka and Orkisz (1980). The basic ideas of this method were proposed in seventies. Jensen (1972) employed the fully arbitrary meshes for finite difference method in his studies. Perrone and Kaos (1975) formulated a two dimensional finite difference method capable of using irregular meshes. Liszka (1977) proposed a local interpolation technique which has an irregular mesh of nodal points. This Liszka's interpolation technique which based on a Taylor series expansion of unknown function combined with minimization of errors is stable and applicable (Liszka, 1984). This technique has also been used as GFDM by Orkisz and Liszka (1980). The GFDM are used in applied mechanics problems (Orkisz and Liszka, 1980; Tworzydlo, 1987). Tworzydlo (1987) used this method to the analyses of large deformations of membrane shell. Benito et al. (2001) investigated the effects of weighting function, radius of influence and stability parameter for time dependent problems in GFDM. Gavete et al. (2003) compared GFDM with the EFG method. They obtained more accurate results in the case of GFDM. Benito et al. (2003) purposed an h-adaptive method in GFDM to avoid ill-condition. Then, Benito et al. (2007) solved parabolic and hyperbolic equations for some randomly distributed nodes with GFDM.

1.4.3 ANALYTICAL AND NUMERICAL METHODS FOR RIGID STRIP COMPLIANCE FUNCTIONS

In the literature, many research studies are conducted to determine the impedance and compliance functions for rigid strip foundations. The problem of vibration of rigid foundation on half space (HS) is a mixed value problem. The displacements under the foundation are imposed and the rest of the surface of the HS is traction

free. Karadushi et al. (1968) conducted a research study on infinitely rigid foundation. In this study, an approximate analytical solution for vertical, horizontal and rocking vibration of this surface foundation on HS are determined. The coupling effects are found to be less significant for surface foundation. Luco (1969) and Luco and Westmann (1972) performed the exact analytical solution of strip foundation using Green function when the Poisson ratio of the soil is ½. In addition, approximate solutions are obtained for other Poisson ratios. Gazetas (1975) studied on dynamic stiffness functions of strip foundation in layered medium using a semi-analytical method employing the fast Fourier transform. Gazetas and Roesset (1979) obtained impedance functions for two-dimensional rigid strip foundations supported on a uniform layer over an elastic half-space. Hryniewicz (1980) suggested a semi-analytical method to determine vertical, horizontal and rocking motion of strip foundation on the surface of the elastic HS. Luco and Apsel (1987) obtained impedance function for embedded foundation in layered viscoelastic half-space with Green`s function technique. Rajapakse and Shah (1988) conducted a research study on embedded rigid strip foundation having an arbitrary geometry in homogenous half space. The solution which is performed to determine the impedance function of embedded trapezoidal shaped foundation reveals that the cross-sectional shape of strip foundation has significant effect on the dynamic responses.

Several authors used discrete methods such as FEM, BEM and hybrid method, to describe compliance or impedance functions for rigid strip foundation. The FEM is started to use in modeling unbounded domains after the first application of artificial boundary condition (ABC) by Lysmer and Kuhlemeyer (1969) in FEM to obtain the stress distribution under the circular footing. Then, the discrete methods are becoming very popular for modeling and analyses of the problems having unbounded domain. Kuhlemeyer (1972) conducted a research study on the vertical vibration of circular footing layered medium using FEM with ABC. Vertical motions of circular region in unbounded domain are also obtained by Waas (1972) using FEM with consistent boundary conditions. Liang (1974)

conducted a research study to determine the compliance functions of embedded strip foundation in layered medium over the bedrock using FEM.

The BEM based on boundary integral equations are known as very applicable for dynamic soil structure interaction (SSI) problems, and this method is widely used for the solution of this type of problems. Using BEM, the radiation of waves towards the infinity in such a problem is automatically included in the model, which is based on an integral representation valid for internal and external regions (Hall and Oliveto, 2003). The first BEM application on dynamic SSI problem is presented by Dominquez (1978). However, first numerical implementation of elastodynamics formulation of BEM is conducted by Cruse and Rizzo (1968). The direct formulation of the BEM is generally applied to evaluate dynamic response of foundation in frequency domain formulation for foundations supported by elastic and viscoelastic half-spaces (HS). Abascal and Dominguez (1984) used BEM to find the dynamic compliance of rigid strip foundation on non-homogenous viscoelastic soil. Von Estorff and Schmid (1984) also performed BEM to analyze of the strip foundation on a soil layer. Spyrakos and Beskos (1986) conducted a research study to determine the dynamic response of a rigid strip foundation using time domain BEM. Ahmad and Israel (1989) and Ahmad and Bharadwaj (1991, 1992) investigated the dynamic response of rigid strip foundation under vertical, horizontal and rocking excitation in layered medium using BEM. Israil and Banerjee (1990) conducted a research study on time domain BEM for 2D wave propagation.

Tzong and Penzien (1983) used the hybrid modeling approach to obtain the dynamic response of rigid strip foundation layered on HS. The hybrid modeling approach splits the entire soil-structure system into a near and far field. The near field which includes foundation and surrounding soil is modeled by discrete method (FEM). However, analytical method is used to simulate far field impedance function.

9

CHAPTER 2

GENERALIZED FINITE DIFFERENCE METHOD

2.1 GENERAL

In this section, the GFDM and its solution procedure are discussed. The main objective of the GFDM method is to approximate the spatial derivatives for a differentiable function in terms of its values at some randomly distributed nodes (Li and Liu, 2004).

GFDM is a truly meshless method which requires only the coordinates of the nodes. Precision at the GFDM can be controlled by either using higher order approximation or by using finer mesh. Physical and geometrical nonlinearity at the problem does not make the algorithm more complicated.

The conventional finite difference method, a mesh based method, is more suitable when the mesh is regular. The earlier studies reveal that the mesh-free difference method yields better results, when compared to conventional finite difference method, for uniform node distribution (Li and Lui, 2004 and Liszka and Orkisz, 1980).

2.2 THE METHOD

In this section, GFDM is formulated for two dimensional problems. Taylor's expansion of a function $f(x,y)$ at a point (x_i, y_i) about a selected (a star) point (x_0, y_0) of a two dimensional region 2D is, when 2D is referred to an x-y rectangular coordinate system,

$$f_i = f_0 + h_i \frac{\partial f_0}{\partial x} + k_i \frac{\partial f_0}{\partial y} + \frac{h_i^2}{2} \frac{\partial^2 f_0}{\partial x^2} + \frac{k_i^2}{2} \frac{\partial^2 f_0}{\partial y^2} + h_i k_i \frac{\partial^2 f_0}{\partial x \partial y} + o(\Delta^3), \quad 1 \le i \le m \qquad (2.1)$$

where the function f is assumed to be continuous and adequately differentiable in 2D, m is number of nodes around the star point and

$$h_i = x_i - x_0, \quad k_i = y_i - y_0, \quad \Delta = \max_{1 \le i \le m} \left(\sqrt{h_i^2 + k_i^2} \right) \qquad (2.2)$$

When the error term in $O(\Delta^3)$ is ignored in Equation 2.1, it approximates the function in the neighborhood (i.e., at the points $[(x_i, y_i) ,(i=1\text{-}m)]$ of the star point (x_0, y_0) in terms of the function and its derivative values at (x_0, y_0)). To simplify the notation, the derivatives at (x_0, y_0) $\left(\frac{\partial^2 f}{\partial x^2} \right)_0 = \frac{\partial^2 f}{\partial x^2}(x_0, y_0)$, etc. are designated in Equation 2.1 by $\frac{\partial^2 f_0}{\partial x^2}$, etc.

To proceed with the development of GFDM, a weighted square error E in the approximation is introduced as:

$$E = \sum_{i=1}^{m} \left[\left(f_0 - f_i + h_i \frac{\partial f_0}{\partial x} + k_i \frac{\partial f_0}{\partial y} + \frac{h_i^2}{2} \frac{\partial^2 f_0}{\partial x^2} + \frac{k_i^2}{2} \frac{\partial^2 f_0}{\partial y^2} + h_i k_i \frac{\partial^2 f_0}{\partial x \partial y} \right) w_i \right]^2 \qquad (2.3)$$

where w_i is the weighting function. The best approximation can be obtained by minimizing the error E, which yields

$$\frac{\partial E}{\partial\{Df\}}=0 \tag{2.4}$$

where

$$\{Df\}^T = \left\{\frac{\partial f_0}{\partial x},\frac{\partial f_0}{\partial y},\frac{\partial^2 f_0}{\partial^2 x},\frac{\partial^2 f_0}{\partial^2 y},\frac{\partial^2 f_0}{\partial x\partial y}\right\} \tag{2.5}$$

From Equations 2.4 and 2.5, the following system of equations is obtained for $\{Df\}$:

$$\underbrace{\begin{pmatrix} \sum w_i^2 h_i^2 & \sum w_i^2 h_i k_i & \frac{1}{2}\sum w_i^2 h_i^3 & \frac{1}{2}\sum w_i^2 h_i k_i^2 & \sum w_i^2 h_i^2 k_i \\ \sum w_i^2 h_i k_i & \sum w_i^2 k_i^2 & \frac{1}{2}\sum w_i^2 k_i h_i^2 & \frac{1}{2}\sum w_i^2 k_i^3 & \sum w_i^2 k_i^2 h_i \\ \frac{1}{2}\sum w_i^2 h_i^3 & \frac{1}{2}\sum w_i^2 k_i h_i^2 & \frac{1}{4}\sum w_i^2 h_i^4 & \frac{1}{4}\sum w_i^2 h_i^2 k_i^2 & \frac{1}{2}\sum w_i^2 h_i^3 k_i \\ \frac{1}{2}\sum w_i^2 h_i k_i^2 & \frac{1}{2}\sum w_i^2 k_i^3 & \frac{1}{4}\sum w_i^2 h_i^2 k_i^2 & \frac{1}{4}\sum w_i^2 k_i^4 & \frac{1}{2}\sum w_i^2 h_i k_i^3 \\ \sum w_i^2 h_i^2 k_i & \sum w_i^2 k_i^2 h_i & \frac{1}{2}\sum w_i^2 h_i^3 k_i & \frac{1}{2}\sum w_i^2 h_i k_i^3 & \sum w_i^2 h_i^2 k_i^2 \end{pmatrix}}_{A_{(5*5)}} \underbrace{\left\{\begin{array}{c} \dfrac{\partial f_0}{\partial x} \\ \dfrac{\partial f_0}{\partial y} \\ \dfrac{\partial^2 f_0}{\partial x^2} \\ \dfrac{\partial^2 f_0}{\partial y^2} \\ \dfrac{\partial^2 f_0}{\partial x\partial y} \end{array}\right\}}_{Df_{(5*1)}}$$

$$=\underbrace{\begin{pmatrix} -f_0\sum w_i^2 h_i + \sum f_i w_i^2 h_i \\ -f_0\sum w_i^2 k_i + \sum f_i w_i^2 k_i \\ -f_0\sum w_i^2 \frac{h_i^2}{2} + \sum f_i w_i^2 \frac{h_i^2}{2} \\ -f_0\sum w_i^2 \frac{k_i^2}{2} + \sum f_i w_i^2 \frac{k_i^2}{2} \\ -f_0\sum w_i^2 h_i k_i + \sum f_i w_i^2 h_i k_i \end{pmatrix}}_{b_{5*1}} \tag{2.6}$$

or, in compact form,

$$ADf = b \tag{2.7}$$

In view of symmetry of *A*, the Cholesky method is generally preferred to solve this system in Equation 2.7, which eliminates the need for the evaluation of inversion of A (Benito et al., 2007).

For computational purposes, the right hand side in Equation 2.7 can be expressed in the form

$$b = Gf \qquad (2.8)$$

where *G* is a 5*(m+1) dimensional matrix and *f* is (m+1) dimensional vector defined by

$$G = \begin{bmatrix} -\sum_{i=1}^{m} w_i^2 h_i & w_1^2 h_1 & w_2^2 h_2 & \cdots & \cdots & w_m^2 h_m \\ -\sum_{i=1}^{m} w_i^2 k_i & w_1^2 k_1 & w_2^2 k_2 & \cdots & \cdots & w_m^2 k_m \\ -\sum_{i=1}^{m} w_i^2 \dfrac{h_i^2}{2} & w_1^2 \dfrac{h_1^2}{2} & w_2^2 \dfrac{h_2^2}{2} & \cdots & \cdots & w_m^2 \dfrac{h_m^2}{2} \\ -\sum_{i=1}^{m} w_i^2 \dfrac{k_i^2}{2} & w_1^2 \dfrac{k_1^2}{2} & w_2^2 \dfrac{k_2^2}{2} & \cdots & \cdots & w_m^2 \dfrac{k_m^2}{2} \\ -\sum_{i=1}^{m} w_i^2 h_i k_i & w_1^2 h_1 k_1 & w_2^2 h_2 k_2 & \cdots & \cdots & w_m^2 h_m k_m \end{bmatrix} \quad f = \begin{Bmatrix} f_0 \\ f_1 \\ f_2 \\ : \\ : \\ f_m \end{Bmatrix} \qquad (2.9)$$

Equation 2.7, which is to be solved at each star point in 2D, is called the star equation. Now the procedure for the solution of a boundary value problem by GFDM is in order:

1. Select the nodes in solution region and on its boundary

2. Write the governing differential equations (GDE) at each of the selected nodes

3.By treating each node as a star point, approximate the derivatives appearing in GDE, through the use of Equation 2.6, in terms of unknown function values at nodes

4.Combine the equations written at all nodes and solve them in view of boundary conditions.

2.3 SELECTION OF PARAMETERS IN STAR EQUATION

The selection of the parameters, such as, the number of points around a star point, the form of weighting function and degree of Taylor's series expansion is crucial for obtaining derivatives from star equation. Selection of the number of nodes around a star point is investigated by several authors. It is important to avoid ill-conditioning to improve accuracy of results and reduce the cost of computation. A hexagon grid is selected by Jensen (1972), which includes six nodes around a star point. Perrone and Kaos (1975) suggest nine control schemes where the domain around a star point is divided into eight equal segments and the closest point to the star point in each segment is selected (see Figure 2.1). The four quadrant criterion (see Figure 2.2) is proposed by Liszka and Orkisz (1980) where the domain surrounding a star point is divided into four quadrants and two nodes closest to the star point are selected in each quadrant. Godoy (1986) suggested a model which includes 12 nodes for bi-harmonic problems. Benito et al. (2003) purposed an h-adaptive method in GFDM to avoid ill-condition.

In the distance type algorithm, used in this study, all the nodes inside the circle of influence of a star point are included in formulation (see Figure 2.3). It is to be noted that all the algorithms or criteria used in literature for the selection of nodes in meshless methods contain the domain of influence since the weighting functions appearing in these algorithms involve the radius dm of the influence circle.

14
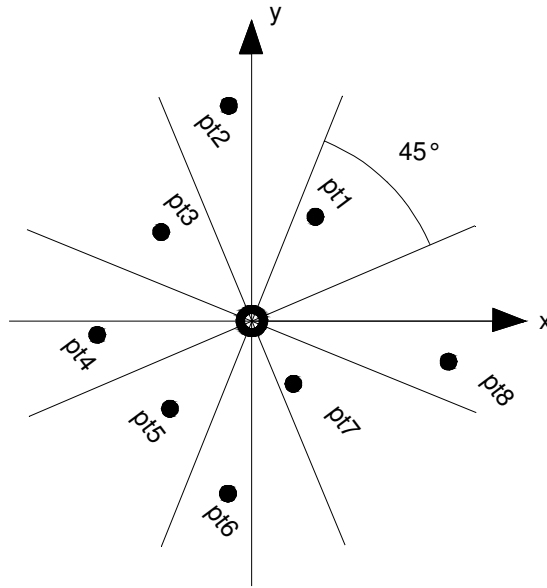
Figure 2.1: Nine control scheme (Perrone and Kaos, 1975)
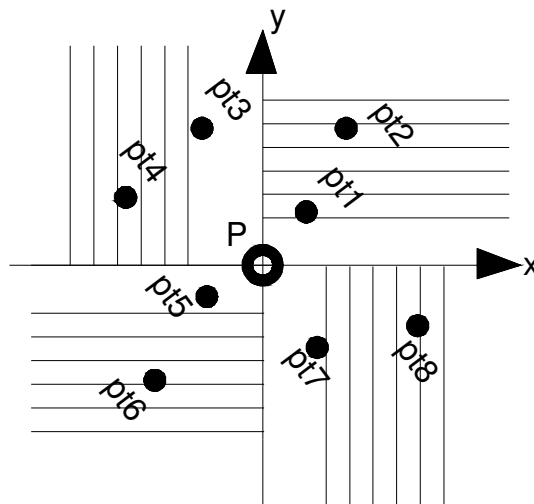
Figure 2.2: Four quadrant algorithm (Liszka and Orkisz, 1980).
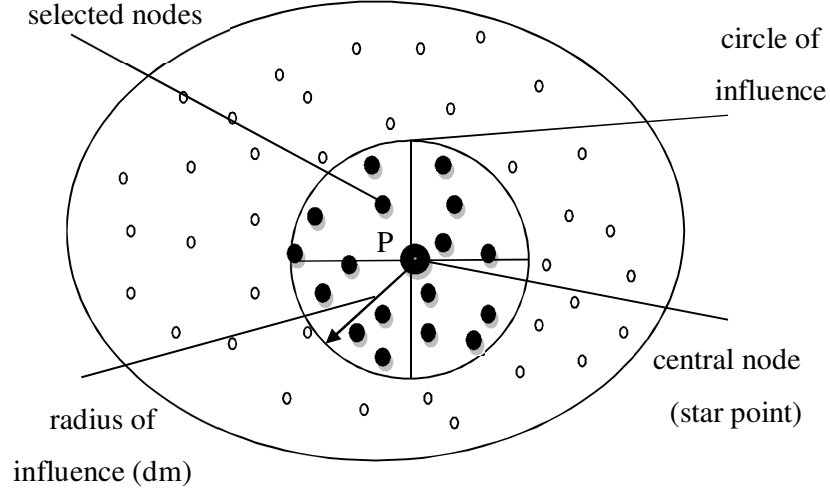
Figure 2.3: Distance type algorithm.

In this study, the following four well-known weighting functions are used for two dimensional problems:

a)   *Cubic distance weighting function:*

$$w_i = \begin{cases} 1/(d_i)^3 \;\; with \; d_i = \sqrt{h_i^2 + k_i^2} \quad for \quad d_i \leq dm \\ w_i = 0 \quad for \quad d_i > dm \end{cases}$$

(2.10)

b)   *Polynomial weighting function (quartic spline):*

$$w_i = \begin{cases} 1 - 6\left(\dfrac{d_i}{dm}\right)^2 + 8\left(\dfrac{d_i}{dm}\right)^3 - 3\left(\dfrac{d_i}{dm}\right)^4 \quad for \quad d_i \leq dm \\ \qquad\qquad 0 \quad for \quad d_i > dm \end{cases}$$

(2.11)

16

c)   Polynomial weighting function (cubic spline):

$$w_i = \begin{cases} \dfrac{2}{3} - 4\left(\dfrac{d_i}{dm}\right)^2 + 4\left(\dfrac{d_i}{dm}\right)^3 & for \ d_i \leq 0.5dm \\[3mm] \dfrac{4}{3} - 4\left(\dfrac{d_i}{dm}\right) + 4\left(\dfrac{d_i}{dm}\right)^2 - \dfrac{4}{3}\left(\dfrac{d_i}{dm}\right)^3 & for \ 0.5dm < d_i \leq dm \\[3mm] 0 & for \ d_i > dm \end{cases} \qquad (2.12)$$

d)   Exponential weigthing function:

$$w_i = \begin{cases} \exp\left(\left(-\left(\dfrac{d_i}{dm}\right)/0.4\right)^2\right) & for \ d_i \leq dm \\[3mm] 0 & for \ d_i > dm \end{cases} \qquad (2.13)$$

It is expected that more accurate results may be obtained when the number of terms in Taylor's series is increased. In the following section, whether this expectation holds or not is also investigated (among other effects, such as the effect of weighting function, on the accuracy) where the results are obtained numerically through the use of GFDM. This investigation is done in view of the fact that if five and nine terms in Taylor's series are retained to solve second order partial differential equations (PDE), it requires respectively, to avoid singularity, at least, five and nine nodes around the star point (excluding the star point). It is to be noted that the five and nine term Taylor's series (TS) for two dimensional (2D) case correspond respectively to TS of order two and three which will be abbreviated in the study as TS2 and TS3.

2.4 AN ASSESSMENT OF GFDM THROUGH A BENCHMARK PROBLEM

In this section, a two-dimensional fictitious plane strain problem, defined in a unit square region, is considered. The problem is solved using GFDM. Three different clouds illustrated in Figures 2.4-2.6 are considered. The first cloud has 144 regular nodes with 44 point at boundary. The second one has 177 irregular nodes having 40 nodes at boundary. The last one contains 232 irregular nodes with 32 nodes at boundary. The distance (*dnodes*) between two successive nodes at boundary for these three clouds is 1/11, 1/10 and 1/8 respectively.
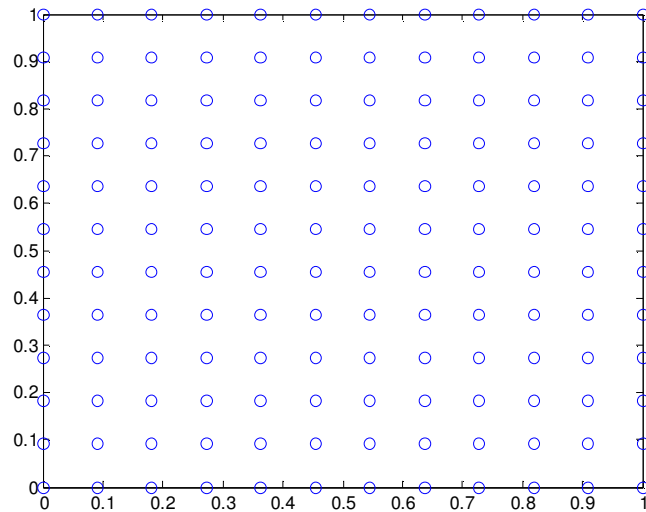
Figure 2.4: Cloud 1: regular 144 nodes
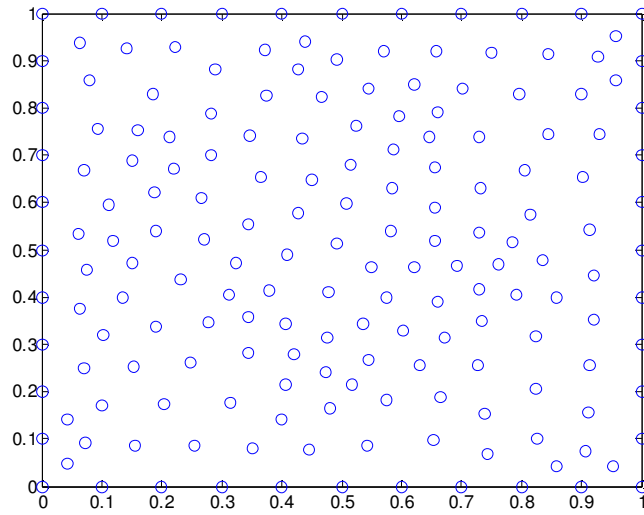
Figure 2.5: Cloud 2: irregular 177 nodes.
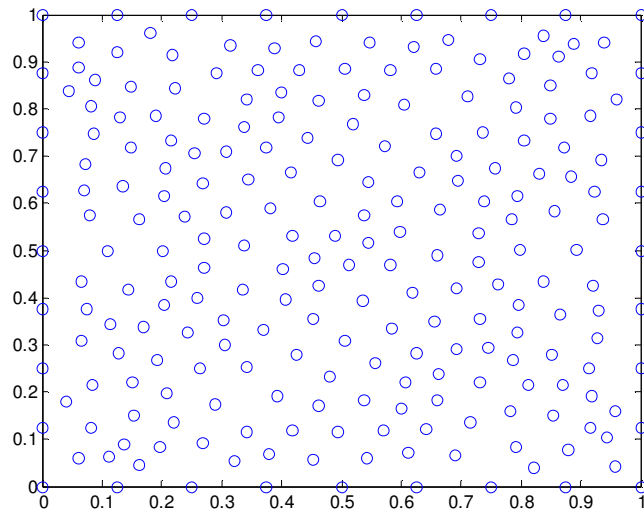
Figure 2.6: Cloud 3: irregular 232nodes.

2D static (equilibrium) equations in Cartesian coordinates *(x, y)* without body forces are

$$\frac{\partial \sigma_{xx}}{\partial x} + \frac{\partial \tau_{xy}}{\partial y} = 0$$

$$\frac{\partial \tau_{yx}}{\partial x} + \frac{\partial \sigma_{yy}}{\partial y} = 0$$

(2.14)

where σ_{xx}, σ_{yy} are normal stresses and τ_{xy} is the shear stress.

The elastic stress-strain relation for plane strain case are given below:

$$\sigma_{xx} = \left(\frac{(1-\upsilon)E}{(1+\upsilon)(1-2\upsilon)} \right) \varepsilon_{xx} + \left(\frac{\upsilon E}{(1+\upsilon)(1-2\upsilon)} \right) \varepsilon_{yy}$$

$$\sigma_{yy} = \left(\frac{\upsilon E}{(1+\upsilon)(1-2\upsilon)} \right) \varepsilon_{yy} + \left(\frac{(1-\upsilon)E}{(1+\upsilon)(1-2\upsilon)} \right) \varepsilon_{xx}$$

(2.15a)

$$\tau_{xy} = \left[\frac{E}{1+\upsilon} \right] \varepsilon_{xy}$$

$$\sigma_{zz} = \left(\frac{\upsilon E}{(1+\upsilon)(1-2\upsilon)} \right) (\varepsilon_{xx} + \varepsilon_{yy})$$

(2.15b)

where E is the elasticity modulus, υ is the Poisson's ratio, σ_{zz} is normal stress in z-direction and ε_{ij} are strains which are related to the displacement components u and v in x and y directions by

$$\varepsilon_{xx} = \frac{\partial u}{\partial x}$$

$$\varepsilon_{yy} = \frac{\partial v}{\partial y}$$

(2.16)

$$\varepsilon_{xy} = \frac{1}{2} \left[\frac{\partial u}{\partial y} + \frac{\partial v}{\partial x} \right]$$

The benchmark problem considered here involves the solution of Equations 2.14-16, which is

$$u(x, y) = -e^{-\pi x} \sin(\pi y)$$
$$v(x, y) = e^{-\pi x} \cos(\pi y)$$

<div align="right">(2.17)</div>

satisfying the following boundary condition for unit square plate:

$$
\begin{aligned}
u(0, y) &= -\sin(\pi y) & v(0, y) &= \cos(\pi y) \\
u(1, y) &= -e^{-\pi} \sin(\pi y) & v(1, y) &= e^{-\pi} \cos(\pi y) \\
u(x, 0) &= 0 & v(x, 0) &= e^{-\pi x} \\
u(x, 1) &= 0 & v(x, 1) &= -e^{-\pi x}
\end{aligned}
$$

<div align="right">(2.18)</div>

where x and y axes of the coordinate system coincide with the lower and left edges of the plate respectively.

In error analysis, the following global error expression defined by (Benito et al., 2001)

$$GlobalError = \frac{\sqrt{\left(\sum_{i=1}^{N} \left(f_i^{appr} - f_i^{exact} \right)^2 \right)} \Big/ N}{\left| \max(f^{exact}) \right|}$$

<div align="right">(2.19)</div>

is used where N is the total number of nodes in the domain and f includes both u and v.

Two different types of node selection algorithm are employed to investigate the accuracy of the GFDM solutions:

i) Distance type algorithm: All nodes inside the circle of influence around a star point (see in Figure 2.3) are included in writing star equation. If the number of nodes is less than eight for TS2 (twelve nodes for TS3), then the radius of circle is multiplied by two until the eight point criterion for TS2 (twelve nodes for TS3) is satisfied.

ii) Quadrant type algorithm: The four quadrant criterion which was proposed by Liszka and Orkisz (1980) is used (see in Figure 2.2). For TS2, two nodes and for TS3, three nodes are considered in each quadrant. If the four quadrants do not exist, for example for the points on the boundary, then the closest twelve points to the star point for TS2 (sixteen points for TS3) are selected. The radius of circle of influence for each star (which is needed for weighting functions) is chosen about 1.6 times of the longest distance of the selected nodes from the star point.

2.4.1 EFFECT OF WEIGHTING FUNCTION

In this section, the effect of weighting function on the global error of distance and quadrant type algorithms is studied. For this purpose, four weighting functions, cubic distance, quartic spline, cubic spline and exponential, are considered and the 2D plane strain problem is solved for each weighting function and for three different clouds where the radius of influence for the distance type algorithm is taken as dm=1/5. The results, which are obtained by using five terms Taylor's series, are presented in Table 2.1 and 2.2. The errors in these tables and in the tables which will be presented subsequently are expressed as percent (%).

Through the comparison of the results presented in Tables 2.1 and 2.2, the following observations can be made:

1. The global errors for the distance and quadrant type algorithms are generally comparable. This implies that the use of quadrant algorithm in the analysis may be advantageous over distance type algorithm since the number of nodes in the star equation of quadrant algorithm is less than (therefore, its computational cost is lower than) that of distance type algorithm.

2. For quadrant algorithms, the best approximation is obtained when the cubic distance weighting functions is used while quartic spline weighting function works better for distance type algorithm. However, Table 2.1 shows that the cubic distance weighting function also yields reasonable results for distance type

algorithm; thus, due to its simplicity, the use of cubic distance weighting function may be suggested for both quadrant and distance type algorithms.

3. The global error increases with the mesh irregularity; but, this increase is not much appreciable for distance type algorithm compared to that of quadrant algorithm.

Table 2.1: The global error for distance type algorithm for various weighting functions (dm=1/5, TS2)

Cloud	Cubic distance	Quartic spline	Cubic spline	Exponential
Cloud1	3.3042e-03	2.6589e-04	2.5744e-03	2.9002e-03
Cloud 2	6.0271e-03	5.7627e-03	6.1977e-03	6.0236e-03
Cloud 3	7.4512e-03	5.3060e-03	5.5493e-03	6.0236e-03

Table 2.2: The global error for quadrant type algorithm with two nodes in each quadrant for various weighting functions (TS2)

Cloud	Cubic distance	Quartic spline	Cubic spline	Exponential
Cloud1	7.0113e-05	6.7071e-04	1.7487e-03	2.0919e-03
Cloud 2	4.9814e-03	7.6678e-03	6.2362e-03	5.8667e-03
Cloud 3	7.0176e-03	1.2292e-02	1.0252e-02	9.5300e-03

2.4.2 EFFECT OF NUMBER OF TERMS IN TAYLOR'S SERIES EXPANSION

Here, the effect of the number of terms in Taylor's series expansion (that is, the effect of the order of TS) on the global error of distance and quadrant type algorithms is studied. Tables 2.3 and 2.4 give the results obtained by using TS2 and TS3. To compare TS2 and TS3 results, for quadrant type algorithm, three nodes are chosen in each quadrant; for distance type algorithm, minimum twelve nodes are chosen around the star point. In the analysis, the radius of circle of influence is chosen as dm=1/4 for the distance type algorithm and the three clouds

in Figures 2.4-2.6 are considered for both algorithms. The selection of dm for quadrant type algorithm is the same as that explained in Section 2.4/ii.

In view of the results in Tables 2.3 and 2.4, one may observe:

1. The global errors in TS3 are generally less than those in TS2 for all weighting functions, except for cubic distance weighting function with quadrant type algorithm using regular mesh. But, it is to be noted that this improvement of TS3 over TS2 is obtained at the expense of the computational cost of the analysis.

2. The global error generally decreases with the amount of mesh irregularity for TS3.

Table 2.3: Influence of number of terms in TS on the global error for distance type algorithm for various weighting functions (dm=1/4)

Cloud	Number of terms in TS	Cubic distance	Quartic spline	Cubic spline	Exponential
1	TS2	0.4214e-02	0.3826e-02	0.2424e-02	0.1815e-02
	TS3	0.2029e-02	0.2400e-02	0.1701e-02	0.0988e-02
2	TS2	0.6530e-02	0.5047e-02	0.4127e-02	0.4216e-02
	TS3	0.2343e-02	0.0857e-02	0.1462e-02	0.1700e-02
3	TS2	0.8400e-02	0.7147e-02	0.6161e-02	0.6197e-02
	TS3	0.1083e-02	0.0927e-02	0.0883e-02	0.0883e-02

Table 2.4: Influence of number of terms in TS on the global error for quadrant type algorithm for various weighting functions

Cloud	Number of terms in TS	Cubic distance	Quartic spline	Cubic spline	Exponential
1	TS2	4.5349e-03	1.1532e-02	9.3874e-03	8.1984e-03
	TS3	4.7724e-03	2.5343e-03	1.1909e-03	1.0598e-03
2	TS2	6.4441e-03	2.0755e-02	1.6153e-02	1.4361e-02
	TS3	1.7374e-03	3.6682e-03	2.6875e-05	2.3229e-03
3	TS2	7.6398-03	1.6682e-02	1.4389e-02	1.3157e-02
	TS3	1.0027e-03	1.6559e-03	1.3734e-03	1.2492e-03

2.4.3 EFFECT OF THE RADIUS OF INFLUENCE FOR DISTANCE TYPE ALGORITHM

In this section, the effect of radius of influence on the global error of distance type algorithm is studied. For this purpose, distance type algorithm with four different radii of 1, 1/3, 1/5 and 1/7 is used to solve the 2D plane strain problem for the four different weighting functions and for various clouds. The emphasis here is given to obtain the optimum value of dm for regular meshes; to this end, two more clouds (Cloud4 and Cloud5), in addition to Cloud1, are considered with 121 and 441 nodes where 40 and 80 points are chosen at boundary. For Cloud4 and Cloud5, the distance of boundary nodes (*dnodes*), between two successive nodes, is 1/10 and 1/20 respectively. The results are presented in Table 2.5 and Table 2.6, which show that:

1. The optimum value of dm varies with the weighting function used and the mesh density chosen.

2. For the regular meshes, the optimum dm for each weighting function is not affected much with mesh density.

3. For the regular meshes, the increase in mesh density reduces the global error.

25

Table 2.5: Effect of the radius of influence on the global error for distance type algorithm for various weighting functions (TS2)

Cloud	dm	Cubic distance	Quartic spline	Cubic spline	Exponential
1	1	2.2566e-02	3.6029e-01	3.1366e-01	2.2561e-01
	1/3	9.0448e-03	1.0671e-02	7.8339e-03	7.1908e-03
	1/5	3.3042e-03	2.6589e-04	2.5744e-03	2.9002e-03
	1/7	7.0113e-05	8.9690e-03	8.9976e-03	8.3816e-03
2	1	2.0068e-02	1.0040	4.2052e-01	3.5759e-01
	1/3	9.0744e-03	1.4612e-02	1.1252e-02	1.0307e-02
	1/5	6.0271e-03	5.7627e-03	6.1977e-03	6.0236e-03
	1/7	5.7426e-03	8.0924e-03	7.5833e-03	6.8501e-03
3	1	2.2511e-02	5.8776e-01	3.3286e-01	8.1406e-01
	1/3	1.0715e-02	1.7886e-02	1.3785e-02	1.2691e-02
	1/5	7.4512e-03	5.3060e-03	5.5493e-03	5.6985e-03
	1/7	5.5702e-03	7.0885e-03	7.2429e-03	6.7393e-03

2.4.4 EFFECT OF NUMBER OF NODES IN EACH QUADRANT

Here, the effect of number of nodes in each quadrant on the global error of quadrant type algorithm is studied. For this purpose, two and three nodes in each quadrant are considered. The 2D plane strain problem is solved for various weighting functions and the clouds 1, 2 and 3. The global errors are given in Table 2.7, showing that, against one's expectations, the error increases with number of nodes. In view of the results presented in Table 2.7, one may state that the best performance is obtained, for solving 2D plane strain problems by GFDM using irregular node distribution, when the quadrant type algorithm with two nodes in each quadrant together with cubic distance weighting function is employed.

Table 2.6: Optimum value of radius of influence minimizing the global error (TS2)

Cloud	Weighting Function	dm	Ave. number of nodes (including star point)	Global Error
1	Cubic distance	1.2-2*dnodes	9	7.0113e-05
	Quartic spline	2.2160*dnodes	13	4.3469e-05
	Cubic spline	2.4200*dnodes	21	6.8161e-05
	Exponential	2.4970*dnodes	21	2.7873e-04
2	Cubic distance	1.6650*dnodes	12	4.7067e-03
	Quartic spline	2.3100*dnodes	24	4.0844e-03
	Cubic spline	2.4750*dnodes	28	4.1139e-03
	Exponential	2.5050*dnodes	24	4.2154e-03
3	Cubic distance	1.1560*dnodes	11	5.4164e-03
	Quartic spline	1.6360*dnodes	25	5.2882e-03
	Cubic spline	1.7280*dnodes	30	5.4024e-03
	Exponential	1.7360*dnodes	30	5.6013e-03
4	Cubic distance	1.4-2*dnodes	9	1.1087e-04
	Quartic spline	2.2163*dnodes	13	6.2082-05
	Cubic spline	2.4200*dnodes	21	9.5267e-05
	Exponential	2.4995*dnodes	21	3.7540e-04
5	Cubic distance	0.14-2*dnodes	9	3.8400e-06
	quartic spline	2.2160*dnodes	13	2.6610e-06
	cubic spline	2.4200*dnodes	21	7.7200e-05
	exponential	2.5120*dnodes	21	3.8141e-05

Table 2.7: Influence of the number of nodes in each quadrant on the global error for quadrant type algorithm (TS2)

Cloud	Number of nodes Each quadrant	Cubic distance	Quartic spline	Cubic spline	Exponential
1	Two nodes	7.0113e-05	6.7071e-04	1.7487e-05	2.0919e-03
	Three nodes	4.5349e-03	1.1532e-02	9.3874e-03	8.1984e-03
2	Two nodes	4.9814e-03	7.6678e-03	6.2362e-03	5.8667e-03
	Three nodes	6.4441e-03	2.0755e-02	1.6153e-02	1.4361e-02
3	Two nodes	7.0176e-03	1.2292e-02	1.0252e-02	0.9530e-02
	Three nodes	7.6398e-03	1.6682e-02	1.4389e-02	1.3157e-02

CHAPTER 3

PERFECTLY MATCHED LAYER (PML) METHOD

The artificial boundary conditions (ABC's), also called transmitting boundary conditions, are generally used in the analysis of unbounded domain problems which arise, for example, from the problems related to modeling of soil-structure interaction (SSI), foundation vibrations, acoustics, electromagnetic waves, etc. The computational analysis of these types of problems by finite element (FE) method or finite difference (FD) method requires the truncation of unbounded domain by some surfaces (called artificial boundaries (AB's)) and performing the analysis in the truncated finite domain by using some special boundary conditions (BC's) on AB's, called ABC's. To predict correctly the dynamic response of unbounded domain from the analysis performed in truncated finite (computational) domain, ABC's should be capable to eliminate, at least, to minimize the reflections on AB's. Various ABC's are already proposed in literature: viscous BC's, paraxial BC's, transmitting BC's for waves propagating in horizontal direction in a layered medium, etc. Extensive list of references for these ABC's may be found in Kausel and Tassoulas (1981), Wolf (1985), Givoli (1991) and Tsynkov (1998). It should be noted that the above mentioned ABC's can only minimize the reflections on AB, not capable to eliminate them completely. For example, viscous BC's can transmit completely, through AB, only the waves of normal incidence and cause some reflections for inclined waves. To cure this shortcoming of ABC's, a method based on putting a perfectly matched layer (PML) around truncated domain is proposed in literature (Berenger 1994, Berenger 1996, Chew and Weedon 1994, Chew and Liu 1996, Hasting et al. 1996, Chew et al. 1997, Collino and Monk 1998). Berenger in his pioneer work in

1994 developed the PML for electromagnetic waves. The PML has a remarkable property: almost zero reflection from this absorbing layer for all directions of incidence and frequencies. The PML decays out the waves exponentially in magnitude, when the wave propagates in the layer (see Figure 3.1).
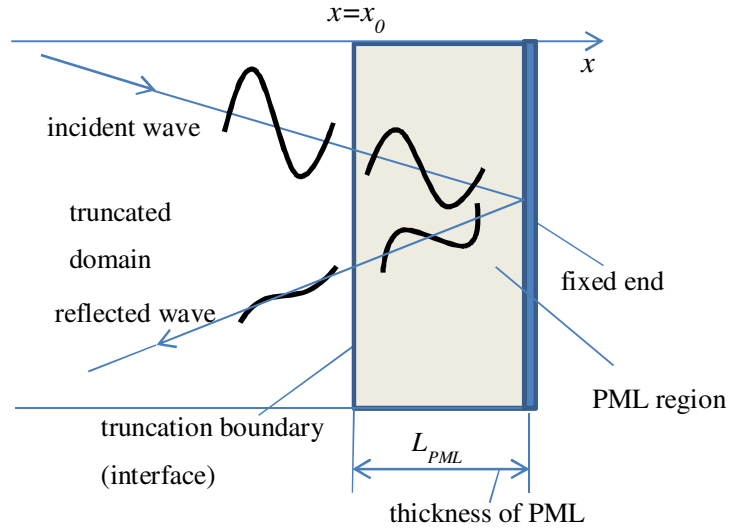
Figure 3.1: Figurative representation of attenuation of waves in a PML region.

Chew and Weedon (1994) reformulated Berenger's PML and introduced complex coordinate stretching for 3D medium. Chew and Liu (1996) used the complex coordinate stretching in elastodynamics. They implemented a code for the PML algorithm using the finite difference time domain (FDTD) technique.

In the PML application, a normal coordinate x (which is perpendicular to truncation boundary, see Figure 3.1) is replaced in frequency space by the stretching coordinate $\tilde{x}$, which is related to x by

$$\tilde{x} = \int_0^x \lambda(s)\,ds \tag{3.1}$$

where λ is a complex valued stretching function. Taking the derivative of the above equation one obtains

$$\frac{\partial}{\partial \tilde{x}} = \frac{1}{\lambda(x)} \frac{\partial}{\partial x} \tag{3.2}$$

To express the governing equations after stretching (in frequency space) in terms of original coordinates, $\frac{\partial}{\partial \tilde{x}}$ appearing in them is to be replaced by $\frac{1}{\lambda(x)} \frac{\partial}{\partial x}$.

When the truncated region is combined with PML, it becomes inhomogeneous; this would be so even in the case of homogenous medium, due to the replacements of the type of $\frac{1}{\lambda(x)} \frac{\partial}{\partial x}$ in PML region. However, the continuity conditions for the variables appearing in the governing equations would be satisfied at the interface between PML and truncated regions, implying that the interface would be invisible for the waves passing across the interface. Thus, if PML attenuates the waves entering it properly, the dynamic response of the truncated region would not be affected much by the waves reflected at a fixed boundary of PML, in other words, the response of truncated region obtained through PML analysis would represent adequately that of unbounded domain.

Various forms of stretching functions are suggested in literature (Chew and Weedon 1994, Mittra and Kuzuoğlu 1996, Fang and Wu 1996). Chew and Weedon (1994) proposed a simple stretching function as

$$\lambda(s) = 1 + \frac{f(s)}{i\omega} \tag{3.3}$$

where i is an imaginary number, ω is frequency and f is an attenuation function satisfying

$$
\begin{aligned}
f = 0 \quad for \quad s \le x_0 \\
f > 0 \quad for \quad s > x_0
\end{aligned}
\tag{3.4}
$$

with x_0 being a coordinate of the point on the truncation boundary (see Figure 3.1).

When Equation 3.3 is inserted into Equation 3.1, one gets

$$
\tilde{x} = \int_{x_0}^{x} \left(1 + \frac{f(s)}{i\omega}\right) ds = x + \frac{1}{i\omega} F(x)
\tag{3.5}
$$

where

$$
F(x) = \int_{x_0}^{x} f(s) \, ds
\tag{3.6}
$$

Equation 3.5 holds for the whole domain (for PML and truncated domains) and reduces to $\tilde{x} = x$ for $x \le x_0$ in truncated domain.

For a harmonic wave entering PML,

$$
u = A \exp\big(i(\omega t - kx)\big)
\tag{3.7}
$$

one can write in PML, when the *exp(iωt)* factor is disregarded,

$$
u(x) = A \exp(-ik\tilde{x}) = A \exp(-ikx) \exp(-\frac{1}{v} F(x))
\tag{3.8}
$$

where

$$
k = \frac{\omega}{v}
\tag{3.9}
$$

is the wave number, v denotes the wave velocity and A is the amplitude of wave. The attenuation is independent of frequency as observed in Equation 3.8.

The simple stretching function in Equation 3.3 is found to be ineffective to absorb evanescent waves which are standing waves with exponential decaying amplitude and imaginary wave number. To overcome this shortcoming of the stretching function in Equation 3.3, various alternative forms are proposed in literature. One of these forms is due to Basu (2004):

$$\lambda(s) = 1 + \frac{f^e(s)}{\omega} + \frac{f^p(s)}{i\omega} \tag{3.10}$$

where f^e and f^p are attenuation functions with the properties in Equation 3.4. f^p in Equation 3.10 attenuates the harmonic waves in PML (which is obvious in view of discussion given for f in Equation 3.3) whereas f^e does that for evanescent waves. In fact, for an evanescent wave, entering PML

$$u = A \exp(i\omega t - kx) \tag{3.11}$$

one can write in PML, when the $exp(i\omega t)$ part is disregarded in Equation 3.11,

$$u = A \exp(-k\tilde{x}) \tag{3.12}$$

This, in view of Equation 3.10, becomes

$$u(x) = A \exp(-(kx + \frac{1}{iv} F^p(x)) \exp(-\frac{1}{v} F^e(x)) \tag{3.13}$$

where

$$F^p(x) = \int_{x_0}^{x} f^p(s)\, ds \quad , \quad F^e(x) = \int_{x_0}^{x} f^e(s)\, ds \tag{3.14}$$

Equation 3.13 shows that f^e is responsible for the attenuation of evanescent waves in PML. It is worth to note that the attenuation implied by the stretching function in Equation 3.10 is frequency independent.

As stated previously, the stretching functions are being used in frequency (Fourier) space. To perform the analysis in the time domain, the governing equation in frequency domain is to be inverted into time space. But, the form of stretching function in Equation 3.10 causes some difficulties in this inversion. For this reason, Basu (2004) suggested a modification to Equation 3.10:

$$\lambda(s) = 1 + f^e(s) + \frac{f^p(s)}{i\omega} \tag{3.15}$$

which implies that the attenuation of evanescent waves in PML is given by the factor $\exp\left(-\frac{\omega}{v}F^e(x)\right)$ which, in turn, indicates that the stretching function in Equation 3.15 does not perform the attenuation properly for low frequency evanescent waves. However, Basu (2004) indicated that reasonable results may be obtained in spite of using the form given in Equation 3.15 for the stretching function.

In the literature, the polynomial attenuation functions are suggested, which may be expressed as

$$f(x) = f_0\left(\frac{x - x_0}{L_{PML}}\right)^m \tag{3.16}$$

where m is the order of attenuation function, L_{PML} is the thickness of PML and f_0 is a constant denoting the attenuation strength. Attenuation function plays significant role for better performance of PML algorithm. The aforementioned parameters (f_0, m and L_{PML}) are to be chosen carefully to mitigate reflections. Basu

(2004) used a linear attenuation function ($m=1$) in his finite element analysis. However, the quadratic form of attenuation is generally preferred by others.

To facilitate the selection of the attenuation strength f_0, some expressions are suggested in literature, expressing it in terms of some physical quantities. For a 1D wave propagation problem, Collino and Tsogka (2001) proposed the following expression for f_0:

$$f_0^p = \frac{(m+1)v_p}{2L_{PML}} \log(\frac{1}{|R|}) \qquad (3.17)$$

where

$$|R| = \exp\left(\frac{-2F^p\left(L_{PML}\right)}{v_p}\right) \qquad (3.18)$$

is the reflection coefficient in PML and v_p is P-wave velocity. The reflection coefficient represents the ratio of the amplitude of the reflected wave from the fixed boundary of PML to the amplitude of incident wave (see Figure 3.1). For the evanescent waves, the following expression is used for f_0, in conjunction with the stretching function in Equation 3.15,

$$f_0^e = \frac{(m+1)b}{2L_{PML}} \log(\frac{1}{|R|}) \qquad (3.19)$$

with

$$|R| = \exp\left(\frac{-2F^e\left(L_{PML}\right)}{b}\right) \qquad (3.20)$$

where b is a characteristic length of the domain.

3.1 PARAMETRIC STUDY

A parametric study is conducted to select the parameters (f_0, m and L_{PML}) appropriately for GFDM. For this purpose, a semi-infinite rod on elastic foundation is considered (see Figure 3.2), which simulates a pile penetrating into soil. The left end of the rod is subjected to an axial displacement u_0. This problem was considered by Wolf (1985 and 1996) to investigate the effect ABC's on the response of unbounded domains. The proper selection of the parameters (f_0, m and L_{PML}) is investigated through the comparison of PML solution (with GFDM) with the analytical. Comparisons will be presented in both frequency and time spaces in the following sections.
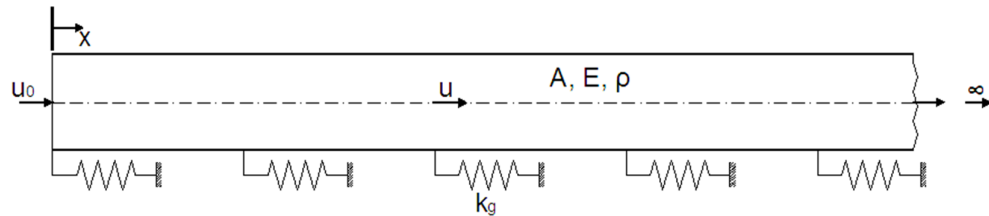
Figure 3.2: Semi-infinite rod on elastic foundation.

3.1.1 PROBLEM DEFINITION

An infinitesimal element from the rod on elastic foundation and the forces acting on it are illustrated in Figure 3.3. As stated previously, the rod is subjected to a dynamic displacement $u_0(t)$ at $x=0$. The waves arising from this displacement excitation radiate to the right. In the Figure 3.3: mass density, static spring stiffness per unit length of the rod, axial force, axial displacement and cross-sectional area are represented by ρ, k_g, N, u, and A, respectively.
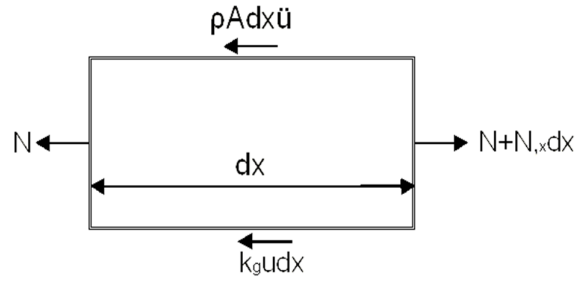
Figure 3.3: Infinitesimal element from the rod on elastic foundation

The equilibrium equation for the infinitesimal element is:

$$N,_x \, dx - k_g \, u \, dx - A \rho \ddot{u} \, dx = 0 \tag{3.21}$$

Substituting the force-displacement relationship $N = EAu,_x$ (E: elasticity modulus) into the above equation, one obtains

$$u,_{xx} - \frac{1}{r_0^2} u - \frac{1}{c_l^2} \ddot{u} = 0 \tag{3.22}$$

where r_0 is a characteristic length and c_l is the longitudinal wave velocity defined by

$$r_0 = \sqrt{\frac{EA}{k_g}} \quad , \quad c_l = \sqrt{\frac{E}{\rho}} \tag{3.23}$$

In the frequency domain, the equation of motion is expressed as

$$\bar{u},_{xx} - \frac{1}{r_0^2} \bar{u} + \frac{1}{c_l^2} \omega^2 \bar{u} = 0 \tag{3.24}$$

36

where the over-bar $(\bar{.})$ denotes the Fourier transform of (.). To simplify the notation, from now on, the over- bars will be dropped in the equations written frequency space.

The solution of the equation of motion in frequency space (of Equation 3.24) may be written as, in view of the BC $u=u_0(a_0)$ at $x=0$,

$$u(a_0) = u_0(a_0)\exp(-i\sqrt{(a_0^2-1)}\frac{x}{r_0})$$ (3.25)

where $a_0 = \dfrac{\omega r_0}{c_l}$ is a nondimensional frequency and $u_0(a_0)$ is Fourier transform of the displacement at $x=0$. The reaction force R at $x=0$ in frequency space can be obtained as, using the force-displacement relation $N = EAu_{,x}$,

$$R(a_0) = \sqrt{k_g EA}\ i\sqrt{(a_0^2-1)}\ u_0(a_0) = S^\infty(a_0)u_0(a_0)$$ (3.26)

which may be considered as the impedance equation relating the force R to the displacement u_0 at $x=0$.

Here S^∞ is the dynamic stiffness (impedance) coefficient. In view of the Equation 3.26, it is obvious that the static stiffness coefficient of the rod on elastic foundation (K^∞) is $\sqrt{EAk_g}$. Thus, the dynamic stiffness normalized with respect to K^∞ becomes

$$S(a_0) = \sqrt{(1-a_0^2)}$$ (3.27)

which is a complex valued quantity with real part being the spring coefficient (k) and the imaginary part, damping coefficient (c), that is

$$S(a_0) = k(a_0) + ia_0 c(a_0)$$ (3.28)

Here, $a_0=1$ is cut-off frequency and

$$for \quad a_0 \leq 1 \quad \rightarrow \quad \begin{array}{c} k(a_0) = \sqrt{(a_0^2 - 1)} \\ c(a_0) = 0 \end{array} \tag{3.29a}$$

$$for \quad a_0 \geq 1 \quad \rightarrow \quad \begin{array}{c} k(a_0) = 0 \\ c(a_0) = \sqrt{\dfrac{a_0^2 - 1}{a_0^2}} \end{array} \tag{3.29b}$$

The Fourier inversion of Equation 3.26 gives the impedance relation (at $x=0$) in the time space (see Wolf (1988)):

$$R(t) = K^\infty \left[\frac{r_0}{c_l} \frac{\partial u}{\partial t} + \int_0^t \frac{1}{t-\tau} J_1 \left(\frac{r_0}{c_l}(t-\tau) \right) u(\tau) d\tau \right] \tag{3.30}$$

where J_1 is the first order Bessel function of first kind.

3.1.2 SELECTION OF ATTENUATION FUNCTION'S PARAMETERS

The use of the PML in the analysis requires the selection of attenuation function's parameters. This section investigates how one may choose them properly. For this purpose, the impedance functions k and c are calculated by PML together with GFDM having regular mesh and using cubic spline weighting function with distance type algorithm; and they are compared with analytical results. The effects of mesh density, attenuation strength (f_0), order of attenuation function (m) and thickness of PML (L_{PML}) on the accuracy of the PML results are investigated in the following sections.

In the PML analysis of the rod, carried out in frequency space, the form of stretching function λ is chosen as that in Equation 3.10 with $f^e = f^p = f$:

$$\lambda(s) = 1 + \frac{f(s)}{a_0} + \frac{f(s)}{ia_0} \qquad (3.31)$$

PML equations of the rod in frequency space can be obtained from Equation 3.24 as, in view of discussions presented previously,

$$\frac{1}{\lambda(x)} \frac{d\varepsilon}{dx} - \frac{1}{r_0^2} u + \frac{1}{c_l^2} \omega^2 u = 0 \qquad (3.32)$$

with

$$\sigma = E\varepsilon \quad , \quad \varepsilon = \frac{1}{\lambda(x)} \frac{du}{dx} \qquad (3.33)$$

where ε: axial strain and σ: axial stress. Spacewise integration of Equations 3.32 and 3.33 may be performed by FEM or FDM or GFDM, which gives an equation of the form, in view of the BC at $x=0$,

$$Ku = P \qquad (3.34)$$

whose solution for u determines the response of the rod in frequency space. In Equation 3.34: K, P and u are respectively frequency dependent stiffness matrix, load and nodal point displacement vectors. In the present study, for spacewise integrations in Equations 3.32 and 3.33, GFDM is employed.

3.1.2.1 EFFECT OF MESH DENSITY

Here, the effect of mesh density on GFDM prediction of the impedance function of the rod on elastic foundation is investigated. In PML analysis, the model shown in Figure 3.4 is employed and parameters (other than mesh density) are chosen as $f_0 = 65$, $m = 4$, $L_{PML} = r_0$, $L = \frac{r_0}{2}$.

The results are given in Figures 3.5 and 3.6. Figure 3.5 gives the variation of the relative errors for the spring and damping coefficient k and c (for various frequencies) with the number of nodes (N_{nod}) used in GFDM, where the errors E_k for the coefficient k and E_c for c are defined by

$$
\begin{aligned}
E_k(a_0) &= \frac{\left|k^{exact}(a_0) - k^{appr}(a_0)\right|}{K^\infty} \\
E_c(a_0) &= \frac{\left|c^{exact}(a_0) - c^{appr}(a_0)\right|}{\max\left|c^{exact}\right|}
\end{aligned}
\tag{3.35}
$$

On the other hand, Figure 3.6 compares the frequency variations of the PML predictions for coefficients k and c with the exact, for various number of nodes employed in GFDM. Examination of the figures may lead to following observations.

1) The results obtained from PML analysis improve with the number of nodes in GFDM.

2) PML results are very sensitive to low frequencies. As already stated in Basu, (2004), the performance of PML is not good in near-zero frequency range, where the use of extrapolation may be suggested from the values in stable frequency zone.

3) The impedance function of the rod on elastic foundation may be estimated properly when the number of nodes are chosen as N_{nod}=61-121.
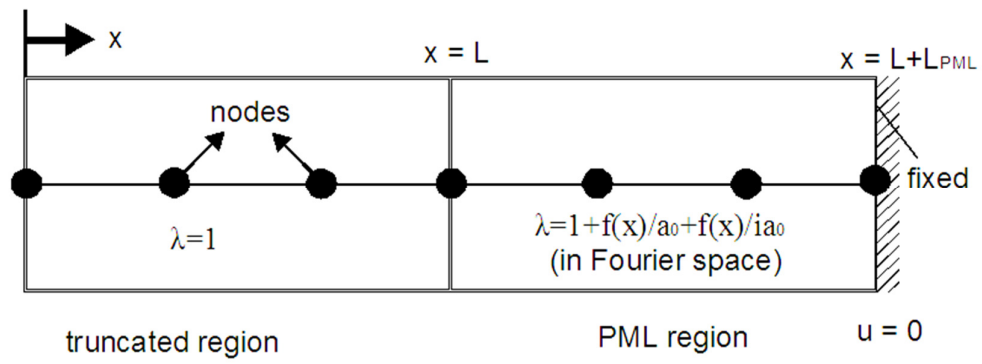
Figure 3.4: PML model of semi-infinite rod.
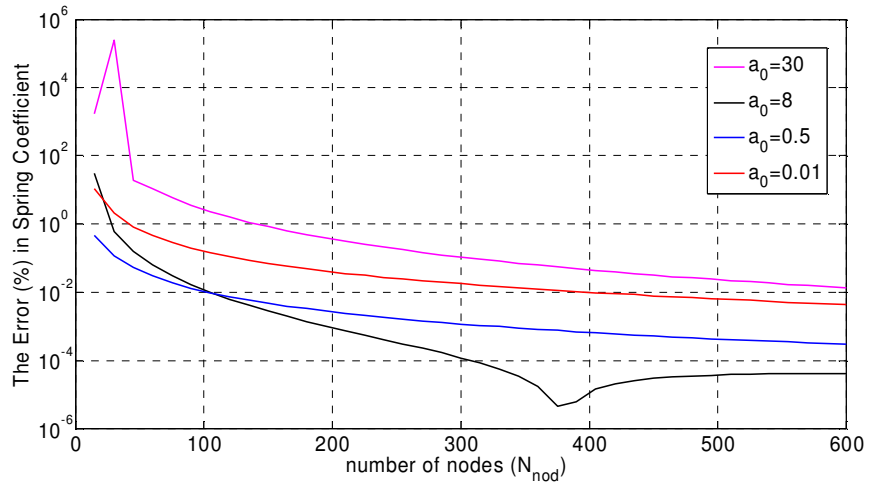
(a)
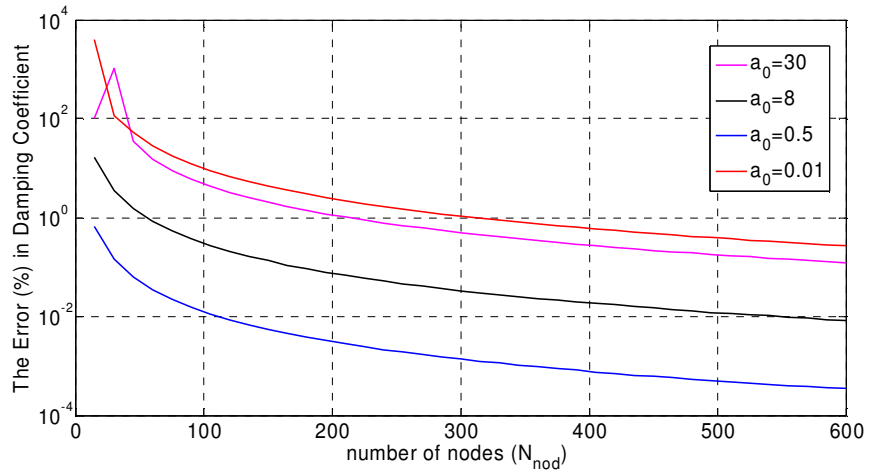
(b)

Figure 3.5: Error versus number of nodes for (a) spring, (b) damping coefficient (obtained from GFDM for various normalized frequencies and for *m=4, f_0=65, L=0.5r_0, L_{PML}=r_0,* and *r_0=1*)

42
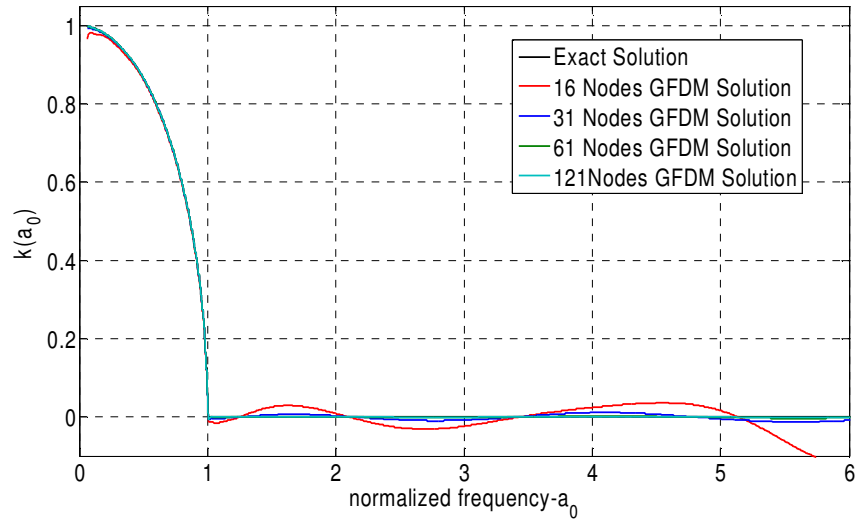
(a)
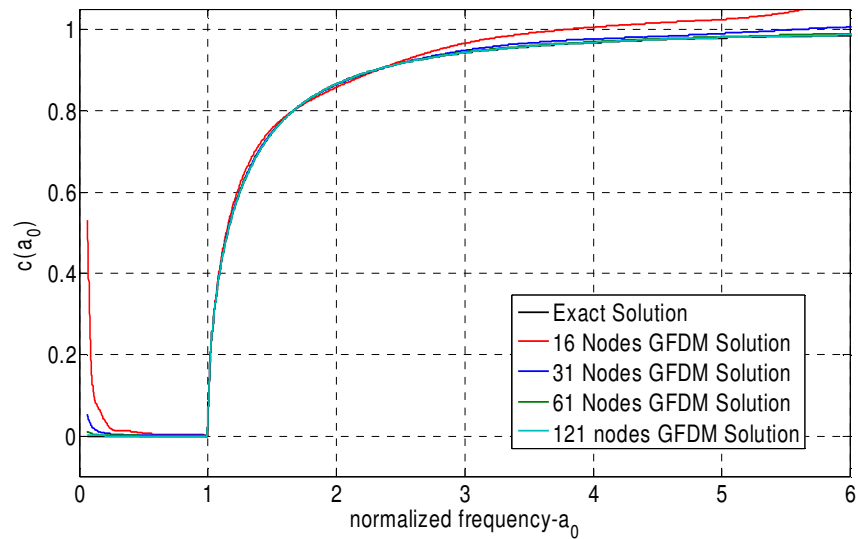
(b)

Figure 3.6: Frequency variation of (a) spring, (b) damping coefficient obtained from GFDM with various number of nodes for *m=4, f₀=65, L=0.5r₀, L_PML=r₀,* and *r₀=1.*

3.1.2.2 EFFECTS OF THE ORDER OF ATTENUATION FUNCTION (*m*) AND ATTENUATION STRENGTH (*f₀*)

Effects of the attenuation strength (*f₀*) and order of attenuation function (*m*) on the accuracy of GFDM results are studied in this section. For this purpose, five different value of *m* (1-5) and 100 different value of *f₀* (1-100) are selected and all possible combination of these two parameters are considered in the GFDM. This leads to 500 different analyses cases for each mesh. In the analyses, the number of nodes (*N_nod*) takes the values 31, 61, 81, 121 and 151, *L_PML* is taken as *r₀* and truncation rod length is chosen as *0.5r₀*. Then, the results of the analysis are used, for a selected *m* value and mesh (*N_nod*), to determine the optimum value of *f₀* which minimizes the combined error *E* defined by

$$E = \sqrt{E_k^{\,2} + E_c^{\,2}} \qquad\qquad (3.36)$$

in an average sense, where the errors *E_k* and *E_c* for the coefficients *k* and *c* were defined in Equation 3.35. This optimization procedure is explained below more clearly. By fixing *m* and *N_nod* and varying *f₀*, one determines, for each *f₀*, *k(a₀)* and *c(a₀)* at the points of the frequency range considered in the analysis, and evaluates the error in Equation 3.36 averaged over frequency points. Then, the *f₀* value which minimizes the average error establishes the optimum value of *f₀* at the considered (fixed) values of m and *N_nod*.

By varying the fixed values of m and *N_nod*, Table 3.1 can be set up for the rod problem under consideration, where each value in *f₀* column gives the optimum value of *f₀* at corresponding values of *m* and *N_nod*. The values of average errors not given here indicate that the best results are obtained when *m* is equal to four which is evident in Figure 3.7. The figure also suggests that the use of linear attenuation function (*m*=1) is not good choice in PML analysis with GFDM.

44

Table 3.1: Optimum value of the attenuation strength f_0 for various orders of attenuation parameter m and for various numbers of nodes (31, 61, 81, 121 and 151), $L_{PML}=r_0$, $L=0.5r_0$, and $r_0=1$.

m	f_0 number of nodes=31	f_0 number of nodes=61	f_0 number of nodes=81	f_0 number of nodes=121	f_0 number of nodes=151
1	4	4	6	5	5
2	12	18	22	26	29
3	27	38	48	56	61
4	34	53	65	72	78
5	41	63	78	86	94
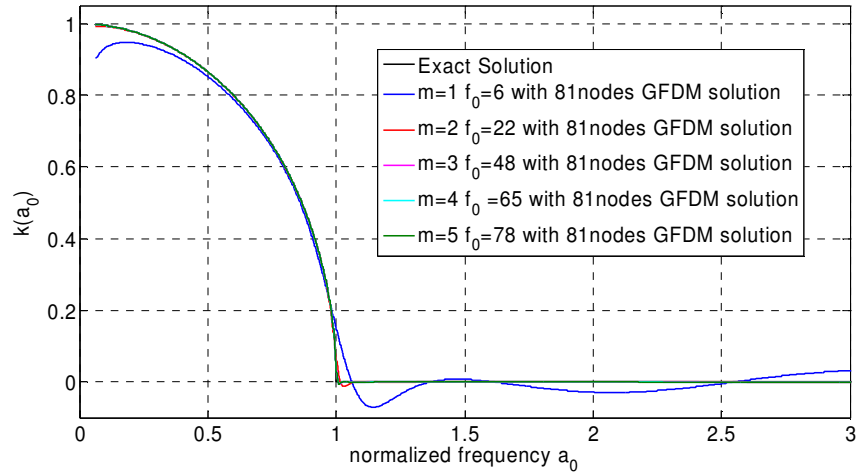
(a)
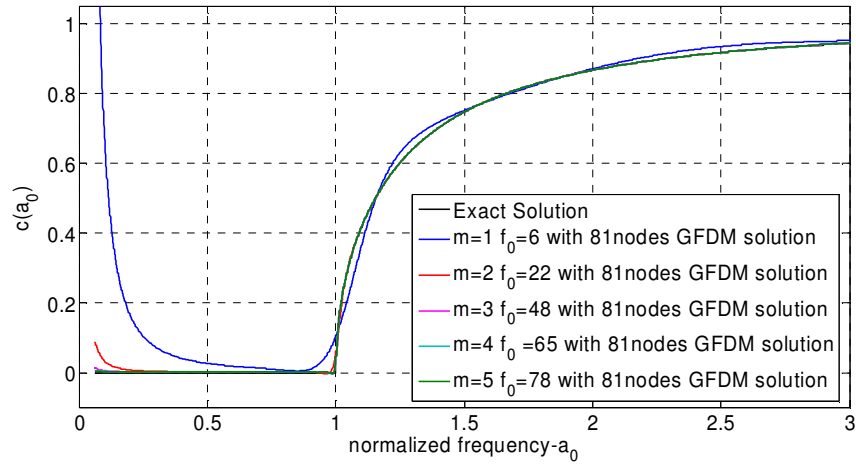
(b)

Figure 3.7: Normalized frequency variation of (a) spring, (b) damping coefficient obtained from GFDM with the optimum value of attenuation strength f_0 corresponding to $N_{nod}=81$ and m=(1,2,3,4,5) with $L_{PML}=r_0$, $L=0.5r_0$, and $r_0=1$.

3.1.2.3 EFFECT OF THICKNESS OF PML (L_{PML})

Here, the effect of thickness of PML on impedance functions (k and c) of the rod on elastic foundation is studied. For that, 16 different values of L_{PML} ranging from *0.25r_0* to *4r_0* are considered. The other parameters are selected to be (*f_0=65, m=4, L=0.5r_0* and *dnodes=0.0125r_0*). As observed from Figure 3.8, the impedance functions are estimated quite accurately when the $L_{PML} \geq r_0$. However, it is to be noted the larger L_{PML} requires increasing the number of nodes to be used in PML region, which obviously increases the computational cost. Figure 3.8 suggests that acceptable results may be obtained with reasonable computational cost *when r_0< L_{PML}<2r_0*, or, in terms of the truncation length L of the rod, when *2L< L_{PML}<4L.*
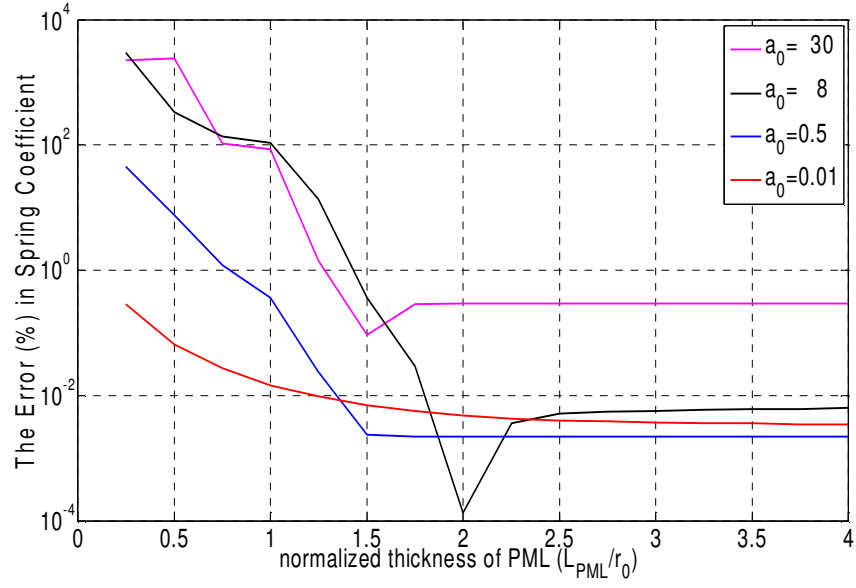
(a)
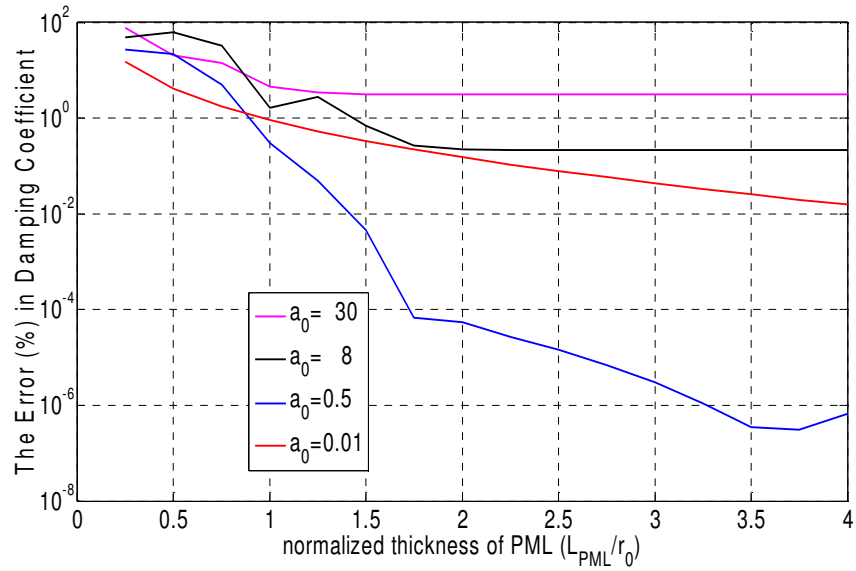
(b)

Figure 3.8: The variation of error with LPML for (a) spring, (b) damping coefficient for various frequencies and *m=4, f_0=65, L=0.5r_0, dnodes=0.0125r_0,* and *r_0=1.*

3.2 TIME DOMAIN PML FORMULATION OF ROD ON ELASTIC FOUNDATION PROBLEM

To carry out the PML analysis of the rod directly in the time domain, its PML equations written in frequency space in Equations 3.32 and 3.33 are to be inverted into time space. For that Equation 3.32 is multiplied by the stretching function λ; then, the inverse Fourier transform is applied to it, which gives (Basu, 2004),

$$\frac{\partial \varepsilon}{\partial x} - \frac{(1+f^e)}{r_0^2}u - \frac{f^p c_l}{r_0^3}\int_0^t u(\xi)d\xi - \frac{(1+f^e)}{c_l^2}\ddot{u} - \frac{f^p}{c_l r_0}\dot{u} = 0 \qquad (3.37)$$

where the stress-strain relationship is

$$\sigma = E\varepsilon \qquad (3.38)$$

and the stretching function is taken as

$$\lambda(s) = 1 + f^e(s) + \frac{f^p(s)}{ia_0} \qquad (3.39)$$

Finally, the strain-displacement relationship in Equation 3.33 is multiplied by $i\omega\lambda(x)$, which gives (Basu, 2004), after inversion

$$(1+f^e)\dot{\varepsilon} + f^p\frac{c_l}{r_0}\varepsilon = \frac{\partial \dot{u}}{\partial x} \qquad (3.40)$$

Equations 3.37and 3.40 constitute the governing PML equations of the rod written in time space. Applying the finite difference formula to the Equation 3.40 for the strain rate, one gets

$$\varepsilon^{n+1} = \left[\frac{1+f^e}{\Delta t} + f^p\frac{c_l}{r_0}\right]^{-1}\left[\frac{\partial \dot{u}^{n+1}}{\partial x} + \frac{1+f^e}{\Delta t}\varepsilon^n\right] \qquad (3.41)$$

where Δt is time increment and superscript n denotes the value of a quantity at the time step "n", that is, at $t=n\Delta t$.

Time integration of u in Equation 3.37 may be calculated as

$$U^{n+1} = \int_0^{t_{n+1}} u(\xi)d\xi \cong \int_0^{t_n} u(\xi)d\xi + u^{n+1}\Delta t \cong U^n + u^{n+1}\Delta t \tag{3.42}$$

where U^n is the total displacement from initial time to n^{th} time step. The displacement is zero at initial time.

Finally, writing Equation 3.37 at $t=(n+1)\Delta t$ and substituting Equations 3.41 and 3.42 into it, the following equation can be obtained:

$$\left(\frac{(1+f^e)}{c_l^2}\right)\ddot{u}^{n+1} + \left(\frac{f^p}{c_l r_0} + \alpha_2 \frac{\partial}{\partial x} - \alpha_1 \frac{\partial^2}{\partial x^2}\right)\dot{u}^{n+1} + \left(\frac{1+f^e}{r_0^2} + \frac{f^p c_l}{r_0^3}\Delta t\right)u^{n+1}$$
$$= \left[(\alpha_4 - \alpha_3)\varepsilon^n + \alpha_5 \frac{\partial \varepsilon^n}{\partial x} - \frac{f^p c_l}{r_0^3}U^n\right] \tag{3.43}$$

where

$$\alpha_0 = \left[\frac{1+f^e}{\Delta t} + f^p \frac{c_l}{r_0}\right] \tag{3.44a}$$

$$\alpha_1 = \frac{1}{\alpha_0} \tag{3.44b}$$

$$\alpha_2 = \frac{\left(\frac{d\alpha_0}{dx}\right)}{\alpha_0^2} \tag{3.44c}$$

$$\alpha_3 = \frac{\left(\frac{1+f^e}{\Delta t}\frac{d\alpha_0}{dx}\right)}{\alpha_0^2} \tag{3.44d}$$

$$\alpha_4 = \frac{\left(\frac{1}{\Delta t}\frac{df^e}{dx}\right)}{\alpha_0} \tag{3.44e}$$

$$\alpha_5 = \frac{\left(\frac{1+f^e}{\Delta t}\right)}{\alpha_0} \tag{3.44f}$$

It is obvious that Equation 3.43 involves both time and space integrations; its time integrations can be performed by the usual methods, such as Newmark's direct integration methods, Runge Kutta's methods, etc.; on the other hand, its space integration can be carried out by FEM or FDM or GFDM. The space integration of Equation 3.43 leads to a matrix equation of the form

$$M\ddot{u}^{n+1} + C\dot{u}^{n+1} + Ku^{n+1} = P^{n+1} \tag{3.45}$$

where the vector u contains the nodal point displacements; *M*, *C* and *K* and P^{n+1} are respectively mass, damping, stiffness matrices, and a load vector which are generated by the coefficients appearing in Equation 3.43as

$$\left(\frac{(1+f^e)}{c_l^2}\right) \Rightarrow M \tag{3.46a}$$

$$\left(\frac{f^p}{c_l r_0} + \alpha_2 \frac{\partial}{\partial x} - \alpha_1 \frac{\partial^2}{\partial x^2}\right) \Rightarrow C \tag{3.46b}$$

$$\left(\frac{1+f^e}{r_0^2} + \frac{f^p c_l}{r_0^3}\Delta t\right) \Rightarrow K \tag{3.46c}$$

$$\left[(\alpha_4 - \alpha_3)\varepsilon^n + \alpha_5 \frac{\partial \varepsilon^n}{\partial x} - \frac{f^p c_l}{r_0^3}U^n\right] \Rightarrow P^n \tag{3.46d}$$

51

3.2.1 NUMERICAL RESULTS FROM TIME DOMAIN ANALYSIS

In this part, the response of the rod on elastic foundation (see Figure 3.2) subjected to two different prescribed displacements $u_0(t)$ is determined by the time domain PML analysis and compared with the exact solution. PML solution of governing equation in Equation 3.43 is obtained by Newmark's method (for details, see Appendix A) together with GFDM with distance type algorithm having cubic spline weighting function. Two different regular meshes with 61 and 81 nodes are used. The truncation length L of the rod is taken as $0.5r_0$ and L_{PML} as $2L$. The order of attenuation function m is chosen four, and its strength as $f_0=53$ for $N_{nod}=61$ and $f_0=65$ for $N_{nod}=81$. PML results for the reaction for R at $x=0$ (that is, at the left end of the semi-infinite rod) are then computed and compared with the exact in Figures 3.9 and 3.10.

The time variation of two types of the imposed displacement $u_0(t)$ at $x=0$, considered in the analyses, are

Type 1 (prescribed displacement employed by Wolf (1988)):

$$u_0(t) = \frac{1}{2}\left[1 - \cos\left(2\pi\frac{t}{t_0}\right)\right] \quad 0 < t < t_0$$
$$u_0(t) = 0 \quad t \geq t_0 \tag{3.47}$$

where t_0 is chosen as 2.

Type 2 (prescribed displacement used by Basu (2004)):

$$u_0(t) = \frac{1}{2}\left[1 - \cos\left(2\pi\frac{t}{T_f}\right)\right] \quad 0 \leq t < T_f/2$$

$$u_0(t) = \cos\left(2\pi\frac{t - T_f/2}{T_f}\right) \quad T_f/2 \leq t < n_c T_f$$

$$u_0(t) = \frac{1}{2}\left[1 - \cos\left(2\pi\frac{t - n_c T_f}{T_f}\right)\right] - 1 \quad n_c T_f \leq t < t_d \tag{3.48}$$

$$u_0(t) = 0 \quad t \geq t_d$$

where n_c denotes the number of cycles, t_d is the duration of time and

$$T_f = \frac{2\pi}{\omega_f} \tag{3.49}$$

is dominant forcing period, with ω_f being the dominant forcing frequency.

Time histories of applied displacement $u_0(t)$ of types 1 and 2 at the left end of the rod together with the corresponding reaction forces there are displayed in Figures 3.9 and 3.10. The excellent match of the numerical results with the exact solution indicates how well the PML functions absorb the incoming waves; it also shows the effectiveness of the use GFDM in PML analysis for the space wise integration of the governing equations.
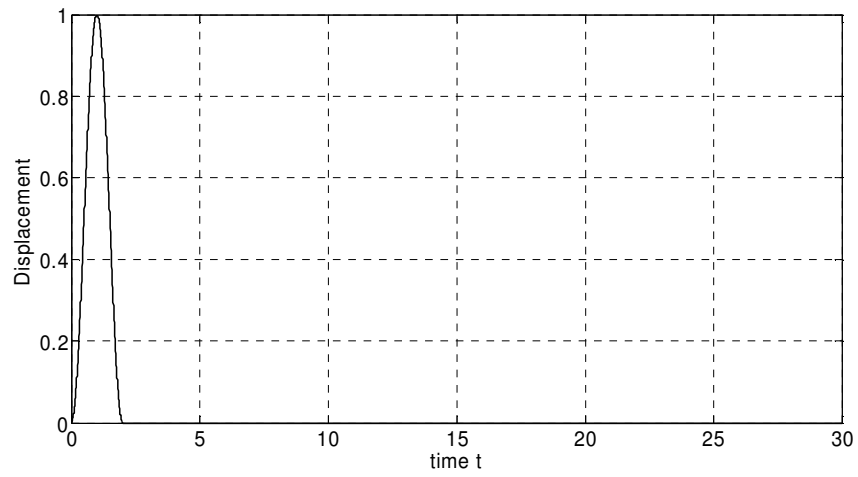
(a)
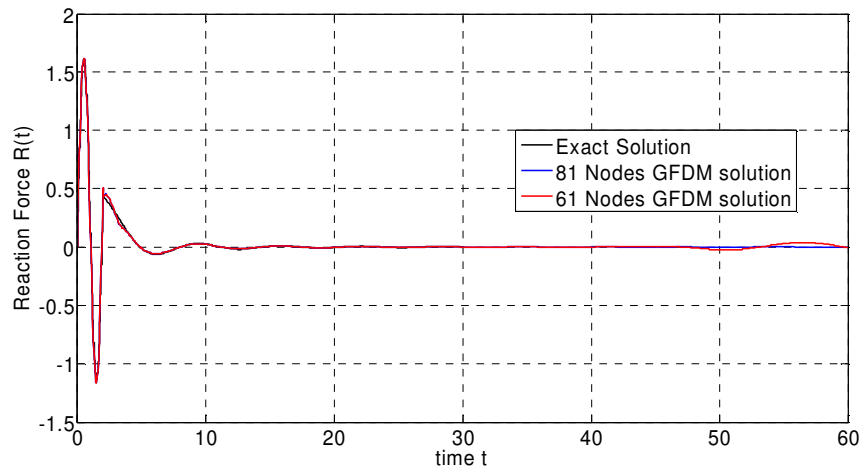
(b)

Figure 3.9: (a) Prescribed displacement (type 1), (b) the corresponding response of the rod on elastic foundation ($m=4$, $f_0 =65$, $L=0.5r_0$, and $L_{PML}= r_0$ for $N_{nod} =81$), ($m=4$, $f_0=53$, $L=0.5r_0$, $L_{PML}= r_0$, and $r_0=1$ for $N_{nod}=61$).
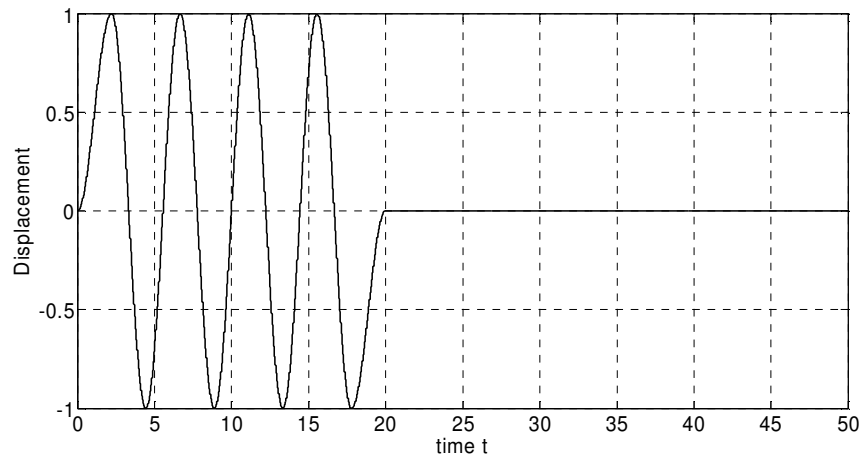
(a)
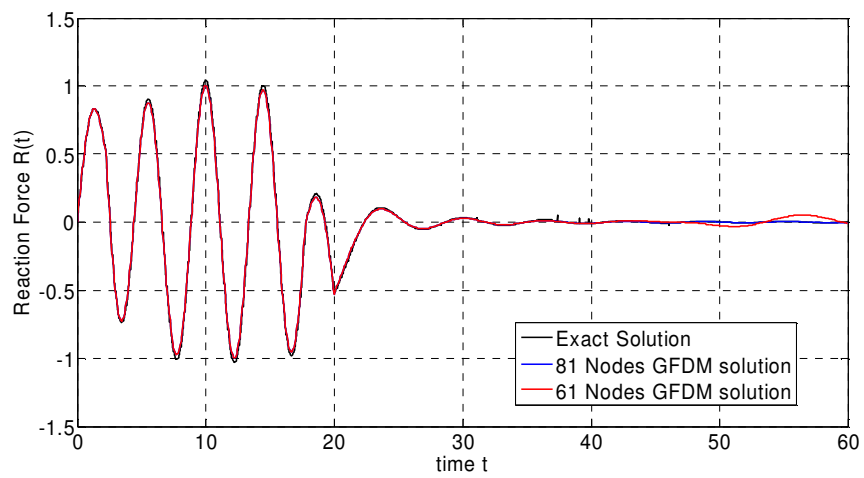
(b)

Figure 3.10: (a) Prescribed displacement (type 2) ($nc=4$, $td=20$, $\omega_f=1.5$), (b) the corresponding response of the rod on elastic foundation, ($m=4$, $f_0=65$, $L=0.5r_0$, and $L_{PML}=r_0$ for $N_{nod}=81$), ($m=4$, $f_0=53$, $L=0.5r_0$, $L_{PML}=r_0$, and $r_0=1$ for $N_{nod}=61$).

CHAPTER 4

DYNAMIC COMPLIANCE FUNCTIONS OF RIGID STRIP FOUNDATION

4.1 INTRODUCTION

During the earthquakes, the waves arising from the seismic excitation propagate through the soil medium from the fault rupture to the structure of interest. Naturally, a dynamic interaction occurs between the foundation of the structure and its surrounding soil medium. This interaction is called "soil-foundation-superstructure interaction" or "soil-structure interaction (SSI)" (Wong, 1975).

The SSI problems are generally modeled using direct (complete) method or substructure method. The direct method models the soil medium and structure together. This method has significant computational cost and requires large computer storage space. On the other hand, in substructure method, the soil medium and structure are modeled separately. First, the soil medium is modeled, mostly as a half space (HS) or layered medium, and analyzed generally in frequency space, and the scattering and impedance properties at the soil structure interface are determined. In the second step, the analysis of the structure is performed by including the influence of soil on its behavior through the use of impedance and scattering relations (Lysmer, 1978).

The impedance relation relates the forces (or moments) to displacements (or rotations) at structure-soil interface and can be written as,

$$P_i(\omega) = K_{ij}(\omega)u_j(\omega) \begin{pmatrix} \textit{summation over the} \\ \textit{repeated index } j \end{pmatrix}$$ (4.1)

where P is interaction force (or moment) and u is displacement (or rotation) and K is frequency (ω) dependent complex stiffness (impedance) coefficient, which depends on the shape of foundation, material properties of soil medium and amount of embedment (Lysmer, 1978).

The real part of complex impedance coefficient denotes the stiffness and inertia of the soil. On the other hand, the imaginary part represents the radiation and material damping of the soil (Gazetas, 1983). Physically, the impedance function may be described by a spring and dashpot representing its real and imaginary components, respectively, that is

$$K(\omega) = k + i\omega c$$ (4.2)

where k and c are stiffness and damping coefficients, respectively.

The dynamic compliance is the ratio of the response of foundation (in the terms of displacements or rotations) and the exciting force (Liang, 1974). The compliance matrix is the inverse of the impedance matrix and satisfies the relation

$$u_i(\omega) = F_{ij}(\omega)P_j(\omega)$$ (4.3)

where F is complex compliance coefficient. Equation 4.3 takes the form, for a rigid strip foundation in Cartesian coordinates,

$$\begin{Bmatrix} u_V \\ u_H \\ bu_R \end{Bmatrix} = \begin{bmatrix} F_{VV} & 0 & 0 \\ 0 & F_{HH} & F_{HR} \\ 0 & F_{RH} & F_{RR} \end{bmatrix} \begin{Bmatrix} P_V \\ P_H \\ P_R/b \end{Bmatrix}$$ (4.4)

where P_V, P_H and P_R are (vertical, horizontal) forces and moment; u_V, u_H and u_R denote (vertical, horizontal) displacements and rotation of the strip foundation; and b is half-width of the foundation (see Figure 4.1). Equation 4.4 shows that the horizontal (swaying) u_H and rotational motion u_R of strip foundation are coupled while its vertical motion u_V is uncoupled (Liang, 1974).
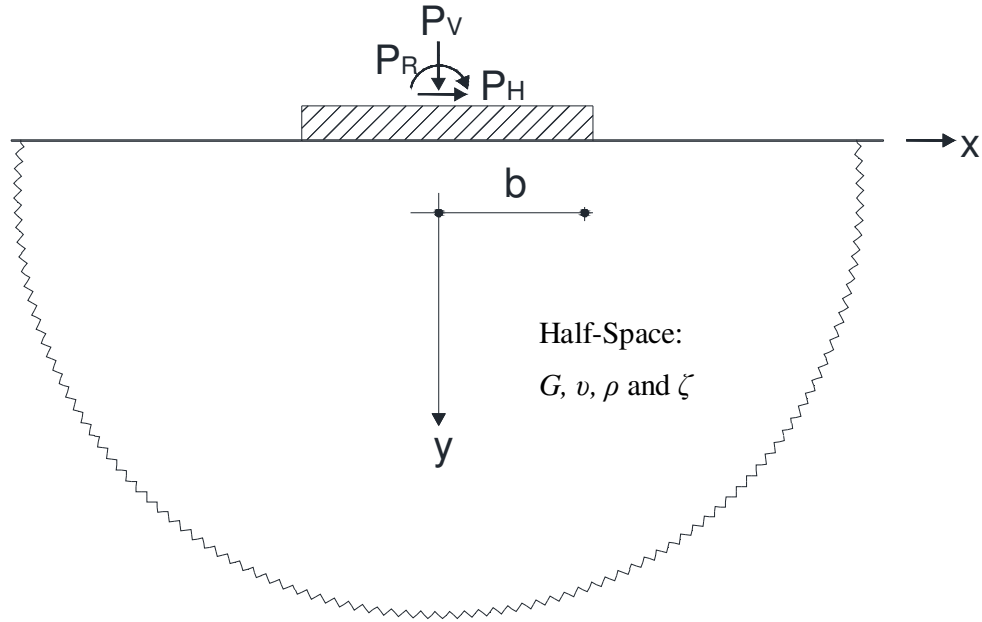
Figure 4.1: Surface rigid strip foundation on HS (G, υ, ρ and ζ represent respectively shear modulus, Poisson's ratio, mass density and damping ratio, respectively)

In this chapter of the thesis, the dynamic compliance functions of a rigid strip foundation are evaluated using GFD method together with PML modeling, and to assess the use of GFD method in PML analysis, the results are then compared with those obtained by other methods. Both surface and embedded rigid strip foundation are considered. In the case of surface foundation, various configurations of the soil foundation are investigated: HS, layer overlying bedrock

and layer on HS. The embedded foundation is considered only when the supporting soil medium is HS. Direct time domain analysis is performed only for a rigid strip foundation on HS.

The soil medium is represented by a homogenous, isotropic and elastic or visco-elastic material. In simulating visco-elastic behavior of soil, the complex elastic modulus $\tilde{E}$ and shear modulus $\tilde{G}$ are expressed as, in frequency space,

$$\tilde{E} = E(1+2i\zeta)$$
$$\tilde{G} = G(1+2i\zeta)$$

(4.5)

where ζ is damping ratio. E and $G = \dfrac{E}{2(1+\upsilon)}$ are respectively elastic and shear moduli at zero frequency, that is, at equilibrium state.

4.2 PML EQUATIONS OF ELASTODYNAMICS FOR PLANE STRAIN CASE (IN FOURIER SPACE)

These equations are needed for determining the compliance or impedance functions for strip foundations by PML method and can be obtained through the steps:

1. Write the equations of elastodynamics for plane strain case and express them in Fourier space.

2. Apply stretching to the coordinates of the equations written in step 1, which establishes the equations (for elastic case) in PML region.

3. If desired, viscoelasticity can be introduced by using the correspondence principle, that is, E and G in the governing equations in the Fourier space are replaced with $\tilde{E}$ and $\tilde{G}$ defined Equation 4.5.

59

Below, first the elastic plane strain equations in Cartesian coordinates x and y will be presented.

The stress equations of motion in the absence of body forces become

$$\frac{\partial \sigma_{xx}}{\partial x} + \frac{\partial \tau_{xy}}{\partial y} = \rho \frac{\partial^2 u}{\partial t^2}$$

$$\frac{\partial \tau_{yx}}{\partial x} + \frac{\partial \sigma_{yy}}{\partial y} = \rho \frac{\partial^2 v}{\partial t^2}$$

(4.6)

where "*t*" stands for time.

The elastic strain- stress equation for 2D case can be expressed as

$$\sigma_{ij} = c_{ijmn}\varepsilon_{mn} \quad i,j,m,n = 1-2 \left(\begin{array}{l} summation\ over\ the \\ repated\ indices\ m\ and\ n \end{array} \right)$$

(4.7)

where c is fourth-order elastic or stiffness tensor and ε is strain tensor. For the plane strain case under consideration, Equation 4.7 becomes, for isotropic material and in matrix form,

$$\sigma = D\varepsilon$$

(4.8)

or, in expanded form,

$$\left\{ \begin{array}{c} \sigma_{xx} \\ \sigma_{yy} \\ \tau_{xy} \end{array} \right\} = \frac{E}{1+v} \left[\begin{array}{ccc} \frac{(1-v)}{(1-2v)} & \frac{v}{(1-2v)} & 0 \\ \frac{v}{(1-2v)} & \frac{(1-v)}{(1-2v)} & 0 \\ 0 & 0 & 1 \end{array} \right] \left\{ \begin{array}{c} \varepsilon_{xx} \\ \varepsilon_{yy} \\ \varepsilon_{xy} \end{array} \right\}$$

(4.9)

where D is plane strain stiffness matrix. Strains are related to the displacement components u and v in x and y direction by

$$\varepsilon_{xx} = \frac{\partial u}{\partial x} \tag{4.10a}$$

$$\varepsilon_{yy} = \frac{\partial v}{\partial y} \tag{4.10b}$$

$$\varepsilon_{xy} = \frac{1}{2}\left[\frac{\partial u}{\partial y} + \frac{\partial v}{\partial x}\right] \tag{4.10c}$$

The Fourier transforms of the stress equations of motion, stress-strain and strain-displacement relations give

stress equations of motion:

$$\frac{\partial \bar{\sigma}_{xx}}{\partial x} + \frac{\partial \bar{\tau}_{xy}}{\partial y} + \rho\omega^2\bar{u} = 0$$

$$\frac{\partial \bar{\tau}_{yx}}{\partial x} + \frac{\partial \bar{\sigma}_{yy}}{\partial y} + \rho\omega^2\bar{v} = 0 \tag{4.11}$$

stress-strain relation:

$$\bar{\sigma} = D\bar{\varepsilon} \tag{4.12}$$

strain displacement relations:

$$\bar{\varepsilon}_{xx} = \frac{\partial \bar{u}}{\partial x}$$

$$\bar{\varepsilon}_{yy} = \frac{\partial \bar{v}}{\partial y} \tag{4.13}$$

$$\bar{\varepsilon}_{xy} = \frac{1}{2}\left[\frac{\partial \bar{u}}{\partial y} + \frac{\partial \bar{v}}{\partial x}\right]$$

where, as mentioned previously, the over-bar denotes the Fourier transform.

In the PML application, its assumed that the truncation boundary is either parallel to x axis or parallel to y axis; x and y coordinates of a point in PML region are replaced by the stretching coordinates $\tilde{x}$ and $\tilde{y}$, defined by

$$\tilde{x} = \int_0^x \lambda_x(s)\,ds \,, \quad \tilde{y} = \int_0^y \lambda_y(s)\,ds \tag{4.14}$$

where s is normal axis to truncation boundary and

for PML normal to x axis:

$$\lambda_x(x) = 1 + \frac{f^e(x)}{a_0} + \frac{f^p(x)}{ia_0} \,, \quad \lambda_y = 1 \tag{4.15a}$$

for PML normal to y axis:

$$\lambda_x = 1 \,, \quad \lambda_y(y) = 1 + \frac{f^e(y)}{a_0} + \frac{f^p(y)}{ia_0} \tag{4.15b}$$

Here, λ_x and λ_y are stretching functions, $a_0 = \dfrac{\omega b}{v_s}$ is a nondimensional frequency; b denotes a characteristic length which will be taken in this study as half-length of foundation width, v_s is shear (S) wave velocity.

f^e and f^p in Equation 4.15 denote the attenuation functions for evanescent and propagating waves, respectively, which satisfy:

1. They are zero in truncated region and on truncation boundary

2. Positive real valued and increasing function of normal axis in PML region.

The first condition implies that $\lambda_x = \lambda_y = 1$ in truncated region, which in turn shows that, in view of Equation 4.15, the stretching functions λ_x and λ_y are continuous

across the truncation boundary. Equation 4.15 indicates further that the stretching functions are nonzero and complex valued in PML region.

In the present study, the attenuation functions for propagating and evanescent waves will be chosen the same, that is, $f^e = f^p = f$ with f being given in polynomial form as

for PML normal to x axis:

$$f(x) = f_0 \left(\frac{|x - x_0|}{L_{PML}} \right)^m \qquad (4.16a)$$

for PML normal to y axis:

$$f(y) = f_0 \left(\frac{|y - y_0|}{L_{PML}} \right)^m \qquad (4.16b)$$

where m is the order of attenuation function, L_{PML} is the thickness of PML, f_0 is a constant denoting the attenuation strength, and x_0 and y_0 are the coordinates of the points on the truncation boundary (see Figure 4.2).

In the view of Equation 4.14, it is obvious that the derivatives with respect to stretching coordinates of a point in the analysis region are related to those with respect to its actual coordinates by

$$\frac{\partial}{\partial \tilde{x}} = \frac{1}{\lambda_x} \frac{\partial}{\partial x}$$
$$\frac{\partial}{\partial \tilde{y}} = \frac{1}{\lambda_y} \frac{\partial}{\partial y} \qquad (4.17)$$

To obtain PML equations of elastodynamics for plane strain case (in Fourier space), first, the derivatives $\dfrac{\partial}{\partial x}$ and $\dfrac{\partial}{\partial y}$ appearing in Equations 4.11-4.13 should

be replaced by $\dfrac{\partial}{\partial \tilde{x}}$ and $\dfrac{\partial}{\partial \tilde{y}}$, then, the expressions in Equation 4.17 should be used for $\dfrac{\partial}{\partial \tilde{x}}$ and $\dfrac{\partial}{\partial \tilde{y}}$. Thus, one can determine the PML equation as

stress equations of motion:

$$\frac{1}{\lambda_x}\frac{\partial \bar{\sigma}_{xx}}{\partial x} + \frac{1}{\lambda_y}\frac{\partial \bar{\tau}_{xy}}{\partial y} + \rho\omega^2\bar{u} = 0$$
$$\frac{1}{\lambda_x}\frac{\partial \bar{\tau}_{yx}}{\partial x} + \frac{1}{\lambda_y}\frac{\partial \bar{\sigma}_{yy}}{\partial y} + \rho\omega^2\bar{v} = 0$$

(4.18)

stress-strain relation:

$$\bar{\sigma} = D\bar{\varepsilon}$$

(4.19)

strain displacement relations:

$$\bar{\varepsilon}_{xx} = \frac{1}{\lambda_x}\frac{\partial \bar{u}}{\partial x}$$
$$\bar{\varepsilon}_{yy} = \frac{1}{\lambda_y}\frac{\partial \bar{v}}{\partial y}$$
$$\bar{\varepsilon}_{xy} = \frac{1}{2}\left[\frac{1}{\lambda_y}\frac{\partial \bar{u}}{\partial y} + \frac{1}{\lambda_x}\frac{\partial \bar{v}}{\partial x}\right]$$

(4.20)

The displacement equations of motion are determined by substituting first, the strain-displacement equations into the stress-strain relations and then, the resulting equations into the stress equations of motion. Multiplying the equations obtained in the last step by $\lambda_x\lambda_y$, one gets the final form of the displacement equations of motion as

$$(\alpha_1 + \alpha_2)\bar{u} + \alpha_3\bar{v} = 0$$
$$\alpha_3\bar{u} + (\alpha_4 + \alpha_5)\bar{v} = 0$$

(4.21)

where

$$\alpha_1 = D_{11}\left[\rho\omega^2\lambda_x\lambda_y - \frac{\lambda_y\dfrac{d\lambda_x}{dx}}{\lambda_x^2}\frac{\partial}{\partial x} + \frac{\lambda_y}{\lambda_x}\frac{\partial^2}{\partial x^2}\right]$$

(4.22a)

$$\alpha_2 = \frac{D_{33}}{2}\left[-\frac{\lambda_x\dfrac{d\lambda_y}{dy}}{\lambda_y^2}\frac{\partial}{\partial y} + \frac{\lambda_x}{\lambda_y}\frac{\partial^2}{\partial y^2}\right]$$

(4.22b)

$$\alpha_3 = \left[\left(D_{12} + \frac{D_{33}}{2}\right)\frac{\partial}{\partial x}\frac{\partial}{\partial y}\right]$$

(4.22c)

$$\alpha_4 = \frac{D_{33}}{2}\left[-\frac{\lambda_y\dfrac{d\lambda_x}{dx}}{\lambda_y^2}\frac{\partial}{\partial x} + \frac{\lambda_y}{\lambda_x}\frac{\partial^2}{\partial x^2}\right]$$

(4.22d)

$$\alpha_5 = D_{22}\left[\rho\omega^2\lambda_x\lambda_y - \frac{\lambda_x\dfrac{d\lambda_y}{dy}}{\lambda_y^2}\frac{\partial}{\partial y} + \frac{\lambda_x}{\lambda_y}\frac{\partial^2}{\partial y^2}\right]$$

(4.22e)
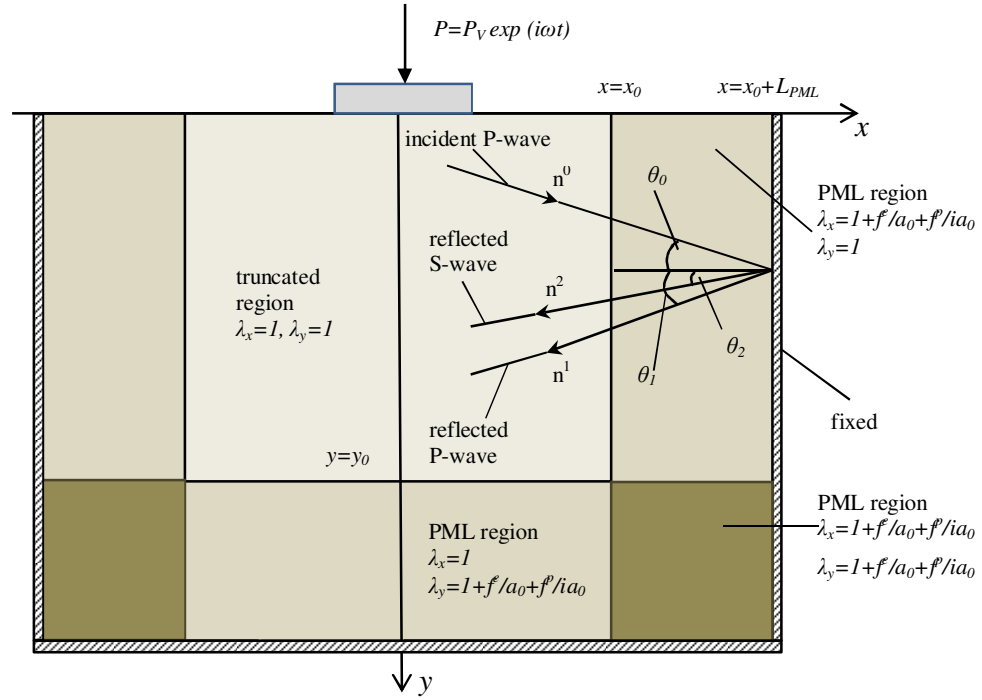
Figure 4.2: Reflections of incident P wave at fixed boundary of PML region.

4.2.1 WAVE REFLECTION COEFFICIENTS FOR PML

Here, the analysis will be performed by referring to Figure 4.2, showing the reflection of an incident P wave of the inclination angle θ_0 from the fixed boundary of PML. The inclination angles of reflected P and S waves are designated respectively by θ_1 and θ_2 in the figure. It is known that θ_1 and θ_2 are related to θ_0 by

$$\theta_1 = \theta_0 \, , \ \ \sin\theta_2 = \frac{v_s}{v_p}\sin\theta_0 \tag{4.23}$$

where v_p and v_s are P and S wave velocities defined by (see, e.g., Achenbach, 1973)

$$v_p = \sqrt{\frac{(1-\upsilon)E}{(1+\upsilon)(1-2\upsilon)\rho}} \ , \ v_s = \sqrt{\frac{E}{2(1+\upsilon)\rho}} \tag{4.24}$$

For the displacement fields induced by incident and reflected waves, one has (Achenbach, 1973):

for incident P wave:

$$u_j^0 = A_p^{inc} n_j^0 \exp\left(i\left(\omega t - k_p\left(n_x^0 \tilde{x} + n_y^0 \tilde{y}\right)\right)\right) \tag{4.25a}$$

for reflected P wave:

$$u_j^1 = A_p^{ref} n_j^1 \exp\left(i\left(\omega t - k_p\left(n_x^1 \tilde{x} + n_y^1 \tilde{y}\right)\right)\right) \tag{4.25b}$$

for reflected S wave:

$$u_j^2 = A_s^{ref} d_j^2 \exp\left(i\left(\omega t - k_s\left(n_x^2 \tilde{x} + n_y^2 \tilde{y}\right)\right)\right) \tag{4.25c}$$

where index "j" stands for x and y, u_x and u_y correspond respectively to the displacements u and v; n^0, n^1 and n^2 are respectively unit vectors in the directions of incident P wave, reflected P and S waves, for which one can write

$$\begin{aligned} n^0 &= (n_x^0,\ n_y^0) = (\cos\theta_0,\ \sin\theta_0) \\ n^1 &= (n_x^1,\ n_y^1) = (-\cos\theta_1,\ \sin\theta_1) \\ n^2 &= (n_x^2,\ n_y^2) = (-\cos\theta_2,\ \sin\theta_2) \end{aligned} \tag{4.26}$$

d^2 in Equation 4.25c is orthogonal to n^2 and given by

$$d^2 = (d_x^2,\ d_y^2) = (\sin\theta_2,\ \cos\theta_2) \tag{4.27}$$

k_p and k_s in Equation 4.25 are wave numbers for P and S waves, respectively, defined by

$$k_p = \frac{\omega}{v_p}, \quad k_s = \frac{\omega}{v_s} \tag{4.28}$$

and $A_p{}^{inc}$, $A_p{}^{ref}$ and $A_s{}^{ref}$ are the amplitudes of incident P wave, reflected P and S waves; $\tilde{x}$ and $\tilde{y}$ are stretching coordinates for the PML considered in Figure 4.2 (normal to x axis) and are given by, in view of Equation 4.14, 4.15a and 4.16a,

$$\tilde{x} = x + \frac{F^e(x)}{a_0} + \frac{F^p(x)}{ia_0}, \quad \tilde{y} = y \tag{4.29}$$

where

$$F^e(x) = \int_{x_0}^{x} f^e(s)\,ds, \quad F^p(x) = \int_{x_0}^{x} f^p(s)\,ds \tag{4.30}$$

and

$$a_0 = \frac{\omega b}{v_s} = k_s b \tag{4.31}$$

At the right end of the PML normal to x axis in Figure 4.2, the total displacement induced by incident P wave, reflected P and S waves should vanish, that is, one should have

$$u_j = u_j^0 + u_j^1 + u_j^2 \quad at \ x = x_0 + L_{PML} \tag{4.32}$$

From this condition, one obtains, after some manipulations and in view of Equations 4.23-4.32,

$$\left|R_{pp}\right| = \left|\frac{A_p^{ref}}{A_p^{inc}}\right| = \left|\frac{\cos(\theta_0 + \theta_2)}{\cos(\theta_0 - \theta_2)}\right| \exp\left(-2\frac{v_s}{v_p}\frac{F^p(L_{PML})}{b}\cos\theta_0\right)$$

$$\left|R_{ps}\right| = \left|\frac{A_s^{ref}}{A_p^{inc}}\right| = \left|\frac{\sin(2\theta_0)}{\cos(\theta_0 - \theta_2)}\right| \exp\left(-\frac{F^p(L_{PML})}{b}\left(\frac{v_s}{v_p}\cos\theta_0 + \cos\theta_2\right)\right) \tag{4.33}$$

where R_{pp} and R_{ps} are reflection coefficients for reflected P and S waves caused by the incident P wave.

The reflection coefficients R_{ss} and R_{sp} (for reflected S and P waves) of the incident S wave can be obtained by using a similar procedure. They are

$$\left|R_{sp}\right| = \left|\frac{A_p^{ref}}{A_s^{inc}}\right| = \left|\frac{\sin(2\theta_0)}{\cos(\theta_0 - \theta_1)}\right| \exp\left(-\frac{F^p(L_{PML})}{b}\left(\frac{v_p}{v_s}\cos\theta_1 + \cos\theta_0\right)\right)$$

$$\left|R_{ss}\right| = \left|\frac{A_s^{ref}}{A_s^{inc}}\right| = \left|\frac{\cos(\theta_0 + \theta_1)}{\cos(\theta_0 - \theta_1)}\right| \exp\left(-2\frac{F^p(L_{PML})}{b}\cos\theta_0\right) \tag{4.34}$$

where θ_0 is the inclination angle of incident S wave and θ_1 is that of the reflected P wave satisfying

$$\sin\theta_1 = \frac{v_p}{v_s}\sin\theta_0 \tag{4.35}$$

It is to be noted that the inclination angle θ_2 of the reflected S wave is equal to that of the incident S wave.

The reflection coefficients have significant effects on the strength f_0 of attenuation function. The following expression for f_0 (for $\theta_0=0$) may be determined from the Equation 4.33.

$$f_0 = \frac{(m+1)v_p b}{2L_{PML}v_s}\log(\frac{1}{\left|R_{pp}\right|}) \tag{4.36}$$

69

Equations 4.33 and 4.34 show that the attenuation function f^p is responsible for PML to absorb propagating waves. The performance of PML increases as the inclination angle of incident wave decreases, that is, as the entrance angle of the wave into PML gets closer to the normal of PML.

It can be shown that the attenuation function f^e causes the absorption of the evanescent waves entering PML, as opposed to the role played by f^p for propagating waves.

4.3 NUMERICAL RESULTS FOR SURFACE RIGID STRIP FOUNDATIONS

In this section, the displacement equations of motion defined in Equation 4.21 are integrated using GFDM together with PML modeling for a rigid strip foundation. The results are presented in terms of vertical, horizontal and rocking compliances obtained for three different configurations of soil medium: HS (Figure 4.1), soil layer on a rigid bedrock (Figure 4.3), and soil layer overlying a HS (Figure 4.4), The PML models for these three cases are shown in Figures 4.5 to 4.7. In the modeling of the computational domain, its symmetry is considered, that is, half of the domain is modeled. Four node quadrilateral elements are used in the formulation by FEM and distance type algorithm is employed with cubic spline weighting function in GFDM. In the FEM and GFDM analyses, the same node distribution is used to compare the predictions of these two methods properly. The mass of the rigid strip foundation is disregarded (it is generally taken into account when superstructure is analyzed).

In the case of a rigid strip foundation over HS, the depth (h) and length (L) of the truncated domain is chosen as *0.5b* and *1.5b*, respectively, where *b*, as mentioned previously, is the half width of the foundation. Thickness of the PML is taken as *b* in both orthogonal directions. Attenuation function parameters are assumed to be $m=1$, $f_0^e=10$ and $f_0^p=10$ for FEM and $m=4$, $f_0^e=25$ and $f_0^p=25$ for GFDM

For the rigid strip foundation on soil layer overlying bedrock, the depth of the soil layer is assumed to be *2b*, the thickness of PML is chosen as b. Attenuation function parameters are taken as $m=1, f_0^e=20$ and $f_0^p=20$ for FEM and the same as those of HS case for GFDM.

For the rigid strip foundation on soil layer overlying the HS, the depth h_1 of the layer is assumed to be *2b* and the depth of the horizontal truncation line in HS from layer–HS interface is taken as $h_2=0.5b$ (see Figure 4.7). In both orthogonal directions, the thickness of PML is chosen as *b*. In the calculation of the nondimensional frequency (a_0) for this case, the S wave velocity of the layer is used. Attenuation function parameters are assumed to be the same of those of HS case.

In three situations described above, a damping ratio of 5% is used for viscoelastic case.
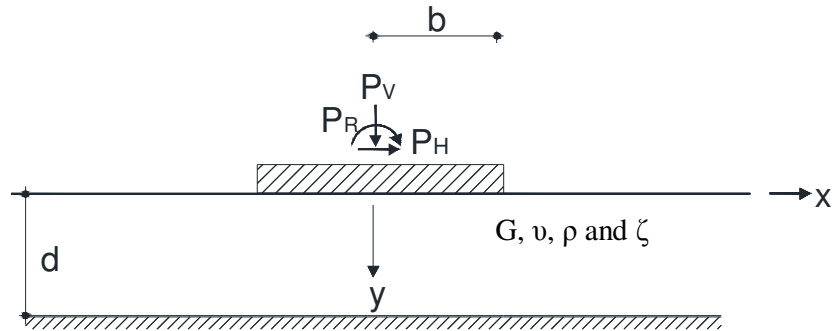

Figure 4.3: Rigid strip foundation overlying rigid bedrock (*G, υ, ρ* and *ζ* represent shear modulus, Poisson's ratio, mass density and damping ratio, respectively).
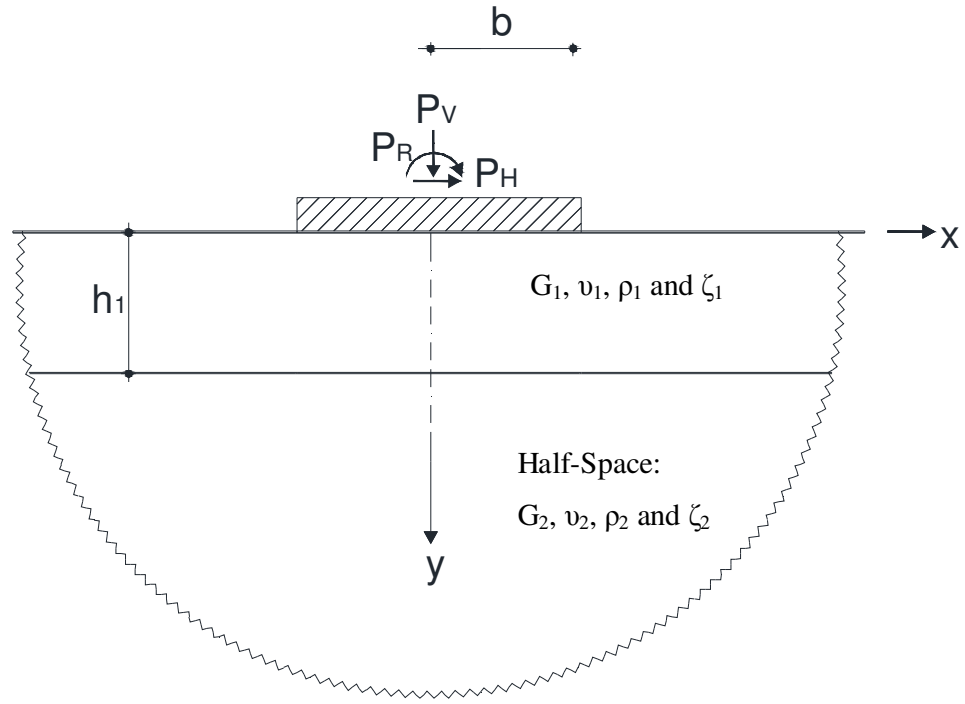
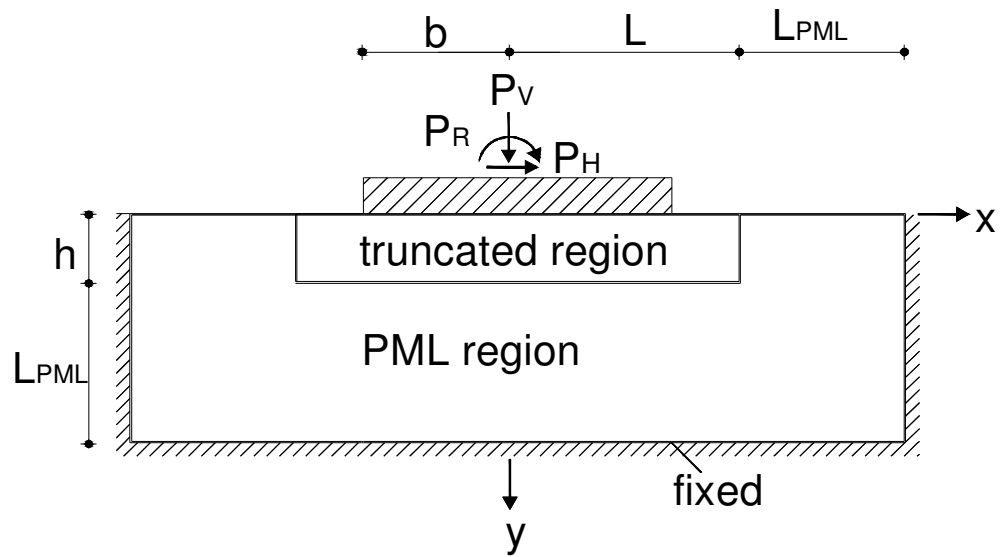**Figure 4.4:** Rigid strip foundation over soil layer overlying HS.

Figure 4.5: PML model for rigid strip foundation overlying HS.
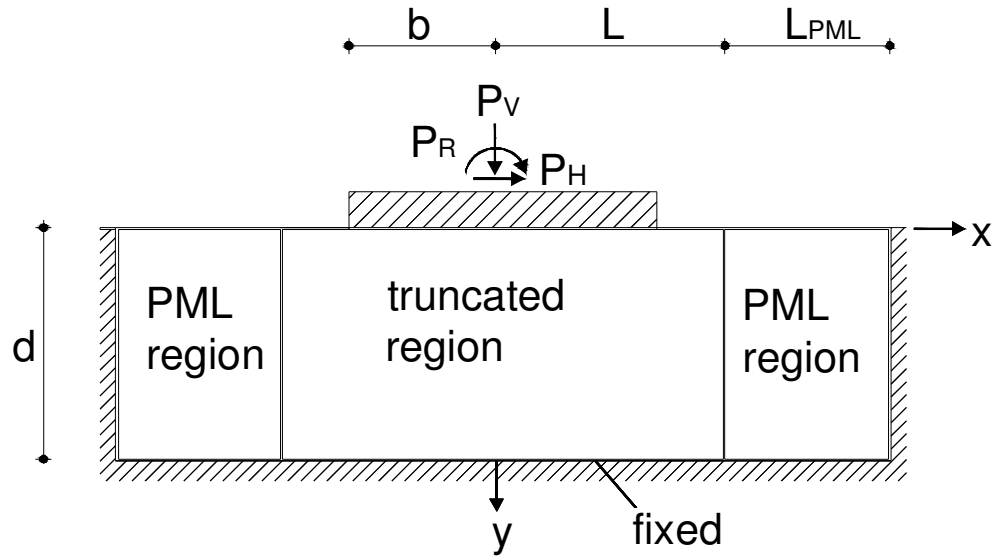
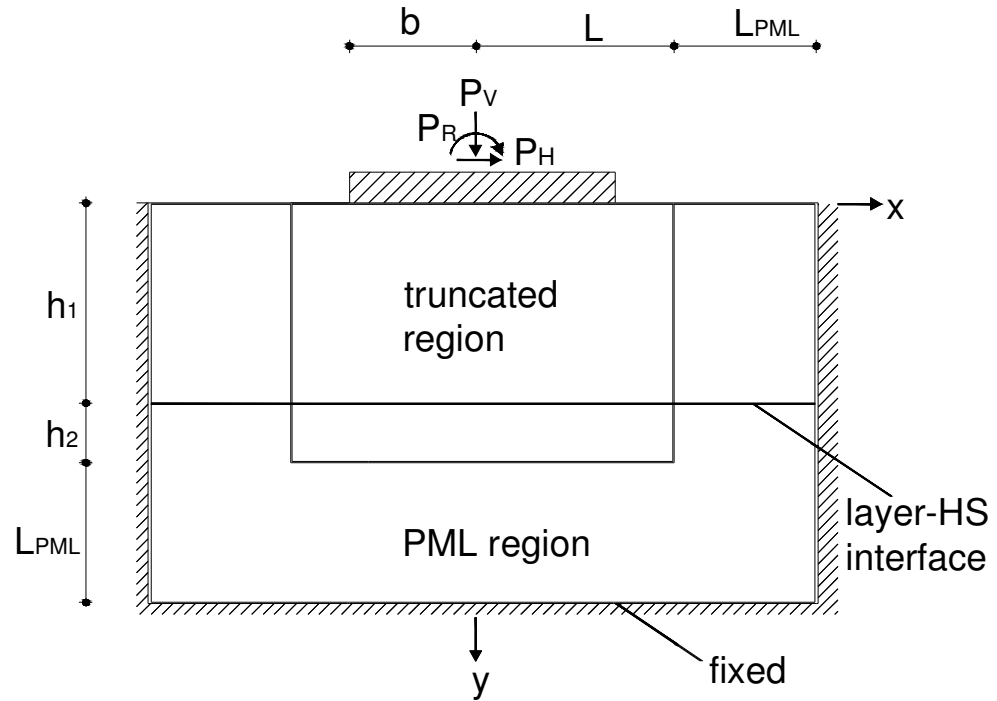**Figure 4.6:** PML model for rigid strip foundation on a layer overlying rigid bedrock.

Figure 4.7: PML model for rigid strip foundation on a layer overlying HS.

4.3.1 ASSESMENT OF THE RESULTS OF GFDM FOR HS CASE

In this section, the dynamic compliances for a rigid strip foundations on HS are calculated by GFDM and they are compared with those of FEM, BEM, and also, when possible, with those obtained by Hryniewicz (1980) using a semi analytical method. The results obtained from these methods are displayed in Figures. 4.8-4.13. In these figures, the compliances are presented as a function of the nondimensional frequencies a_0 which change in the range from 0-6. In the analyses of all considered methods, the soil properties are chosen as $G=1, \upsilon=0.25, \rho=1, \zeta=5\%$, in some suitable units.

Figures 4.8-4.13 indicate that the compliances calculated using GFDM with PML are generally in good agreement with those obtained from the other methods, although some small differences are observed for very small frequencies.
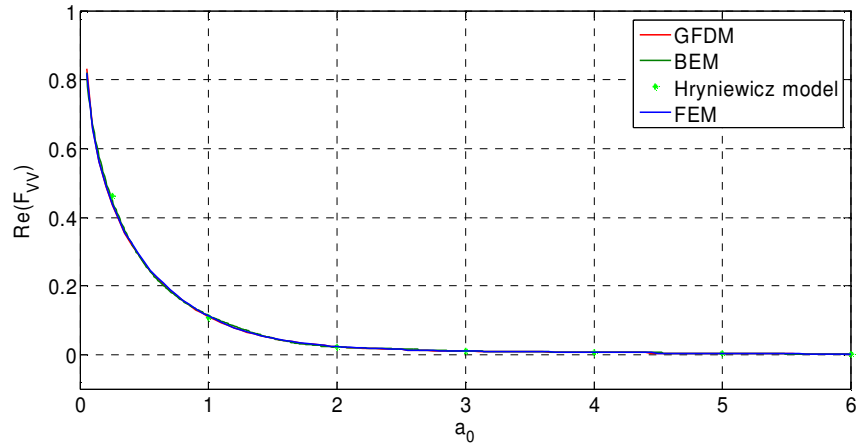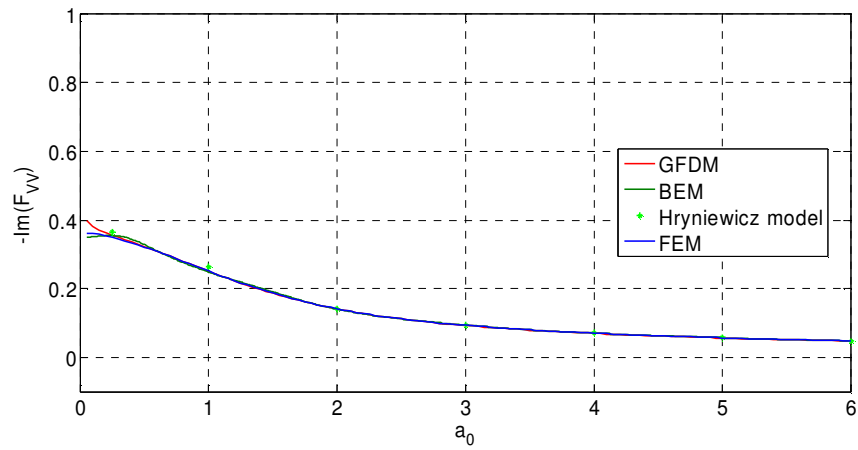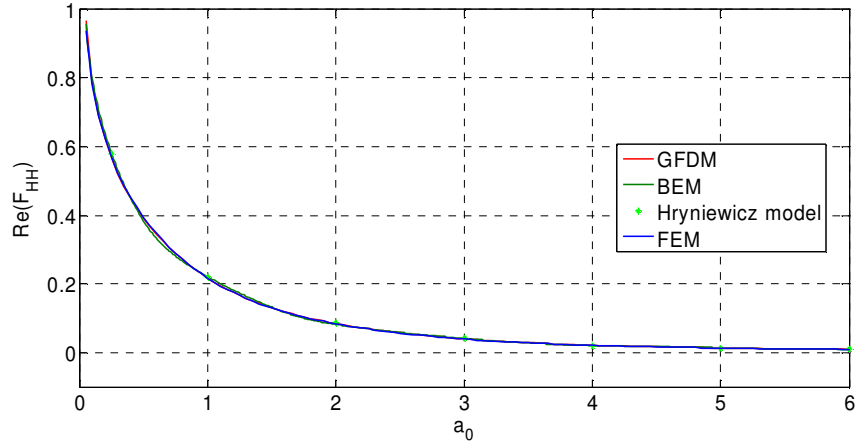
Figure 4.8: Dynamic vertical compliance coefficients of rigid strip foundation on elastic HS for (a) real and (b) imaginary parts ($L=3b/2$, $h=b/2$, $L_{PML}=b$, $b=1$, $G=1$, $\rho=1$ and $\upsilon=0.25$)

(a)

(b)

Figure 4.9: Dynamic horizontal compliance coefficients of rigid strip foundation on elastic HS for (a) real and (b) imaginary parts ($L=3b/2$, $h=b/2$, $L_{PML}=b$, $b=1$, $G=1$, $\rho=1$ and $\upsilon=0.25$).

(a)

(b)

Figure 4.10: Dynamic rocking compliance coefficients of rigid strip foundation on elastic HS for (a) real and (b) imaginary parts ($L=3b/2$, $h=b/2$, $L_{PML}=b$, $b=1$, $G=1$, $\rho=1$ and $\upsilon=0.25$).
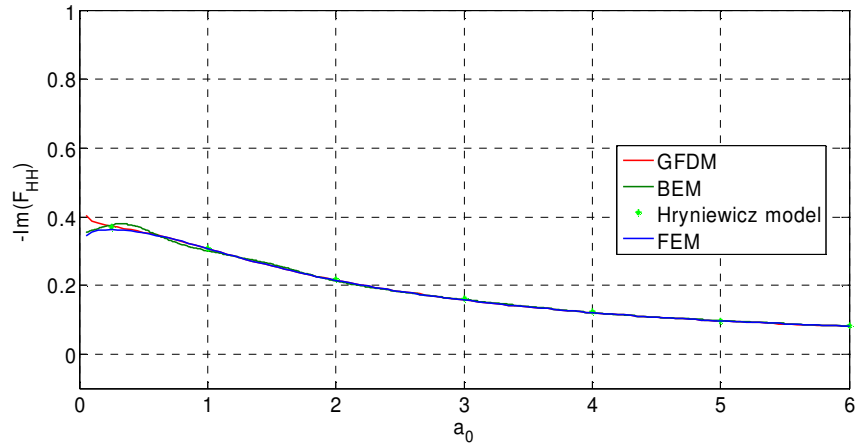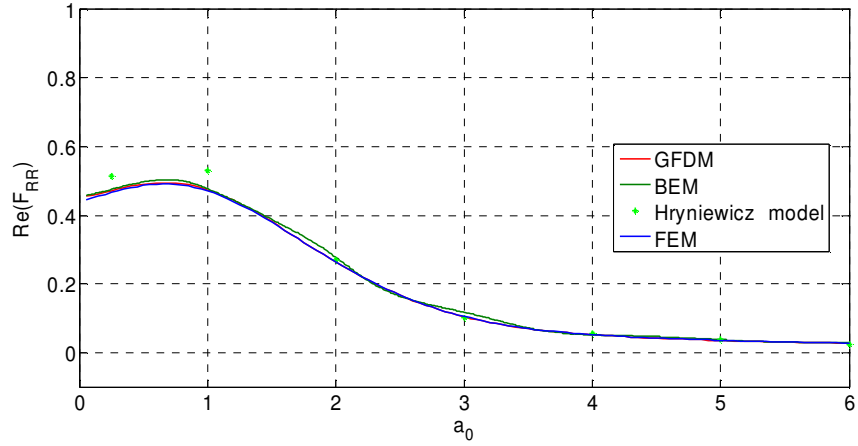
(a)

(b)

Figure 4.11: Dynamic vertical compliance coefficients of rigid strip foundation on visco-elastic HS for (a) real and (b) imaginary parts ($L=3b/2$, $h=b/2$, $L_{PML}=b$, $b=1$, $G=1$, $\rho=1$, $\upsilon=0.25$ and $\zeta=5\%$).
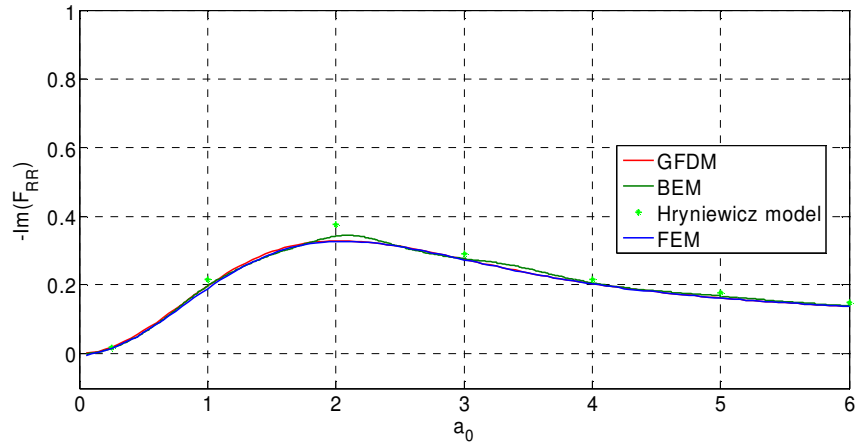
(a)

(b)

Figure 4.12: Dynamic horizontal compliance coefficients of rigid strip foundation on visco-elastic HS for (a) real and (b) imaginary parts (*L=3b/2, h=b/2, L_{PML}=b, b=1, G=1, ρ=1, υ=0.25* and *ζ=5%*).
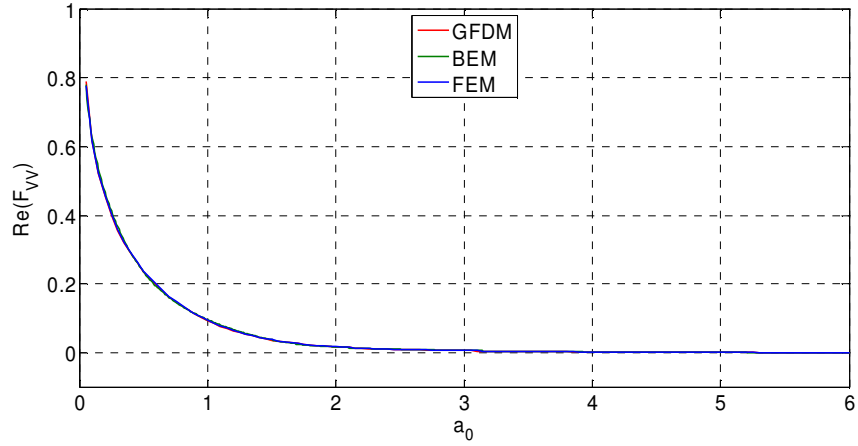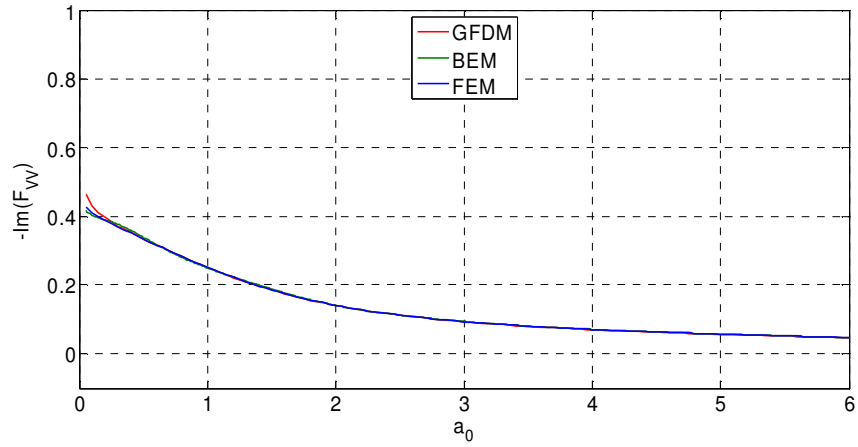
(a)

(b)

Figure 4.13: Dynamic rocking compliance coefficients of rigid strip foundation on visco-elastic HS for (a) real and (b) imaginary parts ($L=3b/2$, $h=b/2$, $L_{PML}=b$, $b=1$, $G=1$, $\rho=1$, $\upsilon=0.25$ and $\zeta=5\%$).
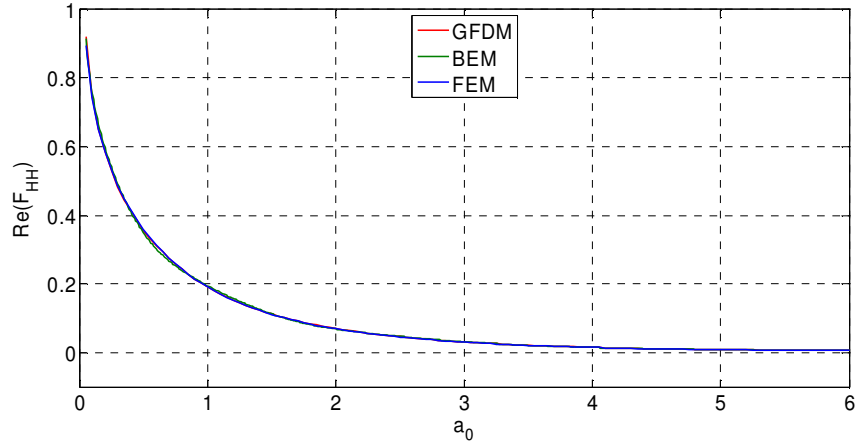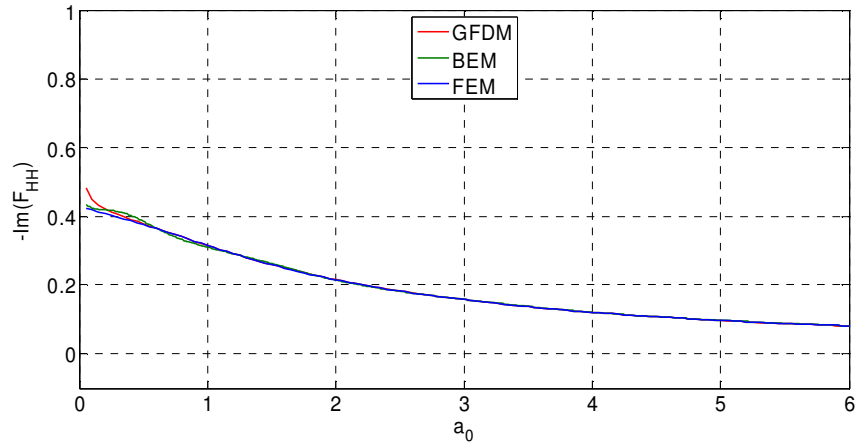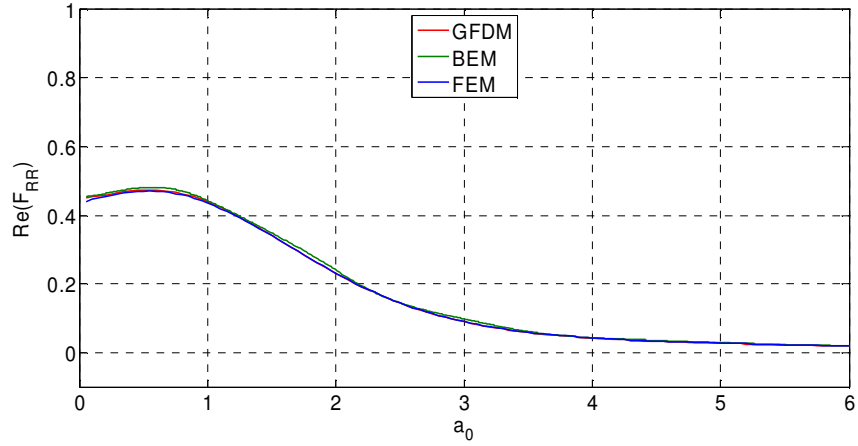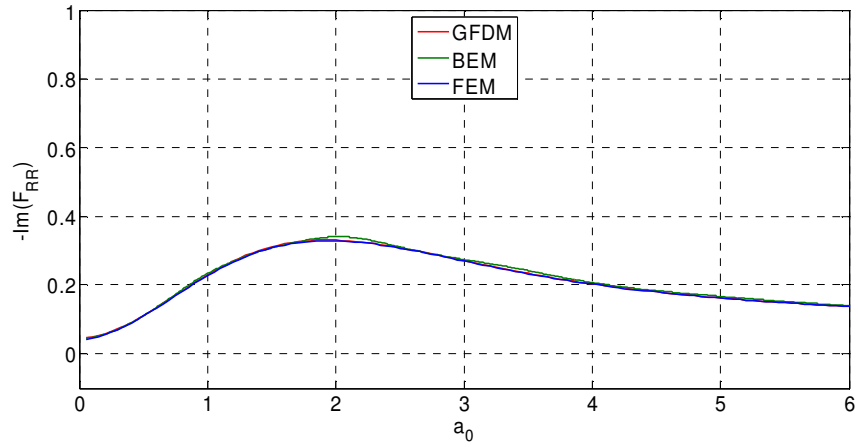
4.3.2 EFFECT OF POISSON AND DAMPING RATIO ON THE COMPLIANCES FOR RIGID STRIP FOUNDATION

In this section, the effect of Poisson ratio and damping ratio of HS on the dynamic compliances of rigid strip foundation is studied (see Figures. 4.14-19). In the Figures 4.14-16, vertical, horizontal and rocking compliances obtained from GFDM with PML are presented as a function of nondimensional frequency for various Poisson ratios. As observed from the Figure 4.14 and 4.16, variation of Poisson ratio has somewhat significant effects on the vertical and rocking compliances. In the case of larger value of Poisson ratio, smaller vertical and rocking compliances are generally obtained. This is mainly due to the fact that the soil material becomes incompressible as Poisson ratio increases, reaching perfectly incompressible state of $\upsilon=0.5$. It is known that the incompressibility increases the soil stiffness against volumetric deformations. This explains why the vertical and rocking compliance values which are governed mainly by volumetric soil behavior get smaller as Poisson ratio increases. However, the effect of Poisson ratio is found to be negligible for horizontal compliances (see Figure 4.15). This obviously results from the fact that the soil behavior in this case is governed by shear, not volumetric deformations.

During the vibration of foundations, some energy is dissipated due to the internal friction between soil particles (called material dissipation) and also due to radiation of waves propagating away from foundation (called radiation damping). The studies reveal that the material dissipation does not depend on frequency in the case of small amplitude of vibration. Accordingly, a linear hysteretic material damping model in Equation 4.5 is used in this study. Figures 4.17-19 investigate the effect of damping ratio on the vertical, horizontal and rocking compliances. As observed from these figures, larger damping ratio generally decreases the real part of compliances, however, increases their imaginary parts, in particular, for lower frequencies. The increase in the imaginary part with the damping should be expected since this part of compliances represents the dissipated energy in soil medium during vibrations of foundation. Figures 4.17-19 also show that the

vertical, horizontal and rocking compliances are insensitive to changing damping ratio for higher frequencies.
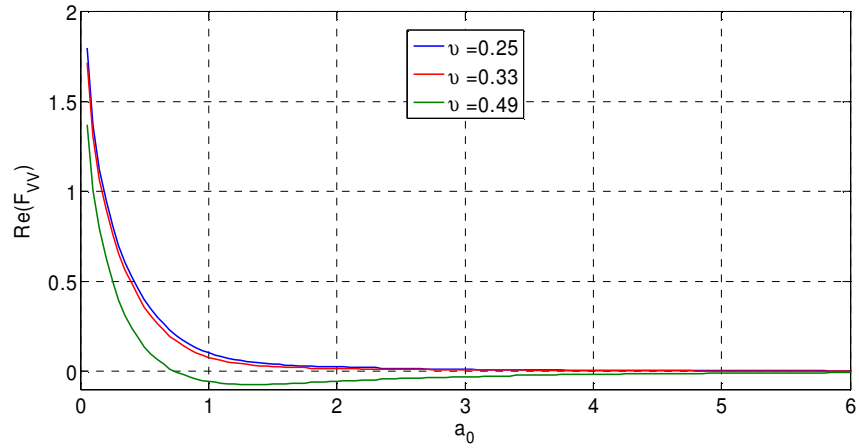
(a)
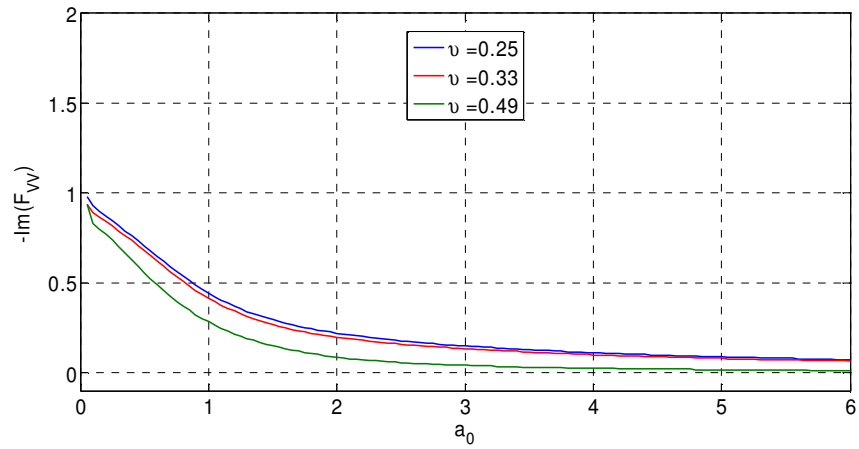
(b)

Figure 4.14: Dynamic vertical compliance coefficients of rigid strip foundation on the elastic HS for (a) real and (b) imaginary parts for various Poisson ratios ($L=3b/2$, $h=b/2$, $L_{PML}=b$, $b=1$, and $E=1$).

(a)

(b)

Figure 4.15: Dynamic horizontal compliance coefficients of rigid strip foundation on the elastic HS for (a) real and (b) imaginary parts for various Poisson ratios ($L=3b/2$, $h=b/2$, $L_{PML}=b$, $b=1$, and $E=1$).
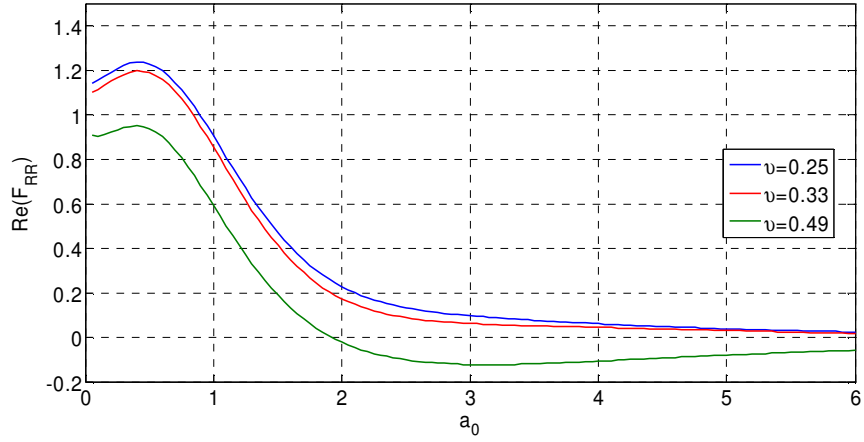
(a)
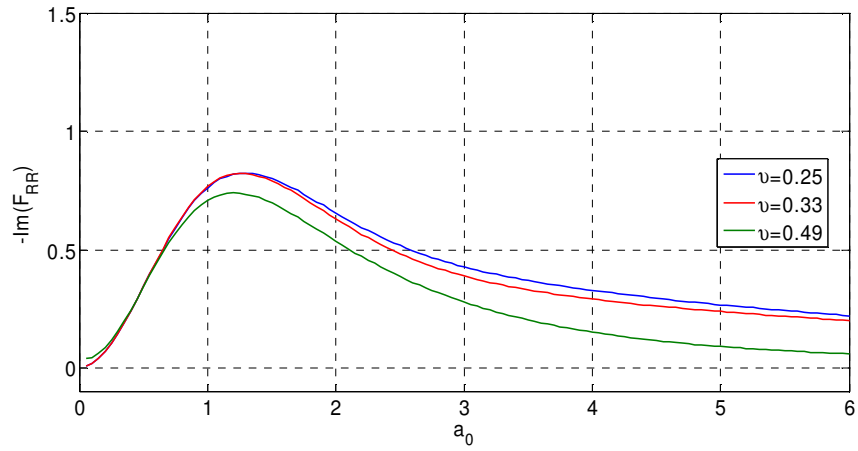
(b)

Figure 4.16: Dynamic rocking compliance coefficients of rigid strip foundation on the elastic HS for (a) real and (b) imaginary parts for various Poisson ratios (*L=3b/2, h=b/2, L$_{PML}$=b, b=1,* and *E=1*).
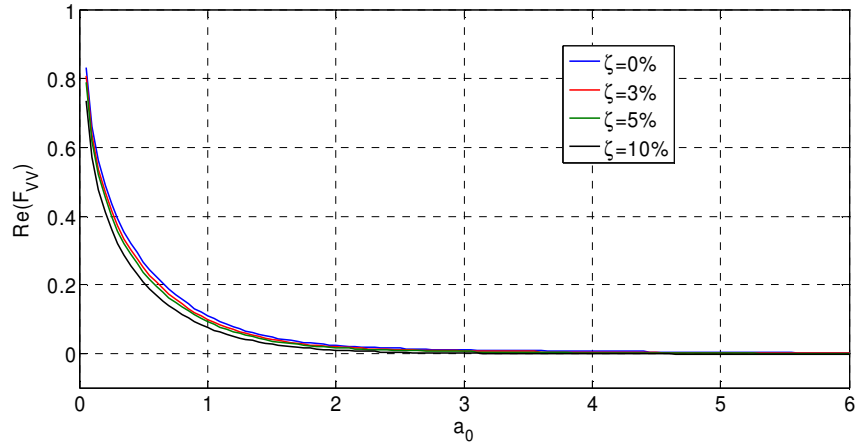
(a)
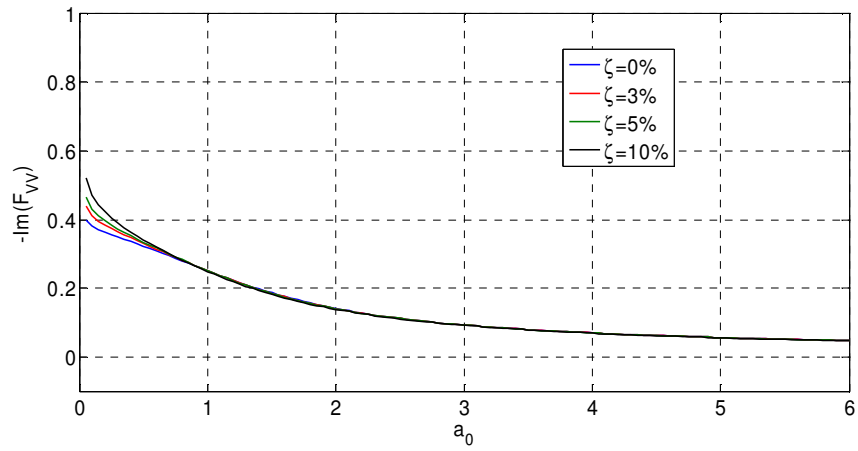
(b)

Figure 4.17: Dynamic vertical compliance coefficients of rigid strip foundation on visco-elastic HS for (a) real and (b) imaginary parts for various damping ratios ($L=3b/2$, $h=b/2$, $L_{PML}=b$, $b=1$, $G=1$, and $\upsilon=0.25$).

85
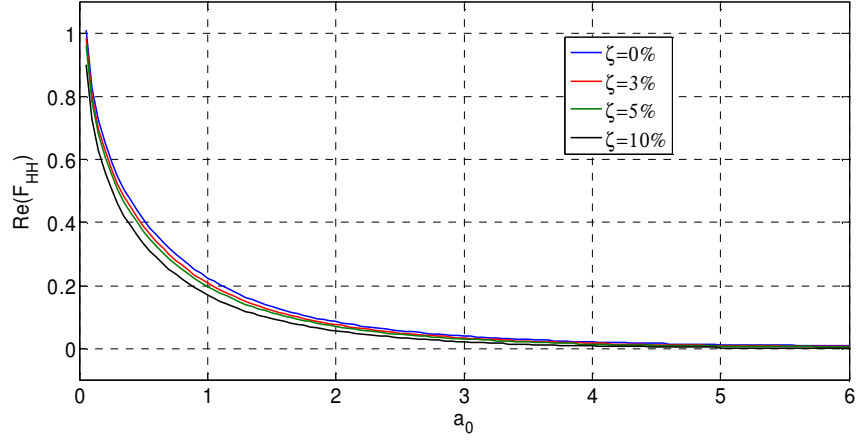
(a)
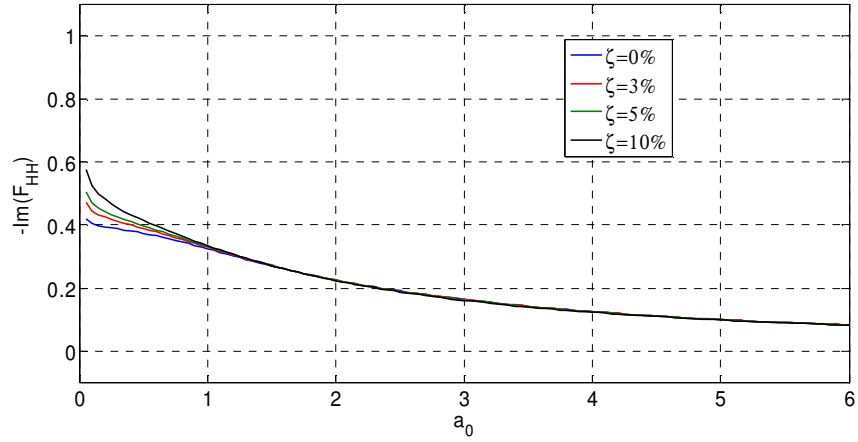
(b)

Figure 4.18: Dynamic horizontal compliance coefficients of rigid strip foundation on visco-elastic HS for (a) real and (b) imaginary parts for various damping ratios ($L=3b/2$, $h=b/2$, $L_{PML}=b$, $b=1$, $G=1$, and $\upsilon=0.25$).
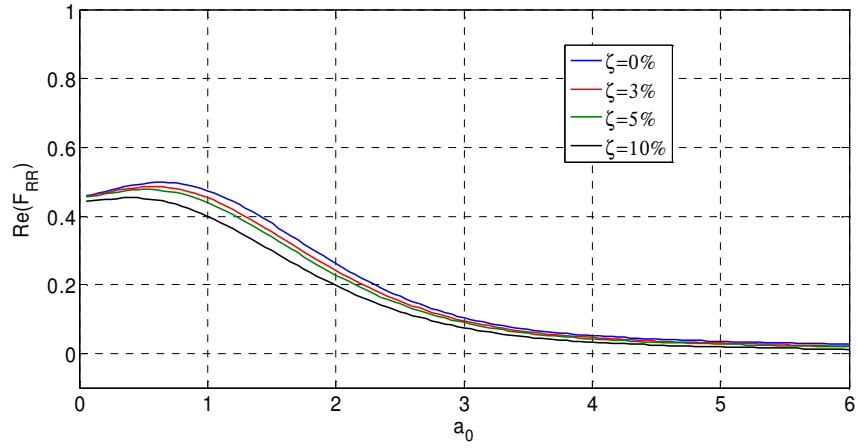
(a)
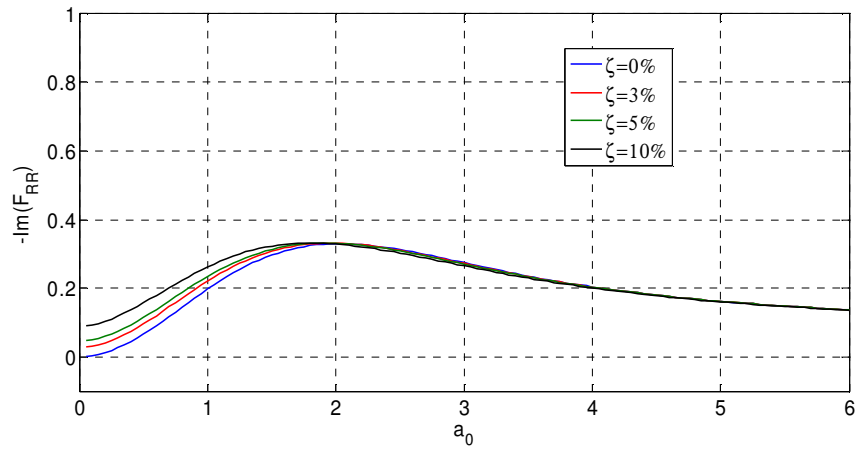
(b)

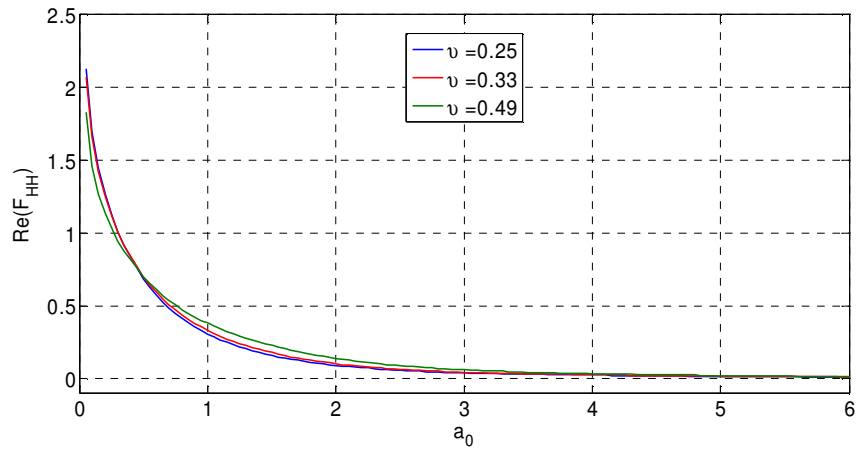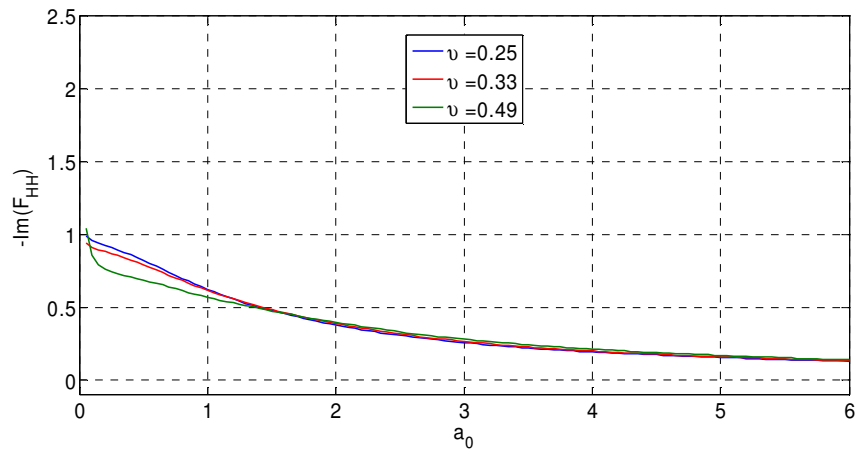**Figure 4.19:** Dynamic rocking compliance coefficients of rigid strip foundation on visco-elastic HS for (a) real and (b) imaginary parts for various damping ratios ($L=3b/2$, $h=b/2$, $L_{PML}=b$, $b=1$, $G=1$, and $\upsilon=0.25$).

4.3.3 COMPARISON OF DYNAMIC COMPLIANCES FOR RIGID STRIP FOUNDATION ON THE SOIL LAYER OVERLYING THE BEDROCK

In this section, the dynamic compliances are calculated using GFDM for rigid strip foundation on the soil layer overlying bedrock and they are compared to those obtained from FEM. The results are given in Figs. 4.20-4.22, where the compliances are presented as functions of nondimensional frequencies ranging between 0 and 6. In the analyses, the Poisson ratio (υ) of the soil layer is assumed to be 0.4 and the shear modulus is chosen as 1. The damping ratio is taken as 5% for viscoelastic soil layer, which reduces the resonance amplitudes considerably.

As seen from figures, the dynamic compliances calculated using GFDM and FEM are generally in good agreement.
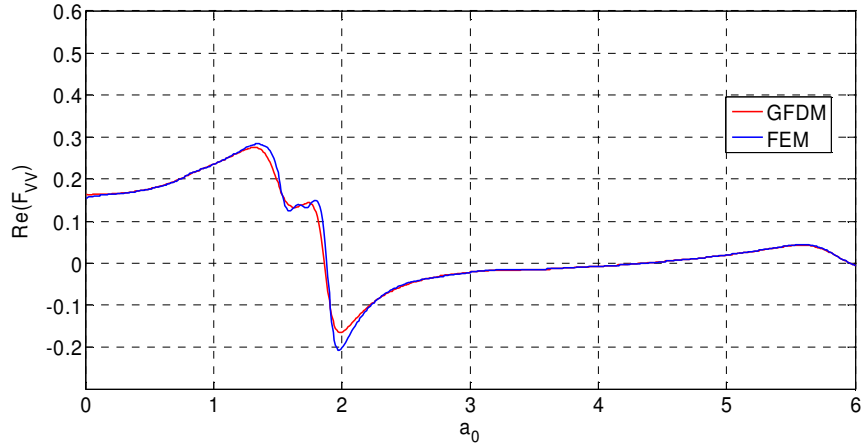
(a)
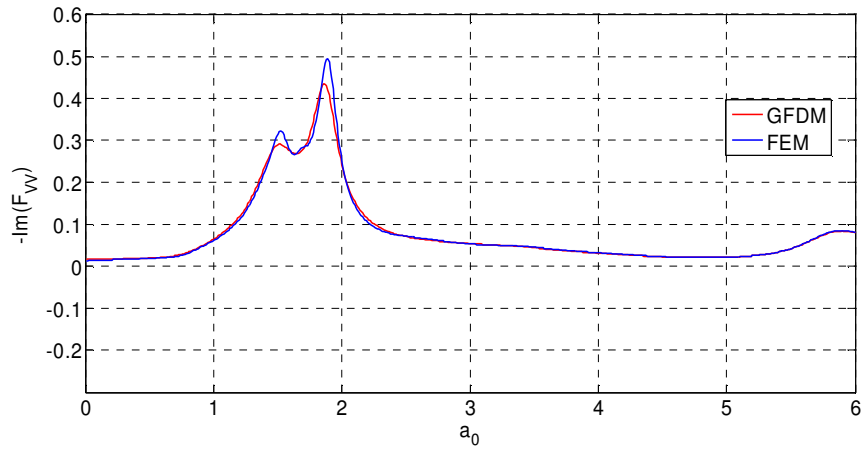
(b)

Figure 4.20: Dynamic vertical compliance coefficients of rigid strip foundation on visco-elastic layer overlying bedrock for (a) real and (b) imaginary parts ($L=3b/2$, $d=2b$, $L_{PML}=b$, $b=1$, $G=1$, $\upsilon=0.4$, and $\zeta=5\%$)
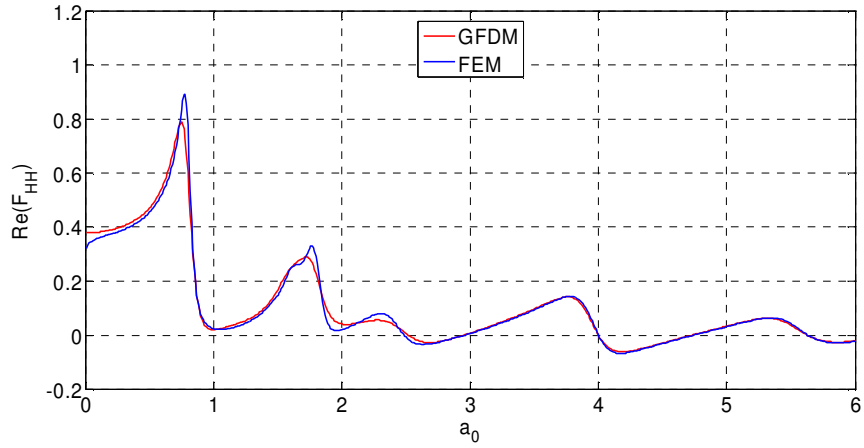
(a)

(b)

Figure 4.21: Dynamic horizontal compliance coefficients of rigid strip foundation on visco-elastic layer overlying bedrock for (a) real and (b) imaginary parts ($L=3b/2$, $d=2b$, $L_{PML}=b$, $b=1$, $G=1$, $\upsilon=0.4$, and $\zeta=5\%$)

90

(a)

(b)

Figure 4.22: Dynamic rocking compliance coefficients of rigid strip foundation on visco-elastic layer overlying bedrock for (a) real and (b) imaginary parts (*L=3b/2, d=2b, LPML=b, b=1, G=1, υ=0.4*, and *ζ=5%*)

4.3.4 EFFECT OF DEPTH OF LAYER OVERLYING BEDROCK ON COMPLIANCES FOR RIGID STRIP FOUNDATION

Here, the dynamic compliances obtained from GFDM for various depths of layer are compared in Figures 4.23-4.25. In the figures, the compliances are presented as functions of nondimensional frequencies ranging between 0 and 6. In the analyses, the Poisson ratio (υ) of the soil layer is assumed to be 0.4 and the shear modulus is chosen as 1. The damping ratio is taken as 5% for viscoelastic soil layer.

Compliance curves of soil layer in the figures are not smooth as observed for HS case. Instead, the compliance functions for layer case exhibit some peaks and valleys. This is mainly due to that the body waves generated by vibrations of foundation are reflected when they reach the bedrock and return back to the foundation at the surface. As a result, when the frequencies are close to natural frequencies of the soil layer, larger amplitude of the foundation motion occurs due to resonance (Gazetas 1983). Resonant nondimensional frequencies for uniform single layered are give by, for vertical P and SV waves,

$$
\begin{aligned}
a_0^p &= (2n-1)\frac{\pi b}{2d}\frac{v_p}{v_s} \\
a_0^s &= (2n-1)\frac{\pi b}{2d} \qquad (n=1,2,3...)
\end{aligned}
\tag{4.37}
$$

where a_0^p and a_0^s are nondimensional resonant frequencies for P and S waves respectively and n is the mode number.

Even though, these formulas were developed for one dimensional wave propagation, the studies in literature reveal that these formulas are also appropriate for 3D problems (Gazetas 1983). The resonant frequencies a_0^p in Equation 4.37 govern approximately the location of peak values of vertical and rocking compliances in Figures 4.23 and 4.25, while a_0^s does that for horizontal compliances in Figure 4.24. This is natural consequence of the fact that the

vertical and rocking compliances are mainly influenced by P waves, whereas the horizontal compliance, by S waves.

The figures indicate further that

- The layer depth has more influence on vertical and rocking compliances compared to horizontal compliance
- As the layer depth increases, the compliance curves become smoother for high frequencies.
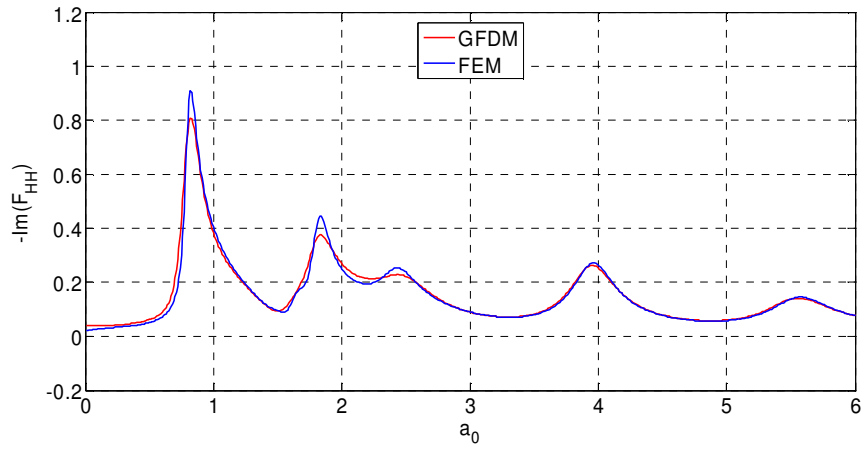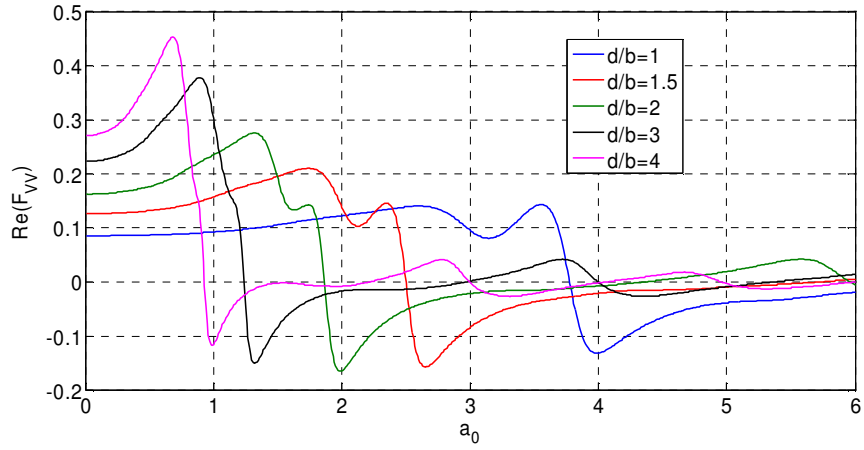
(a)
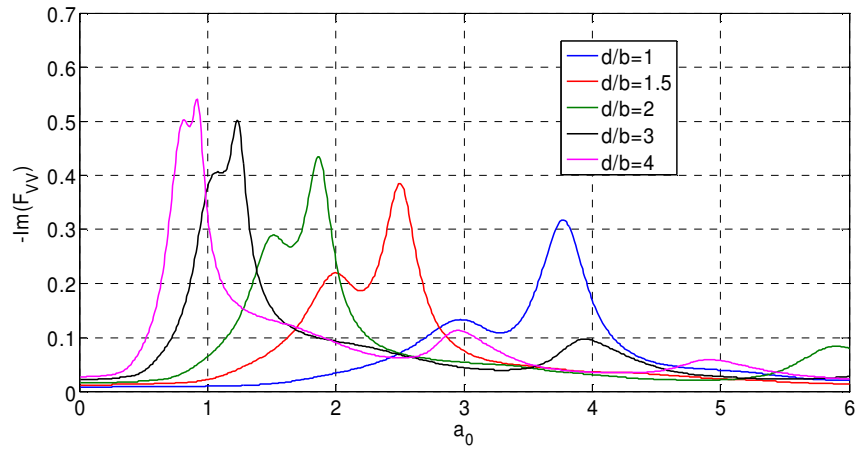
(b)

Figure 4.23: Dynamic vertical compliance coefficients of rigid strip foundation on viscoelastic layer with various depths overlying bedrock (a) real and (b) imaginary parts (*L=3b/2, L_{PML}=b, b=1, G=1, υ=0.4,* and *ζ=5%*)

(a)

(b)

Figure 4.24: Dynamic horizontal compliance coefficients of rigid strip foundation on viscoelastic layer with various depths overlying bedrock (a) real and (b) imaginary parts (*L=3b/2, L_{PML}=b, b=1, G=1, υ=0.4*, and *ζ=5%*)

(a)

(b)

Figure 4.25: Dynamic rocking compliance coefficients of rigid strip foundation on viscoelastic layer with various depths overlying bedrock (a) real and (b) imaginary parts ($L=3b/2$, $L_{PML}=b$, $b=1$, $G=1$, $\upsilon=0.4$, and $\zeta=5\%$)
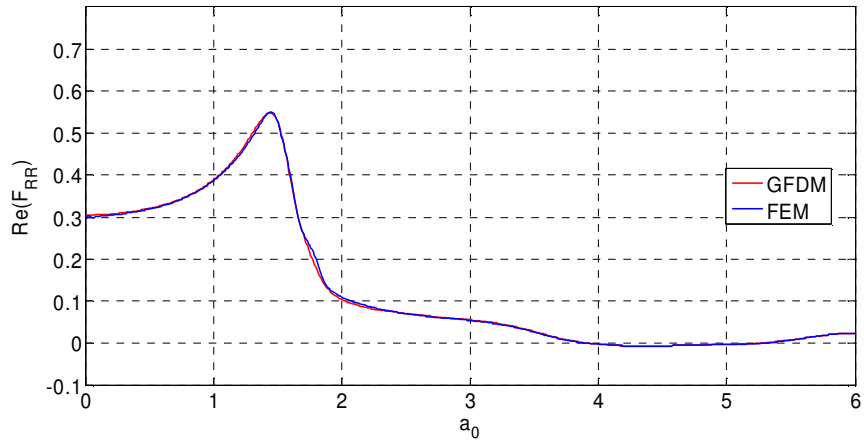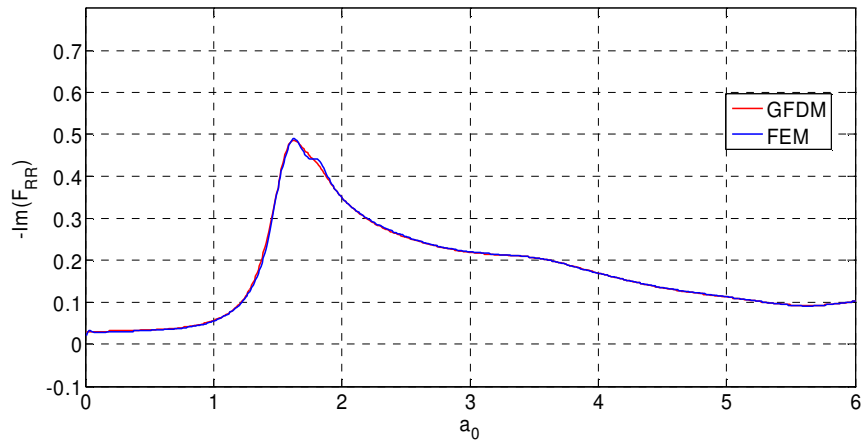
4.3.5 COMPARISON OF DYNAMIC COMPLIANCES FOR RIGID STRIP FOUNDATION ON THE VISCOELASTIC LAYER OVER VISCOELASTIC HS

In this section, the dynamic compliances obtained using GFDM are compared to those calculated from FEM and BEM in Figures. 4.26-28 for the nondimensional frequency range between 0 and 6. In the analyses, the Poisson ratio, damping ratio, mass density and shear modulus of viscoelastic layer are taken as 0.4, 5%, 1 and 1 respectively. The properties of HS are the same as those of the layer, except that its shear modulus is assumed as four.

The figures indicate that the compliances calculated using GFDM with PML compare well with those obtained from FEM and BEM.

It may be noted that the compliance curves in Figures 4.26-28 are rather smooth and contain no noticeable irregularities induced by resonant frequencies as in the case of layer over rigid bedrock. This is mainly due to the fact that the HS below layer permits partially the radiation of the waves generated by vibrations of foundation.

(a)
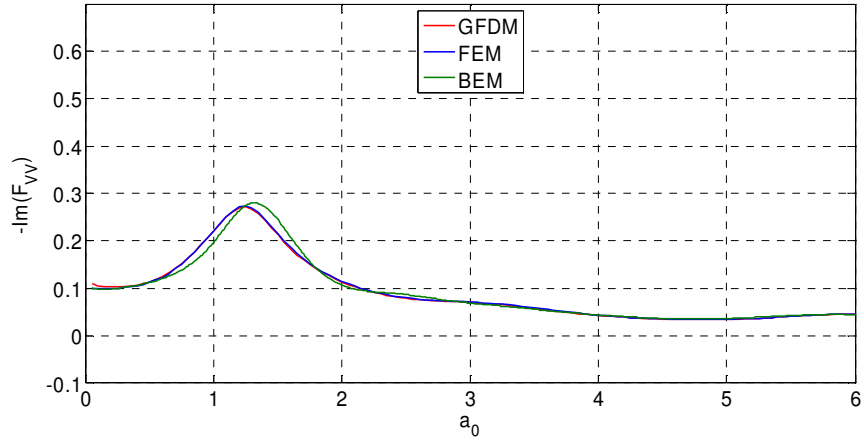
(b)

Figure 4.26: Dynamic vertical compliance coefficients of rigid strip foundation on visco-elastic layer overlying HS for (a) real and (b) imaginary parts (*L=3b/2, h₁=2b, h₂=0.5b, L_PML=b, b=1, G₁=1, G₂=4, υ=0.4,* and *ζ=5%*)
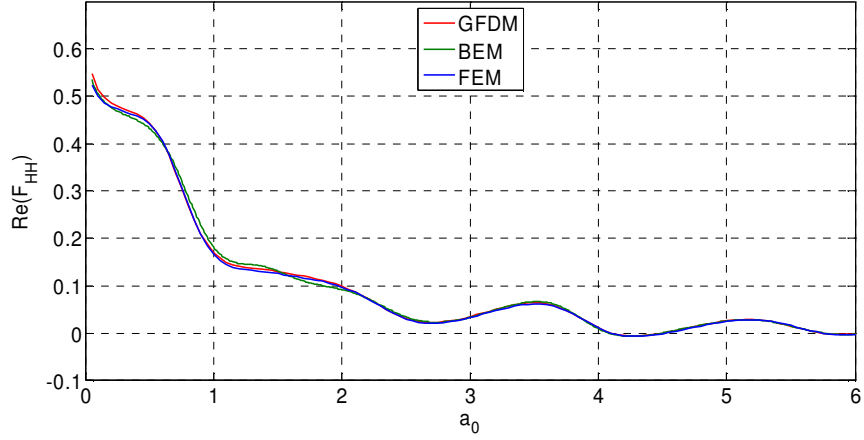
(a)
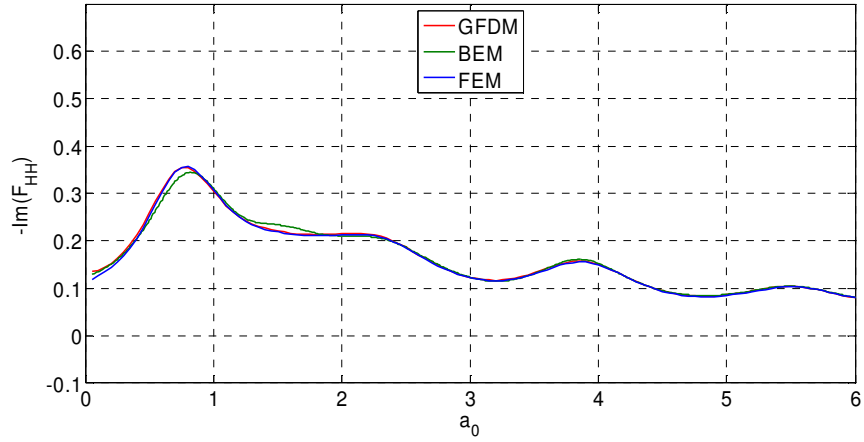
(b)

Figure 4.27: Dynamic horizontal compliance coefficients of rigid strip foundation on visco-elastic layer overlying HS for (a) real and (b) imaginary parts ($L=3b/2$, $h_1=2b$, $h_2=0.5b$, $L_{PML}=b$, $b=1$, $G_1=1$, $G_2=4$, $\upsilon=0.4$, and $\zeta=5\%$)
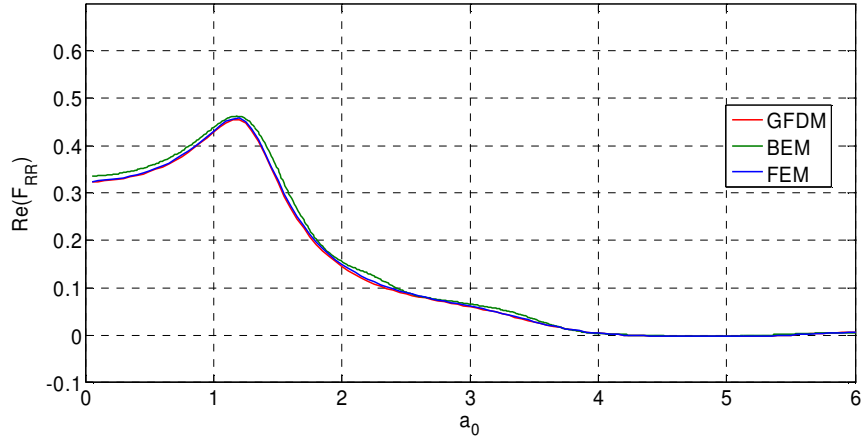
(a)
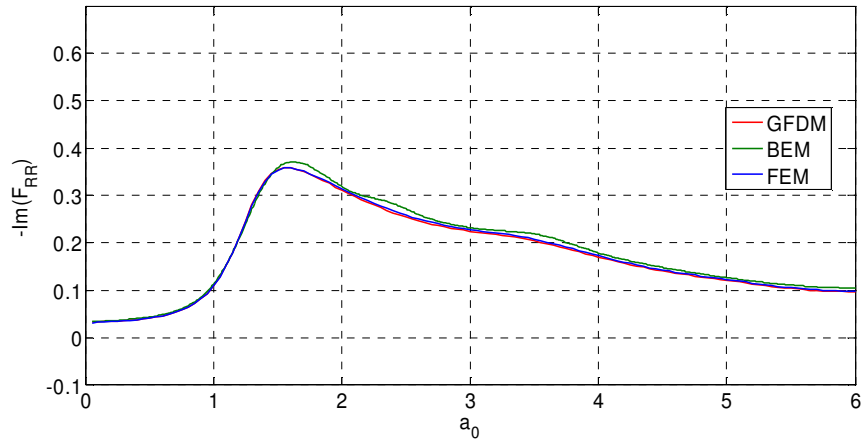
(b)

Figure 4.28: Dynamic rocking compliance coefficients of rigid strip foundation on visco-elastic layer overlying HS for (a) real and (b) imaginary parts ($L=3b/2$, $h_1=2b$, $h_2=0.5b$, $L_{PML}=b$, $b=1$, $G_1=1$, $G_2=4$, $\upsilon=0.4$, and $\zeta=5\%$)

4.3.6 EFFECT OF DEPTH OF LAYER OVERLYING HS ON THE COMPLIANCES FOR RIGID STRIP FOUNDATION

Previous studies reveal that the depth of layer and the ratio of the shear modulus of soil layer and HS are the main parameters which affect the compliances of rigid strip foundation (Gazetas 1983). Accordingly, the effect of the depth of layer overlying HS on dynamic compliances for rigid strip foundation is investigated in this part of the study. The results obtained by GFDM for various depths of the layer are presented in Figures 4.29-31. In the analysis, the properties of the layer and HS are taken as the same as those of the previous section.

The results in figures exhibit larger peak values for deeper top layer on HS. However, the change of vertical compliances as a function of frequency is relatively smoother in the case of shallower soil layer on HS. The resonance does not occur in such layer due to potential energy dissipation of this shallower soil layer on HS (Ahmad and Israil, 1988).
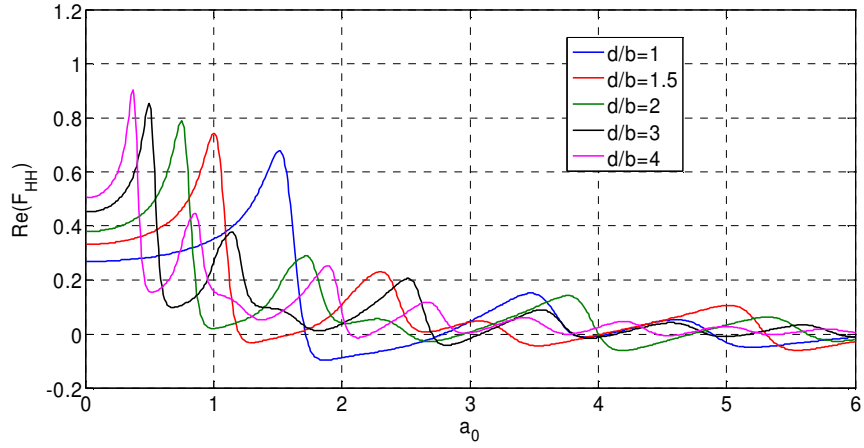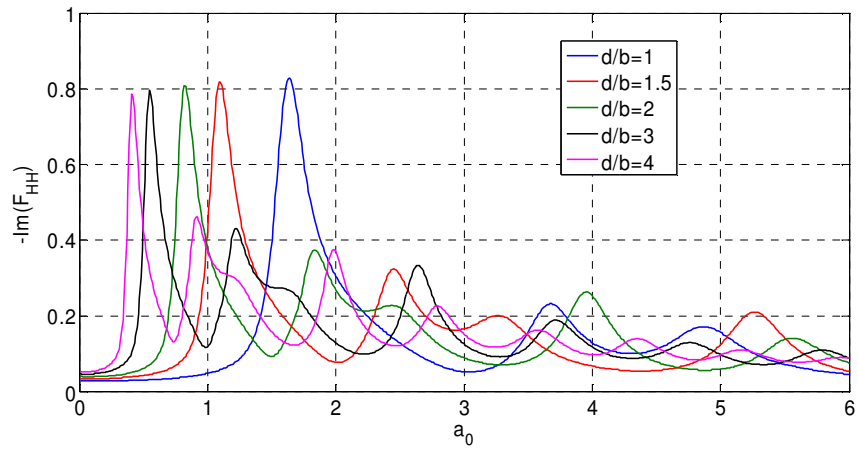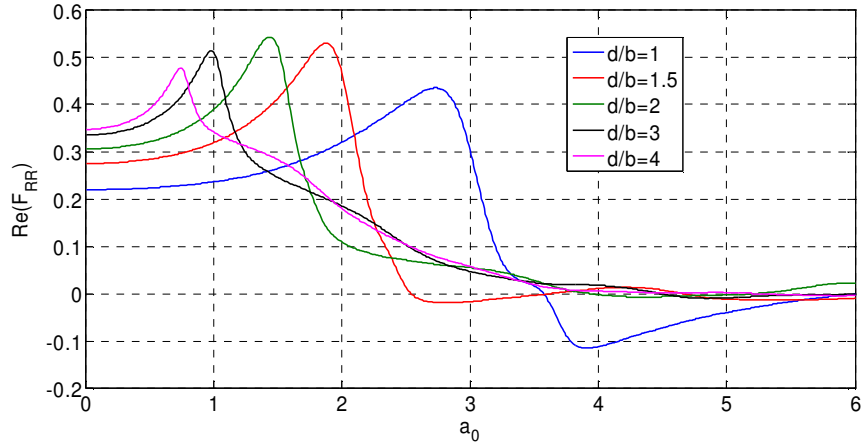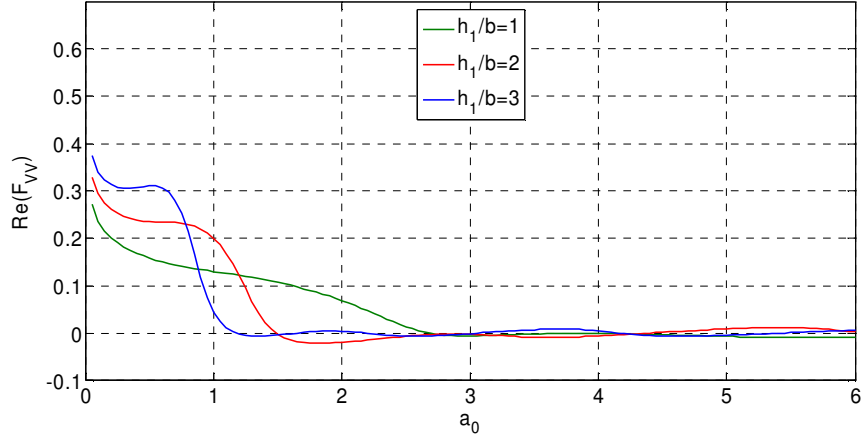
(a)
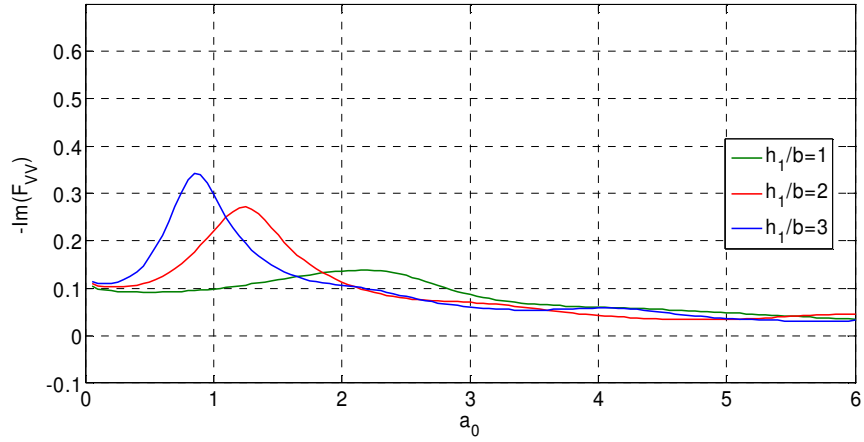
(b)

Figure 4.29: Dynamic vertical compliance coefficients of rigid strip foundation on visco-elastic layer with various depths overlying HS for (a) real and (b) imaginary parts (*L=3b/2, L$_{PML}$=b, b=1, G$_1$=1, G$_2$=4, υ=0.4*, and *ζ=5%*)
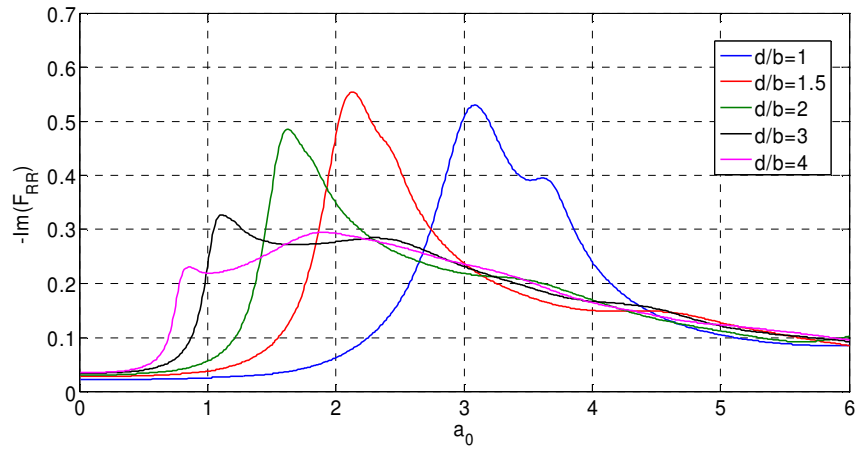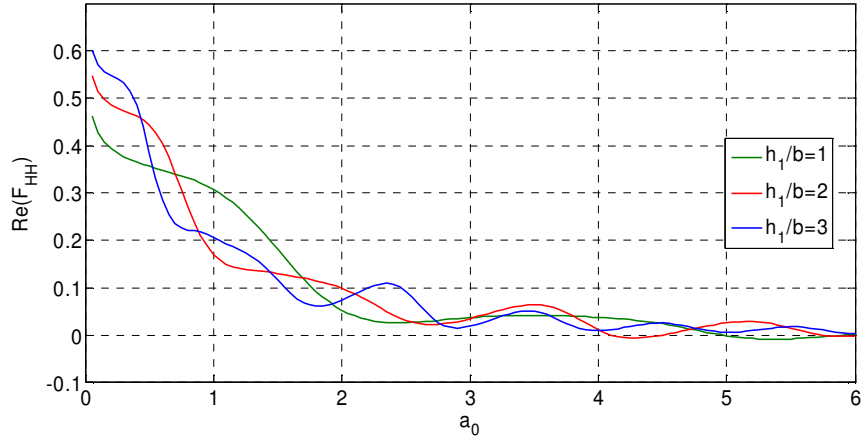
(a)
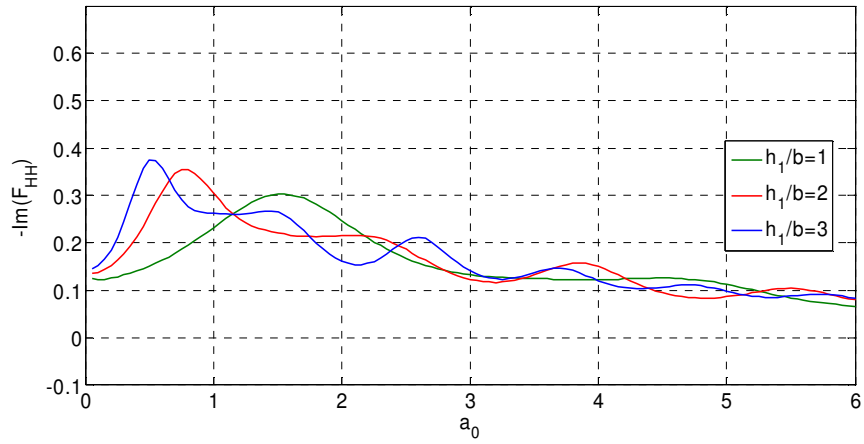
(b)

Figure 4.30: Dynamic horizontal compliance coefficients of rigid strip foundation on visco-elastic layer with various depths overlying HS for (a) real and (b) imaginary parts (*L=3b/2, L_{PML}=b, b=1, G_1=1, G_2=4, v=0.4*, and *ζ=5%)*
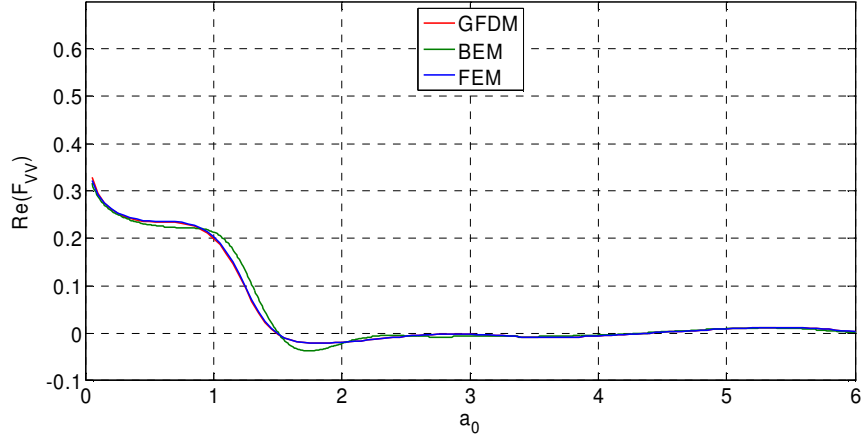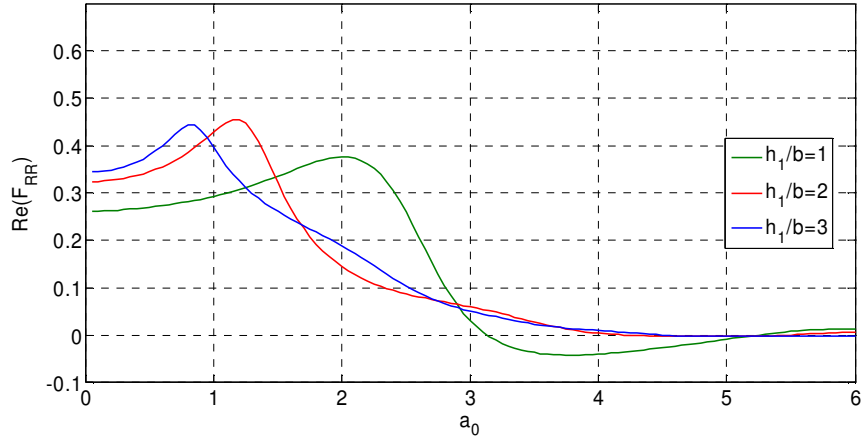
(a)
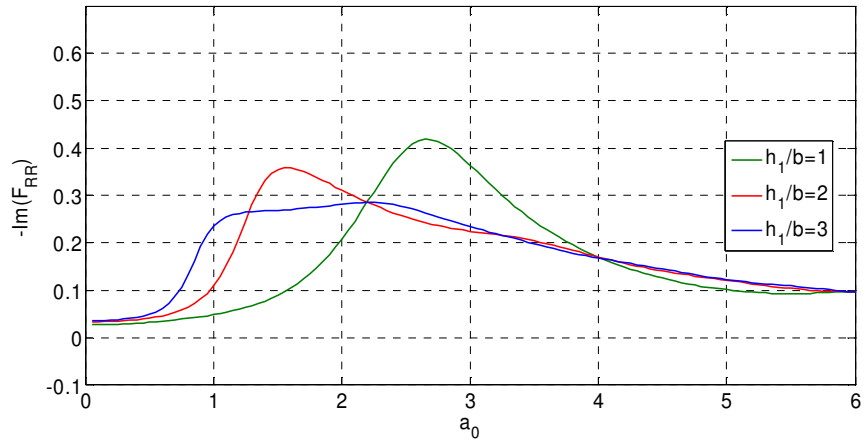
(b)

Figure 4.31: Dynamic rocking compliance coefficients of rigid strip foundation on visco-elastic layer with various depths overlying HS for (a) real and (b) imaginary parts (*L=3b/2, L$_{PML}$=b, b=1, G$_1$=1, G$_2$=4, υ=0.4,* and *ζ=5%*)

4.4 NUMERICAL RESULTS FOR EMBEDDED RIGID STRIP FOUNDATION ON VISCO-ELASTIC HS

Here, the dynamic compliances for embedded rigid strip foundation illustrated in Figure 4.32 are evaluated by GFDM and compared to those obtained from FEM, BEM. The results are displayed in Figures 4.33-35 showing the compliances as a function of nondimensional frequency ranging between 0 and 6. In the analyses, the Poisson ratio (υ) of the HS is assumed to be 0.25, its shear modulus is chosen as 1 and its damping ratio is assumed as 5%.

The comparisons presented in the figures indicate reliability of using GFDM (with PML) in wave propagation analysis.
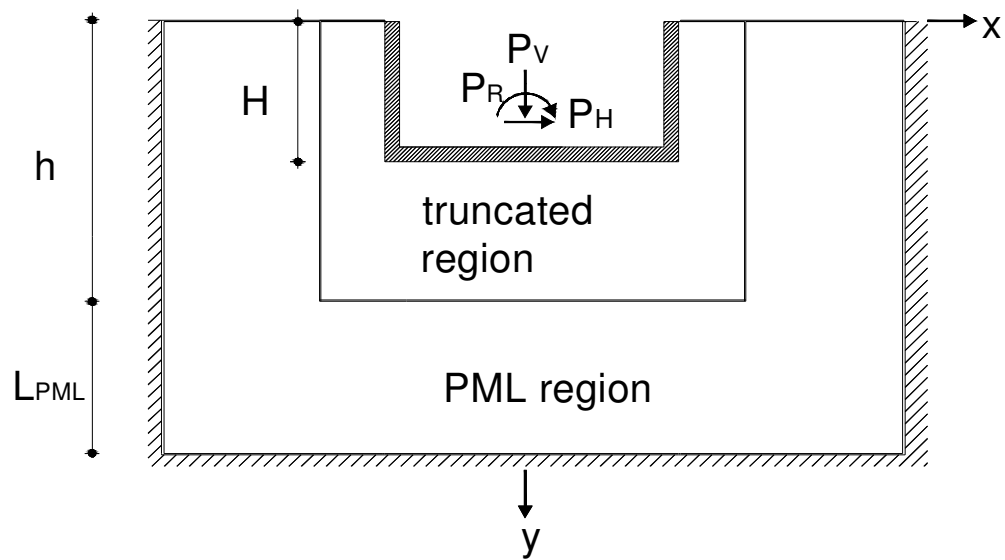
Figure 4.32: PML model for embedded rigid strip foundation on HS under vertical, horizontal and rocking vibrations.
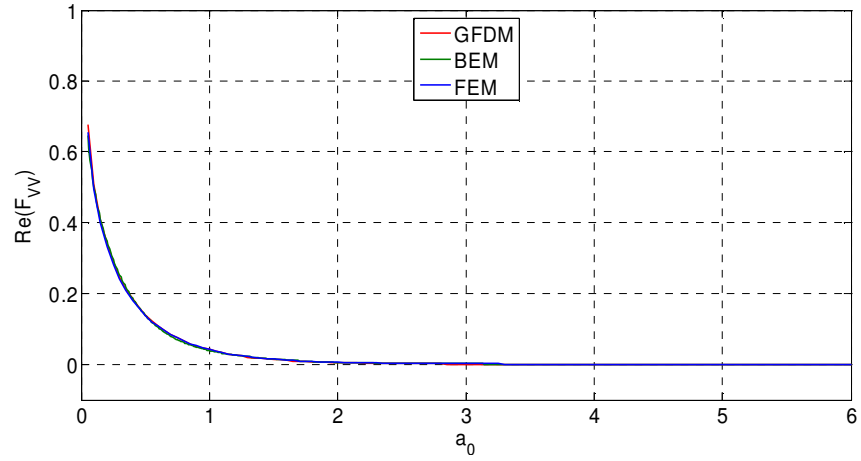
(a)
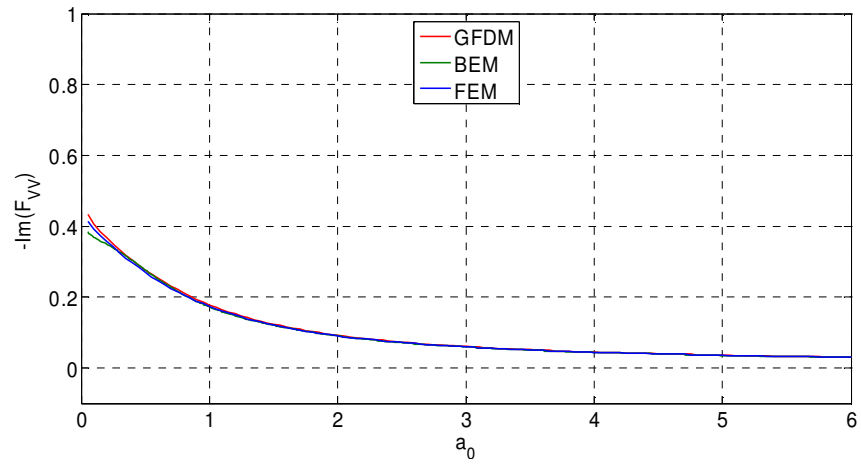
(b)

Figure 4.33: Dynamic vertical compliance coefficients of embedded rigid strip foundation overlying HS for (a) real and (b) imaginary parts ($L=3b/2$, $H=b$, $h=3b/2$, $L_{PML}=b$, $b=1$, $G=1$, $\upsilon=0.25$ and $\zeta=5\%$)
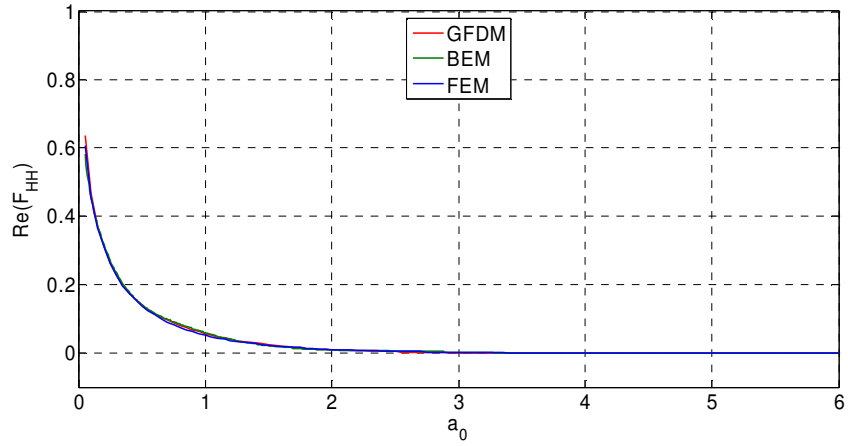
(a)
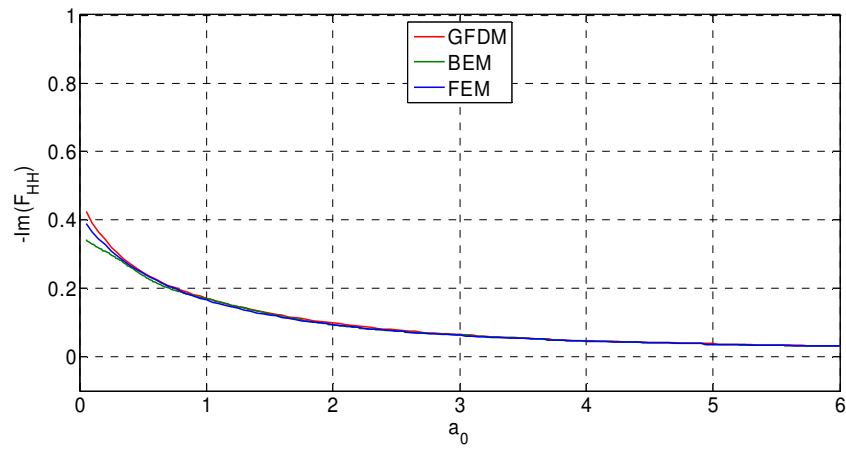
(b)

Figure 4.34: Dynamic horizontal compliance coefficients of embedded rigid strip foundation overlying HS for (a) real and (b) imaginary parts ($L=3b/2$, $H=b$, $h=3b/2$, $L_{PML}=b$, $b=1$, $G=1$, $\upsilon=0.25$ and $\zeta=5\%$)
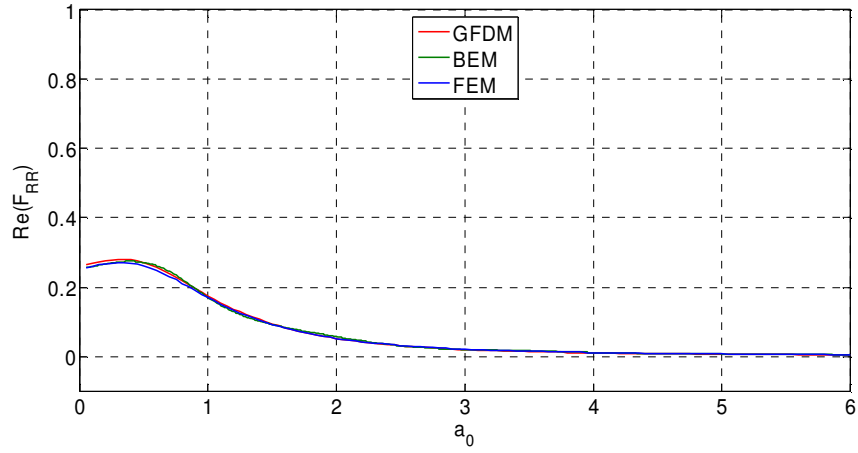
(a)
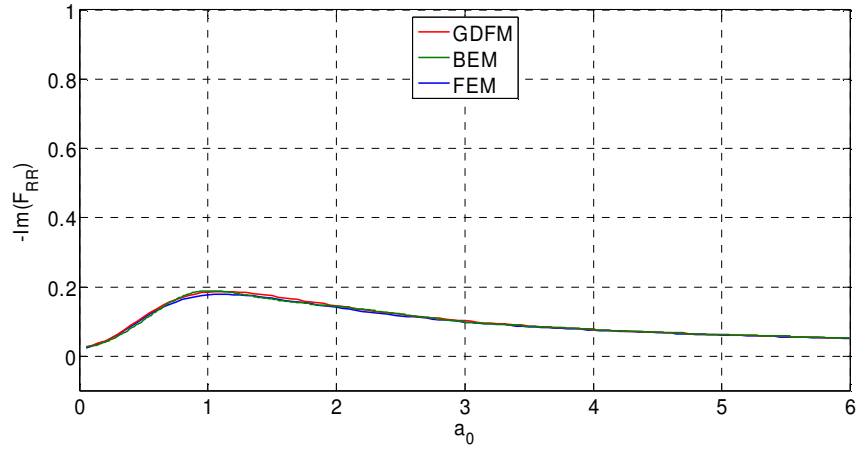
(b)

Figure 4.35: Dynamic rocking compliance coefficients of embedded rigid strip foundation overlying HS for (a) real and (b) imaginary parts ($L=3b/2$, $H=b$, $h=3b/2$, $L_{PML}=b$, $b=1$, $G=1$, $\upsilon=0.25$ and $\zeta=5\%$)

## 4.4.1 EFFECT OF DEPTH OF EMBEDMENT ON THE COMPLIANCES FOR EMBEDDED RIGID STRIP FOUNDATION

In this section, the effect of depth of embedment on dynamic compliances for embedded rigid strip foundations is studied. To this end, the compliances for embedded rigid strip foundation are obtained from GFDM for various depths of embedment and they are compared in Figures 4.36-38. The properties of HS are taken as the same as those of the previous section.

The results in the figures reveal that vertical, horizontal and rocking compliances for embedded rigid strip foundation decreases when the depth of embedment increases. This is because of that the existence of the embedment in the foundation system causes relatively stiffer foundation due to the fact that the area between foundation and soil becomes larger.
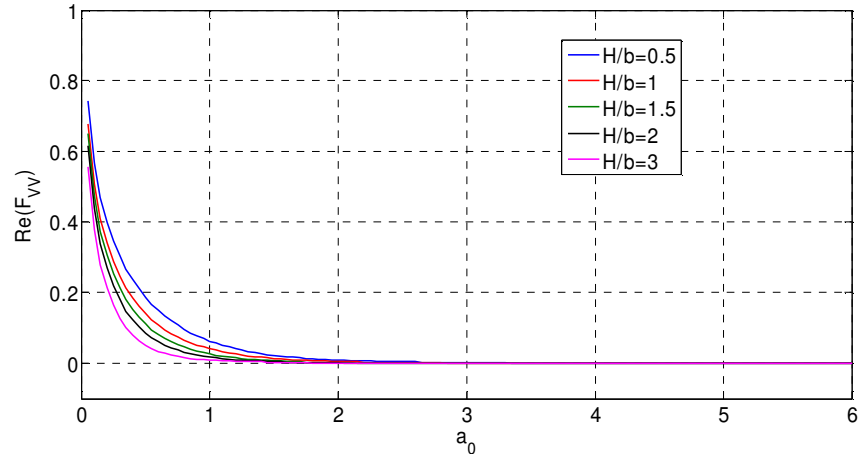
(a)
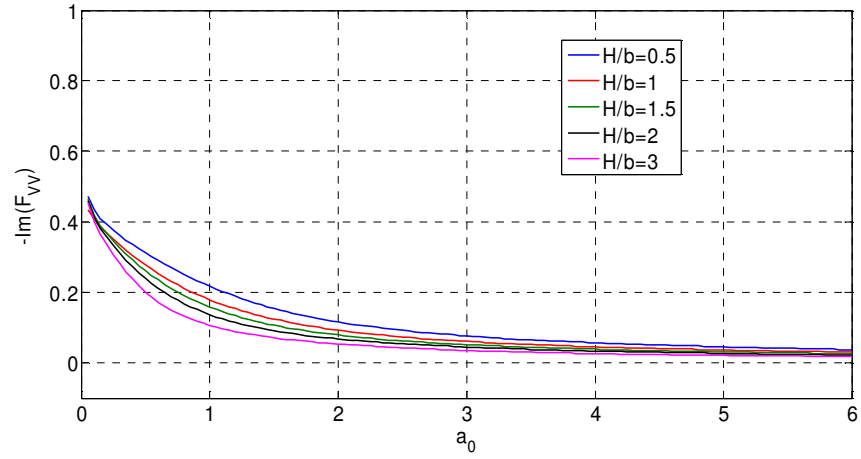
(b)

Figure 4.36: Dynamic vertical compliance coefficients of embedded rigid strip foundation on HS with various depths of embedment for (a) real and (b) imaginary parts (*L=3b/2, h=3b/2, L_{PML}=b, b=1, G=1, υ=0.25*, and *ζ=5%*)
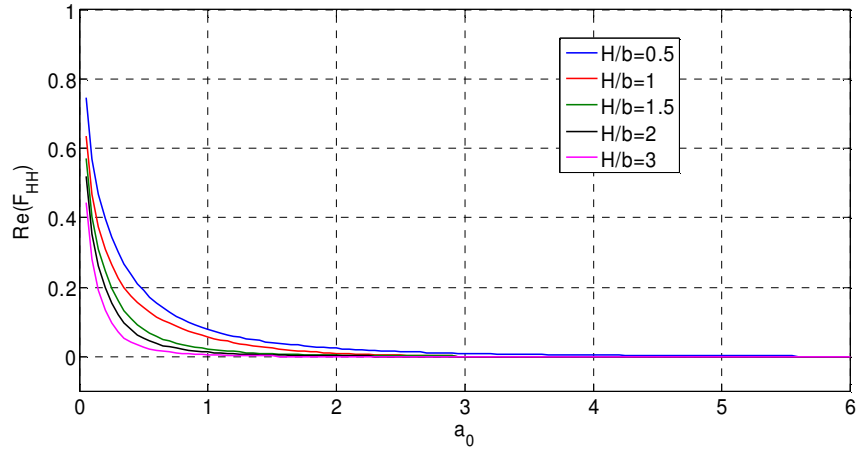
(a)
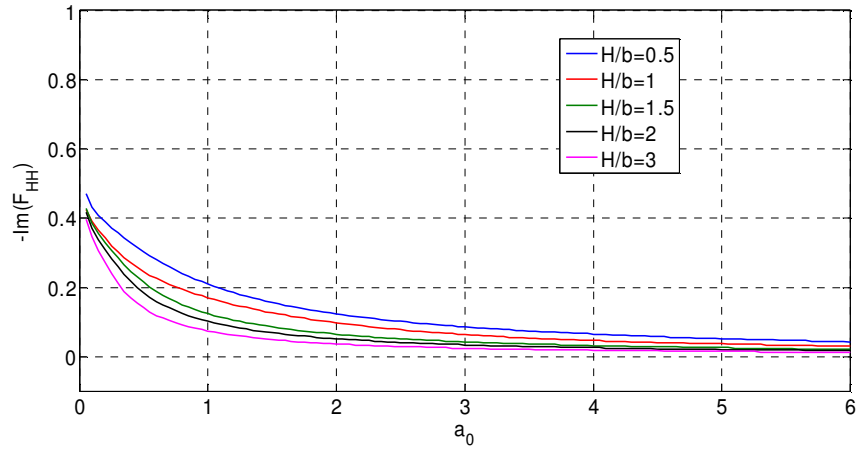
(b)

Figure 4.37: Dynamic horizontal compliance coefficients of embedded rigid strip foundation on HS with various depths of embedment for (a) real and (b) imaginary parts (*L=3b/2, h=3b/2, L_{PML}=b, b=1, G=1, v=0.25*, and *ζ=5%)*
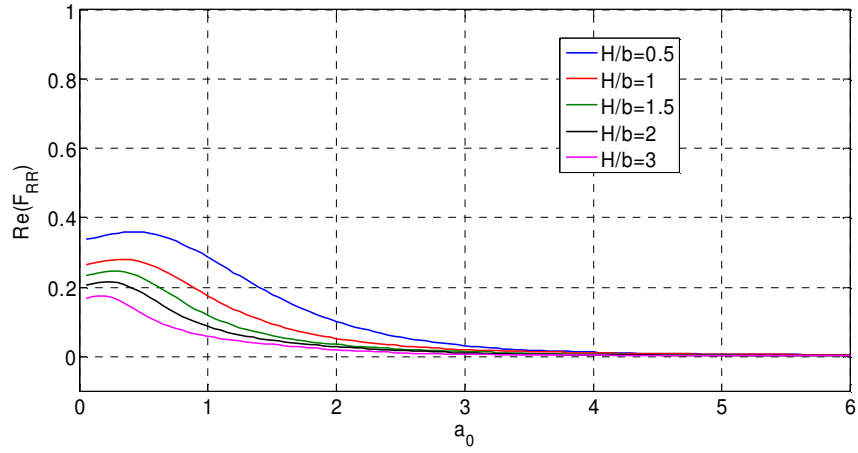
(a)
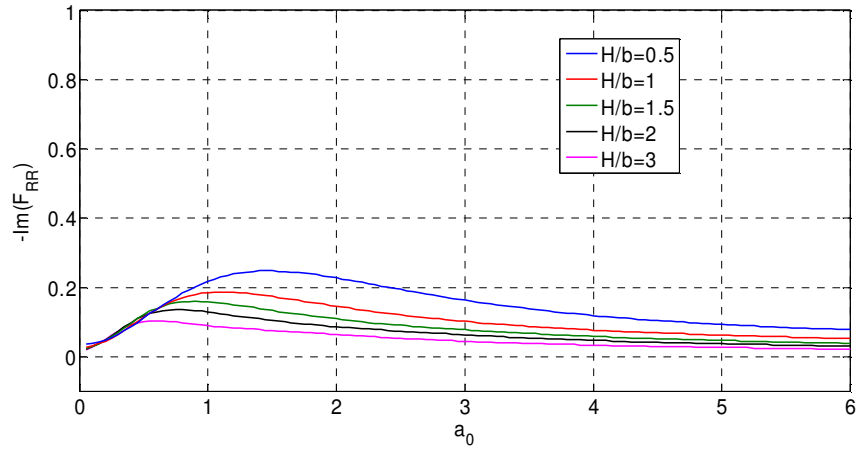
(b)

Figure 4.38: Dynamic rocking compliance coefficients of embedded rigid strip foundation on the HS with various depths of embedment for (a) real and (b) imaginary parts (*L=3b/2, h=3b/2, L_{PML}=b, b=1, G=1, υ=0.25*, and *ζ=5%*)

4.5 DIRECT TIME DOMAIN PML EQUATIONS OF ELASTODYNAMICS FOR PLANE STRAIN PROBLEMS

To carry out the PML analysis of a plane strain problem directly in the time domain, its PML equations written in frequency space in Equations 4.18-20 are to be inverted into the time space. For that Equation 4.18 is multiplied by the product of stretching functions $(\lambda_x \lambda_y)$; then, the inverse Fourier transform is applied to it, which gives (Basu, 2004),

$$
\begin{aligned}
\rho f_m \ddot{u} + \rho f_c \dot{u} + \rho f_k u &= f_{y1} \frac{\partial \sigma_{xx}}{\partial x} + f_{y2} \frac{\partial \Sigma_{xx}}{\partial x} + f_{x1} \frac{\partial \tau_{xy}}{\partial y} + f_{x2} \frac{\partial T_{xy}}{\partial y} \\
\rho f_m \ddot{v} + \rho f_c \dot{v} + \rho f_k v &= f_{y1} \frac{\partial \tau_{xy}}{\partial x} + f_{y2} \frac{\partial T_{xy}}{\partial x} + f_{x1} \frac{\partial \sigma_{yy}}{\partial y} + f_{x2} \frac{\partial \Sigma_{yy}}{\partial y}
\end{aligned}
\tag{4.38}
$$

where, Σ and T are respectively integrated normal and shear stresses defined by

$$
\Sigma = \int_0^t \sigma(\xi) d\xi \quad , \quad T = \int_0^t \tau(\xi) d\xi
\tag{4.39}
$$

The coefficients in Equation 4.38 are defined as

$$
\begin{aligned}
f_{x1} &= (1 + f^e(x)) \\
f_{x2} &= (\frac{f^p(x)v_s}{b}) \\
f_{y1} &= (1 + f^e(y)) \\
f_{y2} &= (\frac{f^p(y)v_s}{b}) \\
f_m &= f_{x1} f_{y1} \\
f_c &= f_{x1} f_{y2} + f_{x2} f_{y1} \\
f_k &= f_{x2} f_{y2}
\end{aligned}
\tag{4.40}
$$

where the stretching functions are assumed to have the forms

$$\lambda_x(x) = 1 + f_x^e(x) + \frac{f_x^p(x)}{ia_0}$$

$$\lambda_y(y) = 1 + f_y^e(y) + \frac{f_y^p(y)}{ia_0}$$
(4.41)

Next, the three strain-displacement relations in Equation 4.20 are multiplied by $i\omega\lambda_x\lambda_x$, $i\omega\lambda_y\lambda_y$ and $i\omega\lambda_x\lambda_y$, respectively. After the inversion, the strain displacement relations become (Basu, 2004),

$$f_{x1}^2\dot{\varepsilon}_{xx} + 2f_{x1}f_{x2}\varepsilon_{xx} + f_{x2}^2 E_{xx} = f_{x1}\frac{\partial\dot{u}}{\partial x} + f_{x2}\frac{\partial u}{\partial x}$$
(4.42a)

$$f_{y1}^2\dot{\varepsilon}_{yy} + 2f_{y1}f_{y2}\varepsilon_{yy} + f_{y2}^2 E_{yy} = f_{y1}\frac{\partial\dot{v}}{\partial y} + f_{y2}\frac{\partial v}{\partial y}$$
(4.42b)

$$f_{x1}f_{x2}\dot{\varepsilon}_{xy} + f_c\varepsilon_{xy} + f_{x2}f_{y2}E_{xy} = \frac{1}{2}\left[f_{x1}\frac{\partial\dot{u}}{\partial y} + f_{x2}\frac{\partial u}{\partial y} + f_{y1}\frac{\partial\dot{v}}{\partial x} + f_{y2}\frac{\partial v}{\partial x}\right]$$
(4.42c)

where $E_{ij}(i,j = x,y)$ are integrated strains defined by

$$E_{ij} = \int_0^t \varepsilon_{ij}(\xi)d\xi \quad (i,j = x,y)$$
(4.43)

Finite difference formulas for strain rates and time integrals of strains are

$$\dot{\varepsilon}^{n+1} = \frac{\varepsilon^{n+1} - \varepsilon^n}{\Delta t}$$

$$E^{n+1} = \int_0^{t_{n+1}} \varepsilon_{ij}(\xi)d\xi = E^n + \varepsilon^{n+1}\Delta t$$
(4.44)

Writing Equations 4.42 at $t=t_{n+1}=(n+1)\Delta t$ and using Equations 4.44 in them, one obtains

114

$$\varepsilon_{xx}^{n+1} = \left(\beta_1\right)^{-1}\left(f_{x1}\frac{\partial \dot{u}^{n+1}}{\partial x} + f_{x2}\frac{\partial u^{n+1}}{\partial x} + \frac{f_{x1}^2}{\Delta t}\varepsilon_{xx}^n - f_{x2}^2 E_{xx}^n\right) \tag{4.45a}$$

$$\varepsilon_{yy}^{n+1} = \left(\beta_2\right)^{-1}\left(f_{y1}\frac{\partial \dot{v}^{n+1}}{\partial y} + f_{y2}\frac{\partial v^{n+1}}{\partial y} + \frac{f_{y1}^2}{\Delta t}\varepsilon_{yy}^n - f_{y2}^2 E_{yy}^n\right) \tag{4.45b}$$

$$\begin{aligned}\varepsilon_{xy}^{n+1} = \left(\beta_3\right)^{-1}\frac{1}{2}(&f_{x1}\frac{\partial \dot{u}^{n+1}}{\partial y} + f_{x2}\frac{\partial u^{n+1}}{\partial y} + f_{y1}\frac{\partial \dot{v}^{n+1}}{\partial x} \\ &+ f_{y2}\frac{\partial v^{n+1}}{\partial x} + \frac{2f_m}{\Delta t}\varepsilon_{xy}^n - 2f_k E_{xy}^n)\end{aligned} \tag{4.45c}$$

where, the β coefficients are defined by

$$\begin{aligned}\beta_1 &= \left[\Delta t\left(\frac{f_{x1}}{\Delta t}+f_{x2}\right)^2\right] \\ \beta_2 &= \left[\Delta t\left(\frac{f_{y1}}{\Delta t}+f_{y2}\right)^2\right] \\ \beta_3 &= \left[\Delta t\left(\frac{f_{x1}}{\Delta t}+f_{x1}\right)\left(\frac{f_{y1}}{\Delta t}+f_{y2}\right)\right]\end{aligned} \tag{4.46}$$

The soil medium is generally represented by a homogenous, isotropic and elastic or visco-elastic material. Two parameter Kelvin model or also called Voigt model is usually used to simulate visco-elastic behavior of the soil. For this model, the complex elastic modulus $\tilde{E}$ and shear modulus $\tilde{G}$ are expressed as

$$\begin{aligned}\tilde{E} &= E\left(1+2ia_0\zeta\right) \\ \tilde{G} &= G\left(1+2ia_0\zeta\right)\end{aligned} \tag{4.47}$$

With use Kelvin model, the stress-strain relation becomes, in frequency space,

$$\sigma = \left(1+2ia_0\zeta\right)D\varepsilon \tag{4.48}$$

After the inversion, the stress-strain relation takes the form

$$\sigma_{xx} = D_{11}\varepsilon_{xx} + D_{12}\varepsilon_{yy} + \left(\frac{2b\zeta}{v_s}\right)\left(D_{11}\dot{\varepsilon}_{xx} + D_{12}\dot{\varepsilon}_{yy}\right)$$

$$\sigma_{yy} = D_{12}\varepsilon_{xx} + D_{22}\varepsilon_{yy} + \left(\frac{2b\zeta}{v_s}\right)\left(D_{12}\dot{\varepsilon}_{xx} + D_{22}\dot{\varepsilon}_{yy}\right) \qquad (4.49)$$

$$\tau_{xy} = 2D_{33}\varepsilon_{xy} + \left(\frac{2b\zeta}{v_s}\right)(2D_{33}\dot{\varepsilon}_{xy})$$

Time integrations of the above equations, up to the current time t give

$$\Sigma_{xx} = D_{11}E_{xx} + D_{12}E_{yy} + \left(\frac{2b\zeta}{v_s}\right)\left(D_{11}\varepsilon_{xx} + D_{12}\varepsilon_{yy}\right)$$

$$\Sigma_{yy} = D_{12}E_{xx} + D_{22}E_{yy} + \left(\frac{2b\zeta}{v_s}\right)\left(D_{12}\varepsilon_{xx} + D_{22}\varepsilon_{yy}\right) \qquad (4.50)$$

$$T_{xy} = 2D_{33}E_{xy} + \left(\frac{2b\zeta}{v_s}\right)(2D_{33}\varepsilon_{xy})$$

Writing Equations 4.49-50 at $t=t_{n+1}$ and using Equations 4.44 in them, one gets

$$\sigma_{xx}^{n+1} = \left(1 + \frac{2b\zeta}{v_s\Delta t}\right)(D_{11}\varepsilon_{xx}^{n+1} + D_{12}\varepsilon_{yy}^{n+1}) - \left(\frac{2b\zeta}{v_s\Delta t}\right)\left(D_{11}\varepsilon_{xx}^{n} + D_{12}\varepsilon_{yy}^{n}\right)$$

$$\sigma_{yy}^{n+1} = \left(1 + \frac{2b\zeta}{v_s\Delta t}\right)(D_{12}\varepsilon_{xx}^{n+1} + D_{22}\varepsilon_{yy}^{n+1}) - \left(\frac{2b\zeta}{v_s\Delta t}\right)\left(D_{12}\varepsilon_{xx}^{n} + D_{22}\varepsilon_{yy}^{n}\right) \qquad (4.51)$$

$$\tau_{xy}^{n+1} = \left(1 + \frac{2b\zeta}{v_s\Delta t}\right)(2D_{33}\varepsilon_{xy}^{n+1}) - \left(\frac{2b\zeta}{v_s\Delta t}\right)(2D_{33}\varepsilon_{xy}^{n})$$

$$\Sigma_{xx}^{n+1} = (D_{11}E_{xx}^{n} + D_{12}E_{yy}^{n}) + \Delta t \left(1 + \frac{2b\zeta}{v_s \Delta t}\right)\left(D_{11}\varepsilon_{xx}^{n+1} + D_{12}\varepsilon_{yy}^{n+1}\right)$$

$$\Sigma_{yy}^{n+1} = (D_{12}E_{xx}^{n} + D_{22}E_{yy}^{n}) + \Delta t \left(1 + \frac{2b\zeta}{v_s \Delta t}\right)\left(D_{12}\varepsilon_{xx}^{n+1} + D_{22}\varepsilon_{yy}^{n+1}\right) \qquad (4.52)$$

$$T_{xy}^{n+1} = (2D_{33}E_{xy}^{n}) + \Delta t \left(1 + \frac{2b\zeta}{v_s \Delta t}\right)(2D_{33}\varepsilon_{xy}^{n+1})$$

Finally, inserting Equations 4.45 into Equations 4.51 and 4.52, and substituting the resulting equations into Equation 4.38 at $t=t_{n+1}$, the following equation is obtained in matrix form:

$$\underbrace{\begin{bmatrix} M_{11} & 0 \\ 0 & M_{22} \end{bmatrix}}_{M}\begin{bmatrix} \ddot{u}^{n+1} \\ \ddot{v}^{n+1} \end{bmatrix} + \underbrace{\begin{bmatrix} C_{11} & C_{12} \\ C_{21} & C_{22} \end{bmatrix}}_{C}\begin{bmatrix} \dot{u}^{n+1} \\ \dot{v}^{n+1} \end{bmatrix} + \underbrace{\begin{bmatrix} K_{11} & K_{12} \\ K_{21} & K_{22} \end{bmatrix}}_{K}\begin{bmatrix} u^{n+1} \\ v^{n+1} \end{bmatrix} = \underbrace{\begin{bmatrix} F_1 \\ F_2 \end{bmatrix}}_{F} \qquad (4.53)$$

where

$$M_{11} = \rho f_m \qquad (4.54a)$$

$$M_{22} = \rho f_m \qquad (4.54b)$$

$$C_{11} = \rho f_c - A_1 \frac{\partial^2}{\partial x^2} - A_2 \frac{\partial}{\partial x} - A_3 \frac{\partial^2}{\partial y^2} - A_4 \frac{\partial}{\partial y} \qquad (4.54c)$$

$$C_{12} = -A_5 \frac{\partial^2}{\partial x \partial y} - A_6 \frac{\partial^2}{\partial x \partial y} - A_7 \frac{\partial}{\partial y} \qquad (4.54d)$$

$$C_{21} = -B_1 \frac{\partial^2}{\partial x \partial y} - B_2 \frac{\partial}{\partial y} - B_3 \frac{\partial^2}{\partial x \partial y} \qquad (4.54e)$$

$$C_{22} = \rho f_c - B_4 \frac{\partial^2}{\partial x^2} - B_5 \frac{\partial}{\partial x} - B_6 \frac{\partial^2}{\partial y^2} - B_7 \frac{\partial}{\partial y} \qquad (4.54f)$$

$$K_{11} = \rho f_k - A_8 \frac{\partial^2}{\partial x^2} - A_9 \frac{\partial}{\partial x} - A_{10} \frac{\partial}{\partial y} - A_{11} \frac{\partial^2}{\partial y^2} \qquad (4.54g)$$

$$K_{12} = -A_{12} \frac{\partial^2}{\partial x \partial y} - A_{13} \frac{\partial}{\partial x} - A_{14} \frac{\partial^2}{\partial x \partial y} \qquad (4.54h)$$

117

$$K_{21} = -B_8 \frac{\partial}{\partial y} - B_9 \frac{\partial^2}{\partial x \partial y} - B_{10} \frac{\partial^2}{\partial x \partial y}$$

<div align="right">(4.54i)</div>

$$K_{22} = \rho f_k - B_{11} \frac{\partial^2}{\partial x^2} - B_{12} \frac{\partial}{\partial x} - B_{13} \frac{\partial^2}{\partial y^2} - B_{14} \frac{\partial}{\partial y}$$

<div align="right">(4.54j)</div>

$$F_1 = \left(A_{15} \frac{\partial}{\partial x} + A_{16} \right) \varepsilon_{11}^n + \left(A_{17} \frac{\partial}{\partial x} - A_{18} \right) E_{11}^n + A_{19} \frac{\partial \varepsilon_{22}^n}{\partial x} + A_{20} \frac{\partial E_{22}^n}{\partial x}$$

$$+ \left(A_{21} + A_{22} \frac{\partial}{\partial y} \right) \varepsilon_{21}^n + \left(A_{24} \frac{\partial}{\partial y} - A_{23} \right) E_{21}^n$$

<div align="right">(4.54k)</div>

$$F_2 = \left(B_{15} + B_{16} \frac{\partial}{\partial x} \right) \varepsilon_{21}^n - \left(B_{18} \frac{\partial}{\partial x} - B_{17} \right) E_{11}^n + B_{19} \frac{\partial \varepsilon_{11}^n}{\partial y} + B_{20} \frac{\partial E_{11}^n}{\partial y}$$

$$+ \left(B_{21} + B_{22} \frac{\partial}{\partial y} \right) \varepsilon_{22}^n - \left(B_{23} - B_{24} \frac{\partial}{\partial y} \right) E_{21}^n$$

<div align="right">(4.54l)</div>

The definitions of the coefficients A_1 to A_{24} and B_1 to B_{24} in the above equations are presented in Appendix B .

It is obvious that Equation 4.53 involves both time and space integrations; therefore its time integrations can be performed by using the usual methods, such as Newmark's direct integration methods (see Appendix A), Runge Kutta's methods (Bogacki and Shampine (1989)), etc.; on the other hand, its space integration can be carried out by FEM or FDM or GFDM.

4.5.1 NUMERICAL RESULTS FROM TIME DOMAIN ANALYSIS

In this part, the response of the strip foundation on elastic or viscoelastic HS (see Figure 4.1) subjected to two different prescribed displacements $u_0(t)$ is determined by the time domain PML analysis and the results are compared with those of FEM and BEM. To integrate the GFD equations with respect to time MATLAB ode12 solver is preferred and used (Bogacki and Shampine (1989)) together with distance type algorithm having cubic spline weighting function. For the time integration of the FEM, Newmark algorithm is used. The order of attenuation function m is chosen two, and its strength as f_0=8 for GFDM; however, for FEM

<div align="center">118</div>

m and f_0 are selected as one and ten respectively. BEM results are first obtained in frequency space and then inverted into time space.

The time variation of two types of the imposed displacement $u_0(t)$, considered in the analyses, are assumed to be given by Equations 3.47 and 3.48.

The analyses results are used to compare the dynamic reaction forces for a rigid strip foundation on HS calculated by GFDM and the other above mentioned methods. The results are displayed in Figures. 4.39-4.44. In the analyses of all considered methods, the soil properties are chosen as, in some suitable units, *G=1, υ=0.25, ρ=1, ζ=5%*.

Figures 4.39-4.42 indicate that the results calculated using GFDM with PML are generally in good agreement with those obtained from other methods.
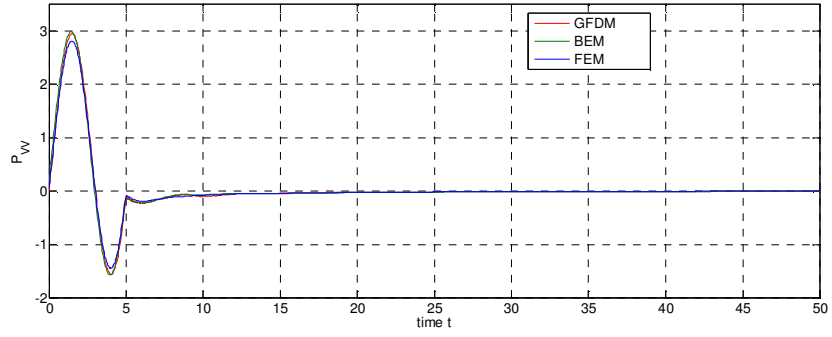
(a)
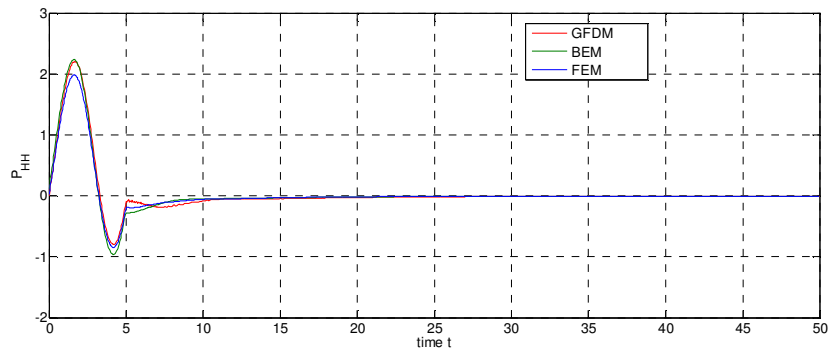
(b)
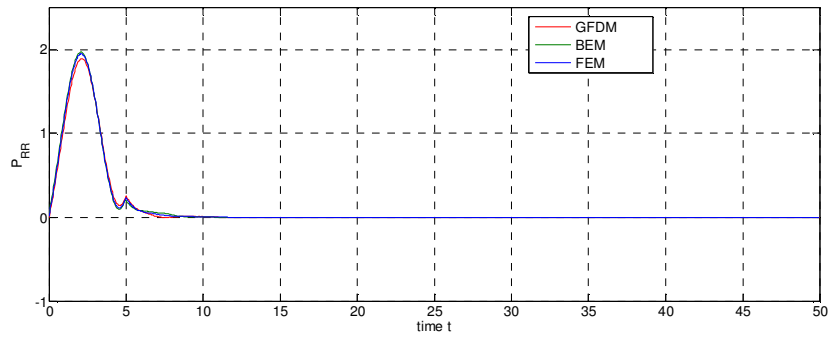
(c)

Figure 4.39: Reactions of rigid strip foundation on elastic HS for (a) vertical (b) horizontal and (c) rocking due to type 1 (Wolf, 1988) prescribed displacement ($t_0=5$) ($L=3b/2$, $h=b/2$, $L_{PML}=b$, $b=1$, $G=1$, $\rho=1$, $\upsilon=0.25$ and $\zeta=0\%$).
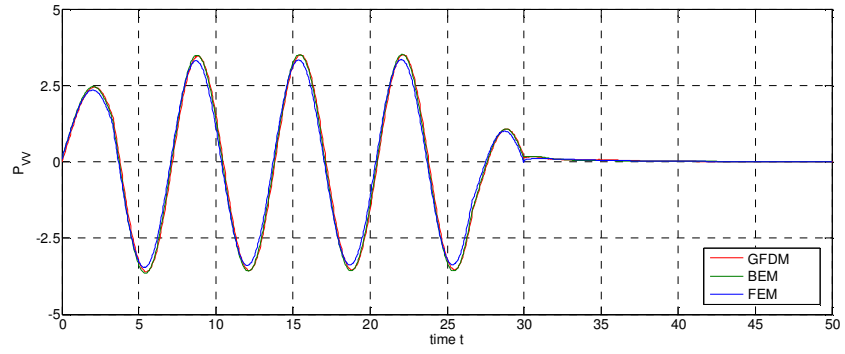
(a)
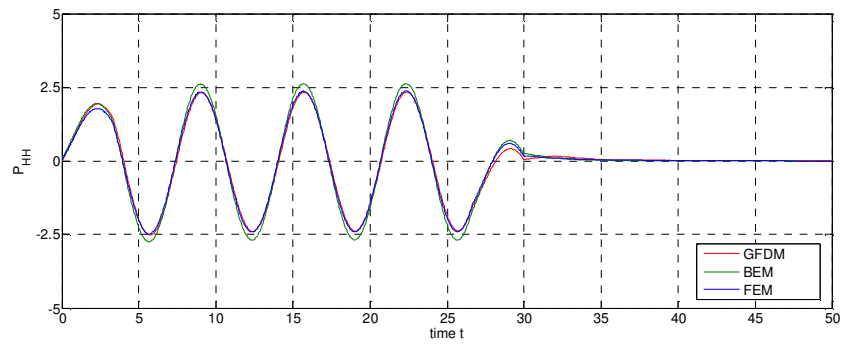
(b)
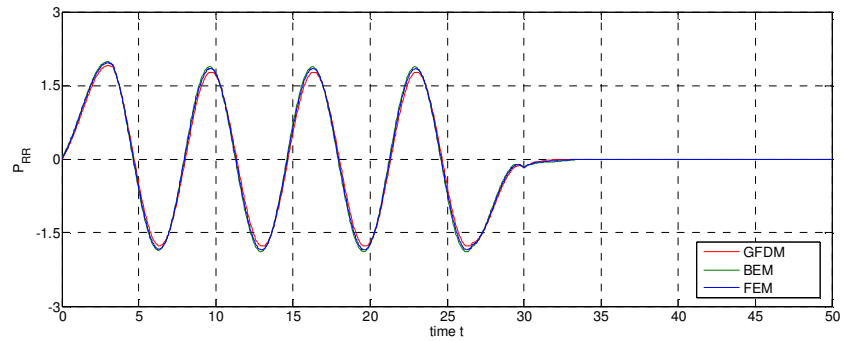
(c)

Figure 4.40: Reactions of rigid strip foundation on elastic HS for (a) vertical (b) horizontal and (c) rocking due to type 2 (Basu, 2004) prescribed displacement ($nc=4$, $td=20$, $\omega_f=1.0$), ($L=3b/2$, $h=b/2$, $L_{PML}=b$, $b=1$, $G=1$, $\rho=1$, $\upsilon=0.25$ and $\zeta=0\%$).
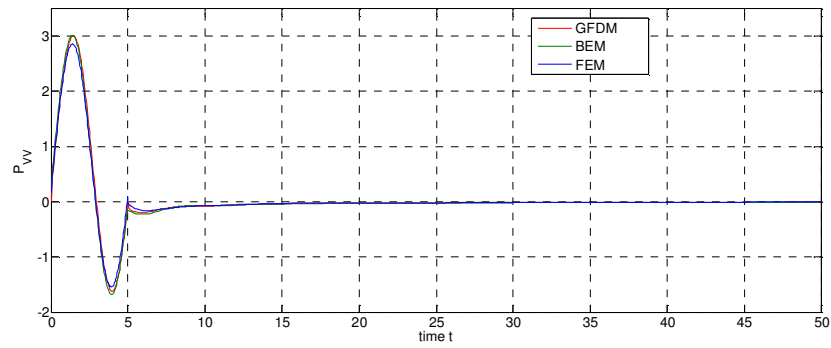
(a)
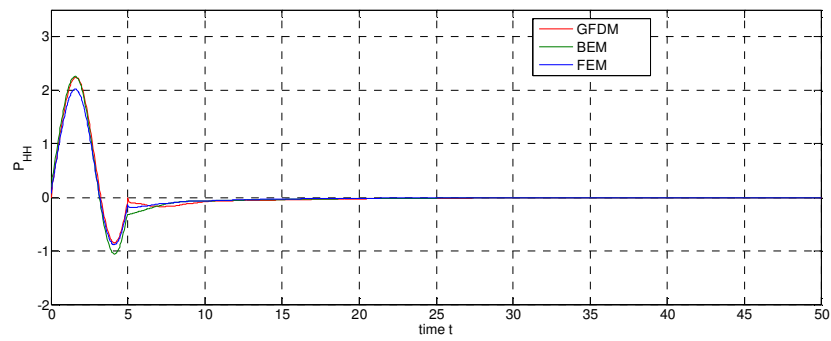
(b)
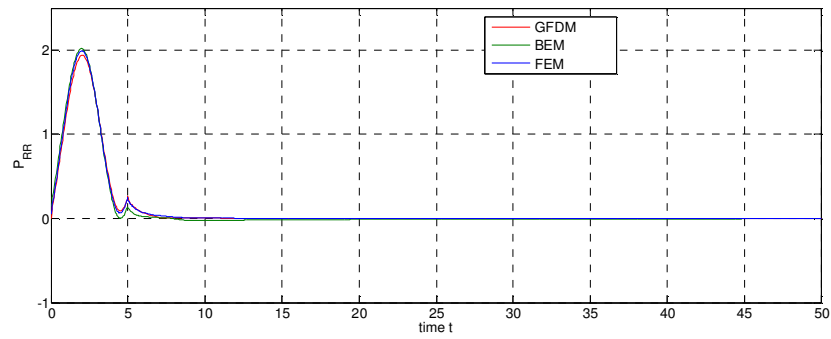
(c)

Figure 4.41: Reactions of rigid strip foundation on visco-elastic HS for (a) vertical (b) horizontal and (c) rocking due to type 1 (Wolf, 1988) prescribed displacement ($t_0=5$) ($L=3b/2$, $h=b/2$, $L_{PML}=b$, $b=1$, $G=1$, $\rho=1$, $\upsilon=0.25$ and $\zeta=5\%$).
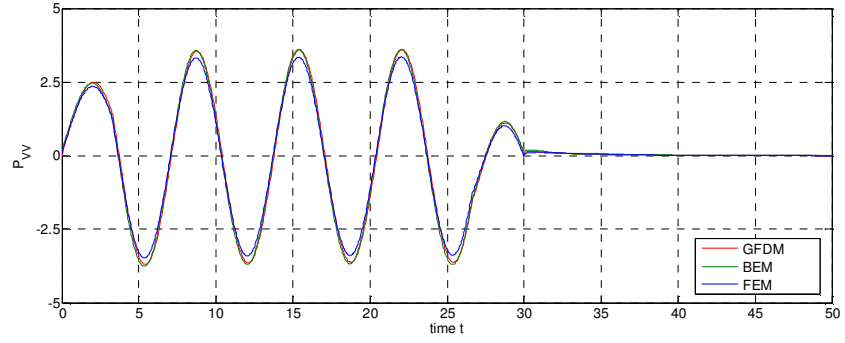
(a)
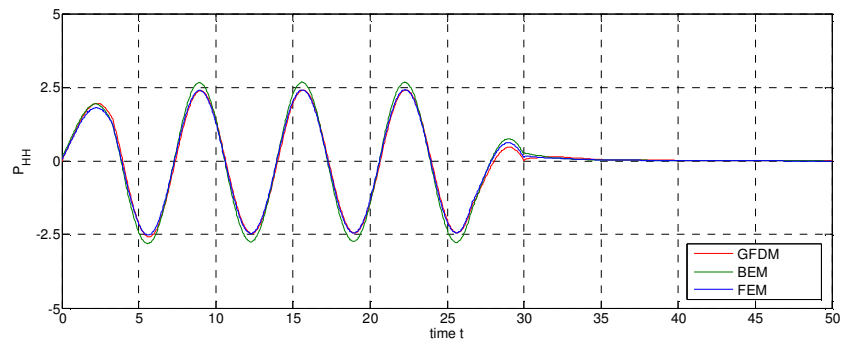
(b)
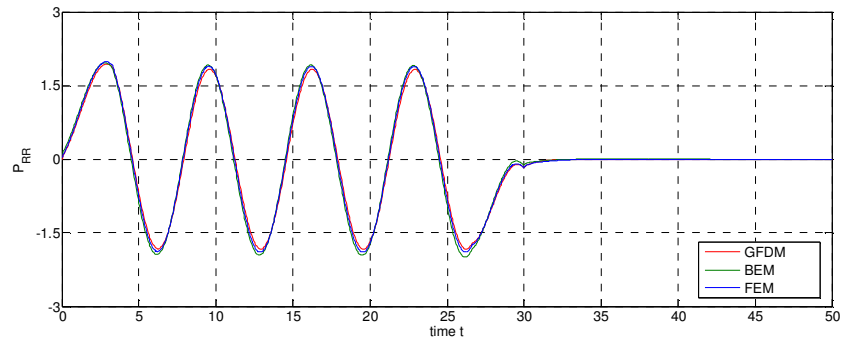
(c)

Figure 4.42: Reactions of rigid strip foundation on visco-elastic HS for (a) vertical (b) horizontal and (c) rocking due to type 2 (Basu, 2004) prescribed displacement (*nc=4, td=20, ω_f=1.0*), (*L=3b/2, h=b/2, L_{PML}=b, b=1, G=1, ρ=1, υ=0.25* and *ζ=5%*).

123

CHAPTER 5

CONCLUSION AND DISCUSSION

In this thesis work, based on GFDM, a formulation is presented for the PML analysis of the problems in wave mechanics. The appropriate choices of the parameter appearing in GFDM and PML are made through the use of parametric studies carried out for some benchmark problems. The proposed formulation is appraised by applying it to the compliance of surface foundation and embedded rigid strip footing supported by a soil foundation. The surface foundation is considered having various configurations: uniform HS, soil layer on rigid bedrock and soil layer on uniform HS. The embedded foundation is considered only when the supporting soil medium is HS. Direct time domain analyses are also performed only for a surface rigid strip foundation on uniform HS. The findings and observations drawn from the study are summarized below.

1. The parametric study which is conducted to determine proper weighting function for distance type and quadrant type GFDM algorithms reveals that using the quartic spline weighting function in the case of distance type algorithm leads to better results. However, using cubic distance weighting function for quadrant type algorithm results in less global error.

2. The parametric study is conducted to determine the effective PML parameters. The results obtained from PML analyses are found to be improved with the increasing number of nodes in GFDM. In addition, PML results are found to be very sensitive to low frequencies. Moreover, linear attenuation function (m=1) is not recommended for PML analyses with GFDM. The reasonable computational

cost is achieved when the thickness of PML is chosen between two and four times of the computational length.

3. The compliance functions are found for rigid strip foundation using GFDM with unsplit PML in frequency domain. The results obtained from this method are compared to those obtained from FEM with unsplit PML and BEM. The compliance functions obtained from GFDM with unsplit PML are found to be comparable with these methods.

4. The compliance functions are also found for rigid strip foundation using GFDM with unsplit PML in time domain. The results obtained from this method are compared to those obtained from FEM with unsplit PML and BEM. The compliance functions obtained from GFDM with unsplit PML are found to be comparable with these methods.

5. GFDM with unsplit PML is generalized in Appendix C for the analyses of problems with arbitrary geometry of truncation region (see Figure C.2). This generalization is important since choosing a particular geometry for PML suitable for the problem under consideration, instead of choosing it as parallel to coordinate axes, maybe needed to decrease the size of analysis region, thus, to reduce the computational cost of PML analysis (for illustrations, see Figure C.2-4).

6. A procedure to perform the PML analysis directly in complex domain, instead of in real domain, is proposed in Appendix D. This approach of the analysis has some advantages over that of real domain analysis:

a) Complex domain PML analysis can be carried out in a homogenous complex domain by keeping the original form of the governing equations together with their symmetry properties.

b) It handles properly the problems arising from the corner points which may appear on truncation boundary. To explain this point, Figure 5.1 will be referred

to, which shows a wedge region of PML associated with a corner (discontinuity) point on truncation boundary. When real domain PML analysis is used, there would be an ambiguity about the selection of the stretching function λ_x and λ_y in the wedge region. On the other hand, the use of the complex domain approach in PML analysis would eliminate this ambiguity; in fact, in the case, the complex nodal point coordinates along the radial directions emanating from the corner point in wedge region (see Figure 5.1) can be generated by using Equation D.7.

The implementation of complex domain PML analysis will be subject of a future work.
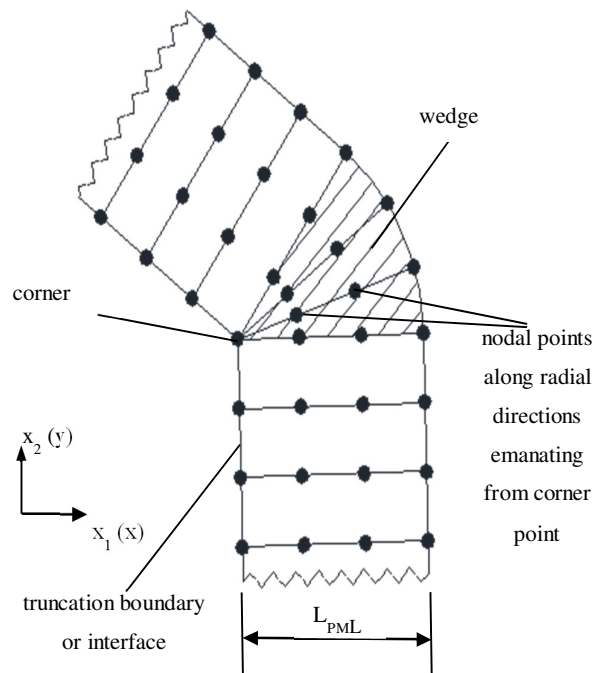
Figure 5.1: Description of wedge region for complex domain PML analysis

7. In this study, GFDM is compared to other numerical methods. The advantages and disadvantages of GFDM are concluded as:

a) Implementation of GFDM for unsplit real and complex domain PML analysis is straigthforward and simpler compared to FEM. The method is also applicable for arbitrary geometry and non-uniform node distribution. Implementation of all type BC is easy. The method enables to more accurate results when using higher order TS expansion, finer mesh, appropriate weighting function and radius of influence. Element transformation, gauss integration and knowledge of connectivity does not required in this method.

b) However, the matrices in GFDM is not banded, ill-condition may be observed in the case of improper node selection and near boundary points.

REFERENCES

Abascal, R., Dominguez, J., (1984) "Dynamic Behavior of Strip Footing on Non-homogenous Viscoelastic Soils" Proceeding of the International Symposium on Dynamic Soil-Structure Interaction, Minneapolis, pp.25-36, A.A. Balkema Publication

Achenbach, J.D., (l973) "Wave Propagation in Elastic Solids" Elsevier Science Publisher, New York, NY, USA

Ahmad, S., Israil, A.S.M., (1988) "Dynamic Compliance of Vertically Loaded Strip Foundations in Multilayered Viscoelastic Soils" Technical Report NCEER-88-0017, State University of New York at Buffalo, Buffalo, USA

Ahmad, S., Israil, A.S.M., (1989) "Dynamic Vertical Compliance Strip Foundations in Layered Soils" Earthquake Engineering and Structural Dynamics, Vol.18, pp.933-950, John Wiley & Sons, Ltd.

Ahmad, S., Bharadwaj, A., (1991) "Horizontal Impedance of Embedded Strip Foundations in Layered Soil" Journal of Geotechnical Engineering, ASCE, Vol.117, No.7, pp.1021-1041

Ahmad, S., Bharadwaj, A., (1992) "Rocking Impedance of Embedded Strip Foundations in Layered Soil" Journal of Geotechnical Engineering, Vol.118, No.5, pp.796-813, ASCE

Appelö, D., Kreiss G., (2006) "A New Absorbing Layer for Elastic Waves" Journal of Computational Physics, Vol.215, pp.642-660

Apsel, R.J., Luco, J.E., (1987) "Impedance Functions for Foundations Embedded in a Layered Medium: an Integral Equation Approach" Earthquake Engineering and Structural Dynamics, Vol.15, pp.213-231, John Wiley & Sons, Ltd.

Basu U., Chopra A.K., (2002) "Perfectly Matched Layers for Transient Elastodynamics of Unbounded Domains" University of California Berkeley Report No: UCB/SEMM-2002/13

Basu U., Chopra A.K., (2003) "Perfectly Matched Layers for time-harmonic elastodynamics of unbounded domains: theory and finite-element implementation" Computer Methods in Applied Mechanics and Engineering. Vol.192, pp.1337-1375

Basu U., (2004) "Perfectly Matched Layers for Acoustic and Elastic Waves: Theory, Finite-Element Implementation and Application to Earthquake Analysis of Dam-Water-Foundation Rock Systems" Ph.D. thesis, University of California, Berkeley, CA, USA

Basu U., (2009) "Explicit finite element perfectly matched layer for transient three-dimensional elastic waves" International Journal of Numerical Methods in Engineering, Vol.77, pp.151-176

Belytschko, T., Lu, Y.Y., Gu, L., (1994) "Element Free-Galerkin Methods" International Journal of Numerical Methods in Engineering, Vol.37, pp.229-256

Benito, J.J., Urena, F., Gavete, L., (2001) "Influence of Several Factors in the Generalized Finite Difference Method" Applied Mathematical Modeling, Vol.25, pp.1039-1053

Benito, J.J., Urena, F., Gavete, L., Alvarez, R., (2003) "An h-Adaptive Method in the Generalized Finite Differences" Computer Methods in Applied Mechanics and Engineering, Vol.192, pp.735-759

Benito, J.J., Urena, F., Gavete, L., (2007) "Solving Parabolic and Hyperbolic Equations by the Generalized Finite Difference Method" Journal of Computational and Applied Mathematics, Vol.209, pp.208-233

Berenger, J.P., (1994) "A Perfectly Matched Layer for the Absorption of Electromagnetic Waves" Journal of Computational Physics, Vol.114, pp.185-200

129

Berenger, J.P., (1996) "Three-Dimensional Perfectly Matched Layer for the Absorption of Electromagnetic Waves" Journal of Computational Physics, Vol.127, pp.363-379

Berenger, J.P., (2007) "Perfectly Matched Layer (PML) for Computational Electromagnetics," Morgan & Claypool Publishers

Bogacki, P., Shampine, L.F., (1989) "A 3(2) Pair of Runge-Kutta Formulas" Applied Mathematics Letters, Vol.2, pp.1-9

Chang-Liang, V., (1974) "Dynamic Response of Structures in Layered Soils" Ph.D. thesis, MIT, Cambridge, Mass. USA

Chew, W.C., Weedon, W.H., (1994) "A 3-D Perfectly Matched Medium from Modified Maxwell Equations with Stretching Coordinates" Microwave and Optical Technology Letters, Vol.7 (13), pp.599-604

Chew, W.C., Liu, Q.H., (1996) "Perfectly Matched Layers for Elastodynamics: A New Absorbing Boundary Condition" Journal of Computational Acoustics, Vol.4, pp.72-79

Chew, W.C., Jin, J.M., Michielssen, E., (1997) "Complex Coordinate Stretching as a Generalized Absorbing Boundary Condition" Microwave and Optical Technology Letters, Vol.15, pp.363-369

Clayton, R., Engquist, B., (1977) "Absorbing Boundary Conditions for Acoustic and Elastic Wave Equations" BSSA, Vol.67 (6), pp.1529-1540

Collino, F., Monk, P.B., (1996) "The Perfectly Matched Layer in Curvilinear Coordinates" SIAM Journal on Scientific. Computing, Vol.19, pp.2061-2090

Collino, F., Monk, P.B. (1998) "Optimizing the Perfectly Matched" Computer Methods in Applied Mechanics and Engineering, Vol.164, pp.157-171

130

Collino, F., Tsogka C., (2001) "Application to Perfectly Matched Absorbing Layer Model to the Linear Elastodynamics Problem in Anisotropic Heterogeneous Media" Geophysics, Vol.66 (1), pp.294-307

Cruse, T.A., Rizzo, F.J., (1968) "A Direct Formulation and Numerical Solution of the General Transient Elastodynamics Problem I" Journal of Mathematical Analysis and Applications, Vol. 22, pp.244-259

Day, S.M., (1977) "Finite Element Analysis of Seismic Scattering Problems" Ph.D. thesis, University of California, San Diego, CA, USA

Dominguez, J., Roesset, J.M. (1978) "Dynamic Stiffness of Rectangular Foundations" Research Report: R78-20, MIT, Cambridge, Mass., USA

Engquist, B., Majda, A., (1977) "Absorbing Boundary Conditions for the Numerical Simulation of Waves" Mathematics of Computation, Vol.31, pp.629-651

Fang, J., Wu, Z., (1996) "High-Performance PML Algorithms" IEEE, Microwave and Guided Wave Letters, Vol.6 (9), pp.335-337

Festa, G., Nielsen, S., (2003) "PML Absorbing Boundaries" BSSA, Vol.93 (2), pp.891-901

Gavete, L., Gavete, M.L., Benito, J.J, (2003) "Improvements of Generalized Finite Difference Method and Comparison with other Meshless Method" Applied Mathematical Modeling, Vol.27, pp.831-847

Gazetas, G., (1975) "Dynamic Stiffness Functions of Strip and Rectangular Footing on Layered Soil" S.M. thesis, MIT, Cambridge, Mass., USA

Gazetas, G., Roesset, J.M., (1979) "Vertical Vibration of Machine Foundations" Journal of the Geotechnical Engineering. Division, ASCE, Vol.105, GT12, pp.1435-1454

Gazetas, G., (1983) "Analysis of Machine Foundation: State of Art" Soil Dynamics and Earthquake Engineering, Vol.2 (1), pp.2-42

Givoli, D., Keller, J.B., (1989) "Exact Non-reflecting Boundary Conditions" Journal of Computational Physics, Vol.82, pp.172-192

Givoli, D., (1991) "Non-reflecting Boundary Conditions" Journal of Computational Physics, Vol.94, pp.1-29

Givoli, D., (1992) "A Spatial Exact Non-reflecting Boundary Condition for Time Dependent Problems" Computational Methods Applied Mechanics Engineering, Vol.95, pp.97-113

Godoy, L.A., (1986) "Ill-conditioned Stars in the Finite Difference Method for Arbitrary Meshes" Computers & Structures, Vol.22, No.3, pp.469-473

Hryniewicz, Z., (1981) "Dynamic Response of a Rigid Strip on an Elastic Half-Space" Computer Methods in Applied and Mechanical Engineering, Vol.25, pp.355-364

Hall, W.S, Oliveto, G., (2003) "Boundary Element Methods for Soil-Structure Interaction" Kluwer Academic Publishers

Hasting, F.D., Schneider, J.B., Broschat, S.L., (1996) "Application of the Perfectly Matched Layer (PML) Absorbing Boundary Condition to Elastic Wave Propagation" Journal of Acoustic Society of America, Vol.100(5), pp.3061-3069

Israil, A.S.M., Banerjee, P.K., (1990) "Advanced Time-Domain Formulation of BEM for Two Dimensional Transient Elastodynamics" International Journal for Numerical Methods in Engineering, Vol.29 (7), pp.1421-1440

Jensen, P., (1972) "Finite Difference Techniques for Variable Grids" Computers & Structures, Vol.2, pp.17-29

Kang, J.E., (2010) "A Mixed Unsplit-Field PML–Based Scheme for Full Waveform Inversion in the Time-Domain Using Scalar Wave" Ph.D. thesis, University of Texas at Austin, TX, USA

Karadushi, P., Keer, L.M., Lee, S.L., (1968) "Vibratory Motion of Body on an Elastic Half-Plane" Journal of Applied Mechanics, ASME, Vol.35, Series E, No.4, pp.697-705

Kausel, E., (1974) "Forced Vibrations of circular Foundations on Layered Media" Ph.D. thesis, MIT, Cambridge, Mass., USA

Kausel, E., Tassoulas, J.L., (1981) "Transmitting Boundaries: A Closed-Form Comparison" BSSA, Vol.71 (1), pp.143-159

Komatitsch, D., Tromp, J., (2003) "A Perfectly Matched Layer Absorbing Boundary Condition for Second-Order Seismic Wave Equation" Geophysics, Vol.154, pp.146-153

Kuhlemeyer, R., (1969) "Vertical Vibrations of Footing Embedded in Layered Media" Ph.D. thesis, University of California, Berkeley, CA, USA

Kuzuoğlu, M., Mittra, R., (1996) "Frequency Dependence of the Constitutive Parameters of Casual Perfectly Matched Anisotropic Absorbers" IEEE, Microwave and Guided Wave Letters, Vol.6 (12), pp.447-449

Kuzuoğlu, M., Mittra, R., (1997) "Investigation of Nonplanar Perfectly Matched Absorbers for Finite Element Mesh Truncation" IEEE Transactıons on Antennas and Propagatıon., Vol.45(3), pp.474-486

Küçükçoban, S., (2010) "The Inverse Medium Problem in PML-Truncated Elastic Media" Ph.D. thesis, University of Texas at Austin, TX, USA

Lehmann, L., (2007) "Wave Propagation in Infinite Domains with Applications to Structure Interaction" Lecture Notes in Applied and Computational Mechanics, Volume 31, Springer

Li, S., Liu, W.K., (2004) "Meshfree Particle Methods" Springer

Liszka, T., Orkisz, J., (1977) "Finite Difference Method at Arbitrary Irregular Meshes and its Application in Nonlinear Problems of Applied Mechanics" In IV SMiRt, San Francisco, CA, USA

Liszka, T., Orkisz, J., (1980) "The Finite Difference Method at Arbitrary Irregular Grids and its Application in Applied Mechanics" Computers & Structures, Vol.11, pp.83-95

Liszka, T., (1984) "An Interpolation Method for an Irregular Net of Nodes" International Journal for Numerical Methods in Engineering, Vol.20, pp.1599-1612

Liu, Q.H., (1999) "Perfectly Matched Layers for Elastic Waves in Cylindrical and Spherical Coordinates" Journal of the Acoustical Society of America, Vol.105 (4), pp.2075-2084

Luco, J.E., (1969) "Application of Singular Integral Equations to the Problem of Forced Vibrations of a Rigid Foundation" Ph.D. thesis, University of California, Los Angeles

Luco, J.E., Westmann, R.A., (1972) "Dynamic Response of a Rigid Footing Bonded to an Elastic Half Space" Journal of Applied Mechanics, ASME, Vol.39, Issue 2, pp.527-534

Lucy, L.B., (1977) "A Numerical Approach to the Testing of the Fission Hypothesis" Astronomical Journal, Vol.82, pp.1013-1024

Lysmer, J., Kuhlemeyer, R.L, (1969) "Finite Dynamic Model for Infinite Media" Journal of the Engineering Mechanics Division, ASCE, Vol.95, pp.859-877

Lysmer, J., Waas, G., (1972) "Shear Waves in Plane Infinite Structures" Journal of the Engineering Mechanics Division, ASCE, Vol.98, pp.85-105

Lysmer, J., (1978) "Analytical Procedures in Soil Dynamics" EERC Report: UCB/EERC-78-29, University of California, Berkeley, CA, USA

Mengi,Y., Tanrikulu, A.H., Tanrikulu, A.K., (1994) 'Boundary Element Method for Elastic Media' Orta Doğu Teknik Üniversitesi Yayinlari, Ankara, Turkey

Ma, S., Liu, P., (2006) "Modeling of the Perfectly Matched Layer Absorbing Boundaries and Intrinsic Attenuation in Explicit Finite-Element Methods" BSSA Vol.96, pp.1779-1794

Maloney, L., Kesler, M., Smith, G., (1997) "Generalization of PML to Cylindrical Geometries", Proceedings of the 13th Annual Review of Progress in Applied Computational Electromagnetics, Vol.2, pp.900-908, Montreal, Canada

Michou, F.E., Koumousis, V.K., (2005) "Absorbing Boundary Conditions and Perfect Matched Layer Models for Plane Soil-Structure Interaction Problems" 5th GRACM International Congress on Computational Mechanics, Limassol

Nayroles, B., Touzot, G., Villon, P., (1992) "Generalizing the Finite Element Method. Diffuse Approximation and Diffuse Elements" Computational Mechanics, Vol.10, pp.307-318

Newmark, N.M., (1959) "A Method of Computation for Structural Dynamics" Journal of the Engineering Mechanics Division, ASCE, Vol.85 (EM3), pp.67-94

Perrone, N., Kaos, R. (1975) "A General Finite Difference Method for Arbitrary Meshes" Computers & Structures, Vol.5, pp.45-58

Rajapakse, R.K.N.D., Shah, A.H., (1988) "Impedances of Embedded Rigid Strip Foundations" Earthquake Engineering and Structural Dynamics, Vol.16, pp.255-273

Spyrakos, C.C., Beskos, D.E., (1986) "Dynamic Response of Rigid Strip-Foundations by a Time-Domain Boundary Element Method" International Journal for Numerical Methods in Engineering, Vol.23, pp.1547-1565

Teixeira, F.L., Chew, W.C., (1997) "PML-FDTD in cylindrical and spherical grids" IEEE, Microwave and Guided Wave Letters, Vol.7 (9), pp.285-287

Tsynkov, S.V., (1998) "Numerical Solution of Problems on Unbounded Domain a Review" Applied Numerical Mathematics, Vol.27, pp.465-532

Tworzydlo, W., (1987) "Analysis of Large Deformations of Membrane Shell by the Generalized Finite Difference Method" Computers and Structures, Vol., 27(1), pp.39-59

Tzong, T., Penzien, J., (1983) "Hybrid modeling of Soil-Structure Interaction in Layered Media" Report No: UCB/EERC-83-22, University of California, Berkeley, CA, USA

Von Estorff, O., Schmid, G., (1984) "Application of the Boundary Element Method to the Analysis of the Vibration Behavior of Strip Foundations on a Soil Layer" Proceeding of the International Symposium on Dynamic Soil-Structure Interaction, Minneapolis, pp.11-17, A.A. Balkema Publication

White, W., Valliappan, S., Lee, I.K., (1977) "Unified Boundary for Finite Dynamic Models" Journal of the Engineering Mechanics Division, ASCE, Vol.103 (5), pp.949-964

Waas, G., (1972) "Linear Two-Dimensional Analyses of Soil Dynamics Problems in Semi-Infinite Layered Media" Ph.D. thesis, University of California, Berkeley, CA, USA

Wolf, J.P., (1985) "Dynamic Soil-Structure Interaction" Prentice-Hall, Englewood Cliffs, New Jersey, USA

Wolf, J.P., (1988) "Soil-Structure-Interaction Analysis in Time Domain" Prentice-Hall, Englewood Cliffs, New Jersey, USA

Wolf, J.P., Song C., (1996) "Finite-Element Modeling of Unbounded Media" John Wiley & Sons, New York, NY, USA

Wolf, J.P., (2003) "The Scaled Boundary Finite Element Method" John Wiley & Sons, New York, NY, USA

Wong, H.L., (1975) "Dynamic Soil Structure Interaction" Ph.D. thesis, California Institute of Technology, Pasadena, CA, USA

Zeng, Y.Q., He, J.Q., Liu, H.Q., (2001) "The Application of the Perfectly Matched Layer in Numerical Modeling of Wave Propagation in Poroelastic Media" Geophysics, Vol.66 (4), pp.1258-1266

Zheng, Y., Huang, X., (2002) "Anisotropic Perfectly Matched Layers for Elastic Waves in Cartesian and Curvilinear Coordinates", Earth Resources Laboratory Industry Consortium Meeting, Dept. of Earth, Atmospheric, and Planetary sciences, Massachusetts Institute of Technology, Cambridge, MA, USA

APPENDIX A

NEWMARK TIME INTEGRATION METHOD

Newmark (1959) developed a time integration method for the solution of structural dynamic problems. The method and its modified forms have been applied to the dynamic analysis for fifty years, especially in the analyses of the structures subjected to the ground excitation. This numerical integration method is used to solve equilibrium equations expressed in the following form,

$$M\ddot{u}^{n+1} + C\dot{u}^{n+1} + Ku^{n+1} = P^{n+1} \tag{A.1}$$

where the vector u contains displacements; M, C, K and P^{n+1} are respectively mass, damping, stiffness matrices, and a load vector.

In Newmark's method truncated Taylor series expansions are used for displacement and velocity and they are given below;

$$u^{n+1} = u^n + \Delta t \dot{u}^n + \frac{\Delta t^2}{2}\ddot{u}^n + \beta \Delta t^3 \dddot{u}$$
$$\dot{u}^{n+1} = u^n + \Delta t \ddot{u}^n + \gamma \Delta t^2 \dddot{u} \tag{A.2}$$

where the coefficient γ is assumed to be 1/2 in linear and average acceleration methods. However, the coefficient β is taken as 1/6 in linear, but 1/4 in average acceleration methods.

Time derivative of acceleration is obtained using finite difference expression;

$$\ddot{u} = \frac{\ddot{u}^{n+1} - \ddot{u}^n}{\Delta t} \qquad (A.3)$$

Substituting the above equation into Equations A.2 following equations are obtained

$$u^{n+1} = A^n + \beta \Delta t^2 \ddot{u}^{n+1}$$
$$\dot{u}^{n+1} = B^n + \gamma \Delta t \ddot{u}^{n+1} \qquad (A.4)$$

where

$$A^n = u^n + \Delta t \dot{u}^n + (\frac{1}{2} - \beta)\Delta t^2 \ddot{u}^n$$
$$B^n = \dot{u}^n + (1 - \gamma)\Delta t \ddot{u}^n \qquad (A.5)$$

The Equations (A.4) are then inserted into the equilibrium equations, to obtain the following formula

$$\bar{K}\ddot{u}^{n+1} = P^n \qquad (A.6)$$

$\bar{K}$ and $\bar{P}^n$ are effective stiffness matrix and effective load vector, respectively.

where

$$\bar{K} = M + C\gamma\Delta t + K\beta\Delta t^2$$
$$\bar{P}^{n+1} = P^{n+1} - CB^n - KA^n \qquad (A.7)$$

Following procedure is used in Newmark method for the calculation of acceleration, velocity and displacement for each time step:

1. First, the effective stiffness matrix is determined from Equations A.7a for initial calculation.

2. Then, the coefficients of A^n and B^n are calculated by using Equations A.5.

3. Next, the effective load vector is determined from Equations A.7b.

4. In the next step, the acceleration is evaluated from Equation A.6.

5) Finally, displacement and velocity vectors are calculated with using Equations A.4. The procedure between steps 2 and 5 is then repeated for each time step.

APPENDIX B

THE COEFFICIENTS OF EQUATIONS 4.54

$$A_1 = \frac{D_{11}\beta_4 f_{x1}}{\beta_1} \tag{B.1}$$

$$A_2 = \frac{D_{11}\beta_4}{\beta_1}\left[\frac{\partial f_{x1}}{\partial x} - \frac{f_{x1}}{\beta_1}\frac{\partial \beta_1}{\partial x}\right] \tag{B.2}$$

$$A_3 = \frac{D_{33}\beta_5 f_{x1}}{\beta_3} \tag{B.3}$$

$$A_4 = -\frac{D_{33}\beta_5 f_{x1}}{(\beta_3)^2}\frac{\partial \beta_3}{\partial y} \tag{B.4}$$

$$A_5 = \frac{D_{12}\beta_4 f_{y1}}{\beta_2} \tag{B.5}$$

$$A_6 = \frac{D_{33}\beta_5 f_{y1}}{\beta_3} \tag{B.6}$$

$$A_7 = \frac{D_{33}\beta_5}{\beta_3}\left[\frac{\partial f_{y1}}{\partial y} - \frac{f_{y1}}{\beta_3}\frac{\partial \beta_3}{\partial y}\right] \tag{B.7}$$

$$A_8 = \frac{D_{11}\beta_4 f_{x2}}{\beta_1} \tag{B.8}$$

$$A_9 = \frac{D_{11}\beta_4}{\beta_1}\left[\frac{\partial f_{x2}}{\partial x} - \frac{f_{x2}}{\beta_1}\frac{\partial \beta_1}{\partial x}\right] \tag{B.9}$$

$$A_{10} = -\frac{D_{33}\beta_5 f_{x2}}{(\beta_3)^2}\frac{\partial \beta_3}{\partial y} \tag{B.10}$$

$$A_{11} = \frac{D_{33}\beta_5 f_{x2}}{\beta_3} \tag{B.11}$$

$$A_{12} = \frac{D_{12}\beta_4 f_{y2}}{\beta_2} \tag{B.12}$$

$$A_{13} = \frac{D_{33}\beta_5}{\beta_3}\left[\frac{\partial f_{y2}}{\partial y} - \frac{f_{y2}}{\beta_3}\frac{\partial \beta_3}{\partial y}\right] \tag{B.13}$$

$$A_{14} = \frac{D_{33}\beta_5 f_{y2}}{\beta_3} \tag{B.14}$$

$$A_{15} = D_{11}\left[\frac{\beta_4}{\beta_1}\left(\frac{f_{x1}^2}{\Delta t}\right) - \frac{2\zeta b}{\Delta t v_s}f_{y1}\right] \tag{B.15}$$

$$A_{16} = \frac{D_{11}\beta_4}{\beta_1}\left[\frac{\partial\left(\frac{f_{x1}^2}{\Delta t}\right)}{\partial x} - \frac{\left(\frac{f_{x1}^2}{\Delta t}\right)}{\beta_1}\frac{\partial \beta_1}{\partial x}\right] \tag{B.16}$$

$$A_{17} = D_{11}\left[f_{y2} - \frac{\beta_4\left(f_{x2}\right)^2}{\beta_1}\right] \tag{B.17}$$

$$A_{18} = \frac{D_{11}\beta_4}{\beta_1}\left[\frac{\partial\left(f_{x2}\right)^2}{\partial x} - \frac{\left(f_{x2}\right)^2}{\beta_1}\frac{\partial \beta_1}{\partial x}\right] \tag{B.18}$$

$$A_{19} = D_{12}\left[\frac{\beta_4}{\beta_2}\left(\frac{f_{y1}^2}{\Delta t}\right) - \frac{2\zeta b}{\Delta t v_s}f_{y1}\right] \tag{B.19}$$

$$A_{20} = D_{12}\left[f_{y2} - \frac{\beta_4\left(f_{y2}\right)^2}{\beta_2}\right] \tag{B.20}$$

$$A_{21} = \frac{2D_{33}\beta_5}{\beta_3}\left[\frac{\partial\left(\frac{f_m}{\Delta t}\right)}{\partial y} - \frac{\left(\frac{f_m}{\Delta t}\right)}{\beta_3}\frac{\partial \beta_3}{\partial y}\right] \tag{B.21}$$

$$A_{22} = 2D_{33}\left[\frac{\beta_5}{\beta_3}\left(\frac{f_m}{\Delta t}\right) - \frac{2\zeta b}{\Delta t v_s}f_{x1}\right] \tag{B.22}$$

$$A_{23} = \frac{D_{33}\beta_5}{\beta_3}\left[\frac{\partial f_k}{\partial y} - \frac{f_k}{\beta_3}\frac{\partial \beta_3}{\partial y}\right] \tag{B.23}$$

$$A_{24} = 2D_{33}\left[f_{x2} - \frac{\beta_5 f_k}{\beta_3}\right] \tag{B.24}$$

$$B_1 = \frac{D_{33}\beta_4 f_{x1}}{\beta_3} \tag{B.25}$$

$$B_2 = \frac{D_{33}\beta_4}{\beta_3}\left[\frac{\partial f_{x1}}{\partial x} - \frac{f_{x1}}{\beta_3}\frac{\partial \beta_3}{\partial x}\right] \tag{B.26}$$

$$B_3 = \frac{D_{12}\beta_5 f_{x1}}{\beta_1} \tag{B.27}$$

$$B_4 = \frac{D_{33}\beta_4 f_{y1}}{\beta_3} \tag{B.28}$$

$$B_5 = -\frac{D_{33}\beta_4 f_{y1}}{(\beta_3)^2}\frac{\partial \beta_3}{\partial x} \tag{B.29}$$

$$B_6 = \frac{D_{22}\beta_5 f_{y1}}{\beta_2} \tag{B.30}$$

$$B_7 = \frac{D_{22}\beta_5}{\beta_2}\left[\frac{\partial f_{y1}}{\partial y} - \frac{f_{y1}}{\beta_2}\frac{\partial \beta_2}{\partial y}\right] \tag{B.31}$$

$$B_8 = \frac{D_{33}\beta_4}{\beta_3}\left[\frac{\partial f_{x2}}{\partial x} - \frac{f_{x2}}{\beta_3}\frac{\partial \beta_3}{\partial x}\right] \tag{B.32}$$

$$B_9 = \frac{D_{33}\beta_4 f_{x2}}{\beta_3} \tag{B.33}$$

$$B_{10} = \frac{D_{12}\beta_5 f_{x2}}{\beta_1} \tag{B.34}$$

$$B_{11} = \frac{D_{33}\beta_4 f_{y2}}{\beta_3} \tag{B.35}$$

$$B_{12} = -\frac{D_{33}\beta_4 f_{y2}}{(\beta_3)^2}\frac{\partial \beta_3}{\partial x} \tag{B.36}$$

$$B_{13} = \frac{D_{22}\beta_5 f_{y2}}{\beta_2} \tag{B.37}$$

$$B_{14} = \frac{D_{22}\beta_5}{\beta_2}\left[\frac{\partial f_{y2}}{\partial y} - \frac{f_{y2}}{\beta_2}\frac{\partial \beta_2}{\partial y}\right] \tag{B.38}$$

$$B_{15} = \frac{2D_{33}\beta_4}{\beta_3} \left[\frac{\partial\left(\frac{f_m}{\Delta t}\right)}{\partial x} - \frac{\left(\frac{f_m}{\Delta t}\right)}{\beta_3} \frac{\partial\beta_3}{\partial x} \right] \tag{B.39}$$

$$B_{16} = 2D_{33} \left[\frac{\beta_4}{\beta_3}\left(\frac{f_m}{\Delta t}\right) - \frac{2\zeta b}{\Delta t v_s} f_{y1} \right] \tag{B.40}$$

$$B_{17} = \frac{2D_{33}\beta_4}{\beta_3} \left[\frac{\partial f_k}{\partial x} - \frac{f_k}{\beta_3} \frac{\partial\beta_3}{\partial x} \right] \tag{B.41}$$

$$B_{18} = 2D_{33} \left[f_{y2} - \frac{\beta_4 f_k}{\beta_3} \right] \tag{B.42}$$

$$B_{19} = D_{12} \left[\frac{\beta_5}{\beta_1}\left(\frac{f_{x1}^{\ 2}}{\Delta t}\right) - \frac{2\zeta b}{\Delta t v_s} f_{x1} \right] \tag{B.43}$$

$$B_{20} = D_{12} \left[f_{x2} - \frac{\beta_5 f_{x2}^{\ 2}}{\beta_1} \right] \tag{B.44}$$

$$B_{21} = \frac{D_{22}\beta_5}{\beta_2} \left[\frac{\partial\left(\frac{f_{y1}^{\ 2}}{\Delta t}\right)}{\partial y} - \frac{\left(\frac{f_{y1}^{\ 2}}{\Delta t}\right)}{\beta_2} \frac{\partial\beta_2}{\partial y} \right] \tag{B.45}$$

$$B_{22} = D_{22} \left[\frac{\beta_5}{\beta_2}\left(\frac{f_{y1}^{\ 2}}{\Delta t}\right) - \frac{2\zeta b}{\Delta t v_s} f_{x1} \right] \tag{B.46}$$

$$B_{23} = \frac{D_{22}\beta_5}{\beta_2} \left[\frac{\partial f_{y2}^{\ 2}}{\partial y} - \frac{f_{y2}^{\ 2}}{\beta_2} \frac{\partial\beta_2}{\partial y} \right] \tag{B.47}$$

$$B_{24} = D_{22} \left[f_{x2} - \frac{\beta_5 f_{y2}^{\ 2}}{\beta_2} \right] \tag{B.48}$$

where

$$\beta_4 = \left[f_{y1} + 2\zeta f_y^p + f_{y2}\Delta t + \frac{2\zeta b}{\Delta t v_s} f_{y1} \right]$$
$$\beta_5 = \left[f_{x1} + 2\zeta f_x^p + f_{x2}\Delta t + \frac{2\zeta b}{\Delta t v_s} f_{x1} \right] \tag{B.49}$$

APPENDIX C

THE USE OF THE STRETCHING FUNCTIONS FOR A PML HAVING ARBITRARY GEOMETRY

Here, a general situation involving a PML region of arbitrary geometry is studied. For simplicity, 2D case is considered in the discussions (see Figure C.1). It is worth to note that choosing a particular geometry for PML suitable for the problem under consideration, instead of choosing it as parallel to coordinate axes, may be needed to decrease the size of analysis region, thus, to reduce the computational cost of PML analysis (for illustrations, see Figures C.2-4).

The discussions will be presented by referring to Figure C.1, where the shape of the truncation boundary (interface) is simulated through its subdivision by some straigth line (SL) segments. Based on each SL segment, a PML element is generated as shown in the Figure C.1. The PML elements are separated by the lines bisecting the angle between the normals of two adjacent SL segments.

In the discussions two types of coordinate axes are used: $x_1 x_2$ global coordinate system, and n-s local coordinate system (see Figure C.1). In the latter coordinate system, to which a PML element is referred, n denotes the normal axis directed outwards from interior (truncated) region and s is the tangential axis directed in α direction as the PML element is viewed from interior region, with α being the rotational direction from x_1 to x_2 axis. For the unit vector $\hat{n}$ in the n direction, one can write

$$\hat{n}_1 = \cos(\theta) \quad , \hat{n}_2 = \sin(\theta) \tag{C.1}$$

where θ is the angle of n axis from x_1 measured in α direction. On the other hand, for unit vector $\hat{s}$ of the tangential axis, one has

$$\hat{s}_1 = -\sin(\theta) \quad , \hat{s}_2 = \cos(\theta) \tag{C.2}$$

In view of Equation C.2 and Figure C.1 (b), one can write for $\cos\theta$ and $\sin\theta$, in terms of the coordinates of the end points of the line segment (LS) $\overline{12}$,

$$\sin(\theta) = -\hat{s}_1 = -\frac{x_1^{(2)} - x_1^{(1)}}{L}$$

$$\cos(\theta) = \hat{s}_2 = \frac{x_2^{(2)} - x_2^{(1)}}{L} \tag{C.3}$$

where L is the length of the LS $\overline{12}$:

$$L = \sqrt{\left(x_1^{(2)} - x_1^{(1)}\right)^2 + \left(x_2^{(2)} - x_2^{(1)}\right)^2}$$

and $(x_1^{(1)}, x_2^{(1)})$ and $(x_1^{(2)}, x_2^{(2)})$ are (x_1, x_2) coordinates of the end points (1) and (2).

The stretching functions for a PML are given by, when the simplest form of stretching function given in Equation 3.3 is used,

$$\lambda_n(\beta) = 1 + \frac{f_n(\beta)}{i\omega}$$

$$\lambda_s(\beta) = 1 \tag{C.4}$$

where f_n is the attenuation function (associated with n-direction), and λ_n and λ_s are stretching functions for n and s directions of the PML element. For the stretching coordinates $(\tilde{n}, \tilde{s})$ of a point in PML element, one can write, in local coordinates,

$$\tilde{n} = \int_0^n \lambda_n(\beta)\, d\beta = n + \frac{F_n(n)}{i\omega}$$

$$\tilde{s} = \int_0^s \lambda_s(\beta)\, d\beta = s$$

(C.5)

where

$$F_n(n) = \int_0^n f_n(\beta)\, d\beta$$

(C.6)

The stretching coordinates $(\tilde{x}_1, \tilde{x}_2)$ of a point in PML element in $x_1 x_2$ global coordinate system are related to its local stretching coordinates $(\tilde{n}, \tilde{s})$ by

$$\begin{bmatrix} \tilde{x}_1 \\ \tilde{x}_2 \end{bmatrix} = \begin{bmatrix} \cos\theta & -\sin\theta \\ \sin\theta & \cos\theta \end{bmatrix} \begin{bmatrix} \tilde{n} \\ \tilde{s} \end{bmatrix} + \begin{bmatrix} x_1^0 \\ x_2^0 \end{bmatrix}$$

(C.7)

where (x_1^0, x_2^0) are (x_1, x_2) coordinates of the midpoint of the LS $\overline{12}$ (see Figure C.1).

When Equation C.5 is inserted into Equation C.7, one gets the stretching coordinates $(\tilde{x}_1, \tilde{x}_2)$,

$$\tilde{x}_1 = x_1 + \cos\theta \frac{F_n(n)}{i\omega}$$

$$\tilde{x}_2 = x_2 + \sin\theta \frac{F_n(n)}{i\omega}$$

(C.8)

with n being the normal coordinate of a point in PML element which is related to its (x_1, x_2) coordinates by

$$n = (x_1 - x_1^0)\hat{n}_1 + (x_2 - x_2^0)\hat{n}_2$$
$$= (x_1 - x_1^0)\cos\theta + (x_2 - x_2^0)\sin\theta$$

(C.9)

147

It is known that, to obtain the stretch equations in PML analysis, one makes the following replacements in the original differential equations:

$$\frac{\partial}{\partial x_1} \rightarrow \frac{\partial}{\partial \tilde{x}_1}, \quad \frac{\partial}{\partial x_2} \rightarrow \frac{\partial}{\partial \tilde{x}_2} \tag{C.10}$$

Thus, to establish the stretch equations in terms of the actual coordinates (x_1, x_2), one should express $\dfrac{\partial}{\partial \tilde{x}_1}$ and $\dfrac{\partial}{\partial \tilde{x}_2}$ in terms of $\dfrac{\partial}{\partial x_1}$ and $\dfrac{\partial}{\partial x_2}$. For this purpose, one writes, first,

$$\frac{\partial}{\partial \tilde{x}_1} = \frac{\partial}{\partial x_1}\frac{\partial x_1}{\partial \tilde{x}_1} + \frac{\partial}{\partial x_2}\frac{\partial x_2}{\partial \tilde{x}_1}$$

$$\frac{\partial}{\partial \tilde{x}_2} = \frac{\partial}{\partial x_1}\frac{\partial x_1}{\partial \tilde{x}_2} + \frac{\partial}{\partial x_2}\frac{\partial x_2}{\partial \tilde{x}_2}$$

or, in matrix form,

$$\begin{bmatrix} \dfrac{\partial}{\partial \tilde{x}_1} \\[2ex] \dfrac{\partial}{\partial \tilde{x}_2} \end{bmatrix} = \underbrace{\begin{bmatrix} \dfrac{\partial x_1}{\partial \tilde{x}_1} & \dfrac{\partial x_2}{\partial \tilde{x}_1} \\[2ex] \dfrac{\partial x_1}{\partial \tilde{x}_2} & \dfrac{\partial x_2}{\partial \tilde{x}_2} \end{bmatrix}}_{A} \begin{bmatrix} \dfrac{\partial}{\partial x_1} \\[2ex] \dfrac{\partial}{\partial x_2} \end{bmatrix} \tag{C.11}$$

To evaluate the coefficient matrix A in Equation C.11, one may consider the identity, written in indicial form,

$$\frac{\partial \tilde{x}_i}{\partial \tilde{x}_j} = \sum_{k=1}^{2} \frac{\partial \tilde{x}_i}{\partial x_k}\frac{\partial x_k}{\partial \tilde{x}_j} = \delta_{ij} \quad (i, j = 1, 2) \tag{C.12}$$

where δ_{ij} is the usual Kronecker's delta ($\delta_{ij} = 1$ for $i = j$; $\delta_{ij} = 0$ for $i \neq j$). Equation C.12 shows that the coefficient matrix A appearing in Equation C.11 is the inverse of the matrix B defined by

148

$$B = \begin{bmatrix} \dfrac{\partial \tilde{x}_1}{\partial x_1} & \dfrac{\partial \tilde{x}_2}{\partial x_1} \\[4mm] \dfrac{\partial \tilde{x}_1}{\partial x_2} & \dfrac{\partial \tilde{x}_2}{\partial x_2} \end{bmatrix}$$

which becomes, in view of Equations C.8 and C.9

$$B = \begin{bmatrix} 1 + \cos^2 \theta \dfrac{f_n(n)}{i\omega} & \sin\theta\cos\theta \dfrac{f_n(n)}{i\omega} \\[4mm] \sin\theta\cos\theta \dfrac{f_n(n)}{i\omega} & 1 + \sin^2 \theta \dfrac{f_n(n)}{i\omega} \end{bmatrix} \tag{C.13}$$

With the use of Equation C.13, inserting $A = B^{-1}$ into Equation C.11, one gets

$$\begin{bmatrix} \dfrac{\partial}{\partial \tilde{x}_1} \\[4mm] \dfrac{\partial}{\partial \tilde{x}_2} \end{bmatrix} = \dfrac{1}{\left(1 + \dfrac{f_n(n)}{i\omega}\right)} \begin{bmatrix} 1 + \sin^2 \theta \dfrac{f_n(n)}{i\omega} & -\sin\theta\cos\theta \dfrac{f_n(n)}{i\omega} \\[4mm] -\sin\theta\cos\theta \dfrac{f_n(n)}{i\omega} & 1 + \cos^2 \theta \dfrac{f_n(n)}{i\omega} \end{bmatrix} \begin{bmatrix} \dfrac{\partial}{\partial x_1} \\[4mm] \dfrac{\partial}{\partial x_2} \end{bmatrix} \tag{C.14}$$

where, it may be noted, n coordinate of a point in PML element is related to its (x_1, x_2) coordinates by Equation C.9. Below Equation C.14 is presented for some special cases.

Special case 1:

For a vertical truncation boundary (interface) with the normal in x_1 direction (see Figure C.1), one has $\theta = 0$, which reduces Equation C.14, as expected, to

$$\frac{\partial}{\partial \tilde{x}_1} = \frac{1}{\left(1 + \dfrac{f_1(r)}{i\omega}\right)} \frac{\partial}{\partial x_1} = \frac{1}{\lambda_1(r)} \frac{\partial}{\partial x_1}$$

$$\frac{\partial}{\partial \tilde{x}_2} = \frac{\partial}{\partial x_2}$$

with $r = x_1 - x_1^0$.

Special case 2:

For *a* horizontal truncation boundary (interface) with the normal in x_2 direction (see Figure C.1), one has $\theta = {}^{\pi}/_2$, which reduces Equation C.14, as expected, to

$$
\frac{\partial}{\partial \tilde{x}_1} = \frac{\partial}{\partial x_1}
$$

$$
\frac{\partial}{\partial \tilde{x}_2} = \frac{1}{\left(1 + \dfrac{f_2(r)}{i\omega}\right)} \frac{\partial}{\partial x_2} = \frac{1}{\lambda_2(r)} \frac{\partial}{\partial x_2}
$$

with $r = x_2 - x_2^0$.
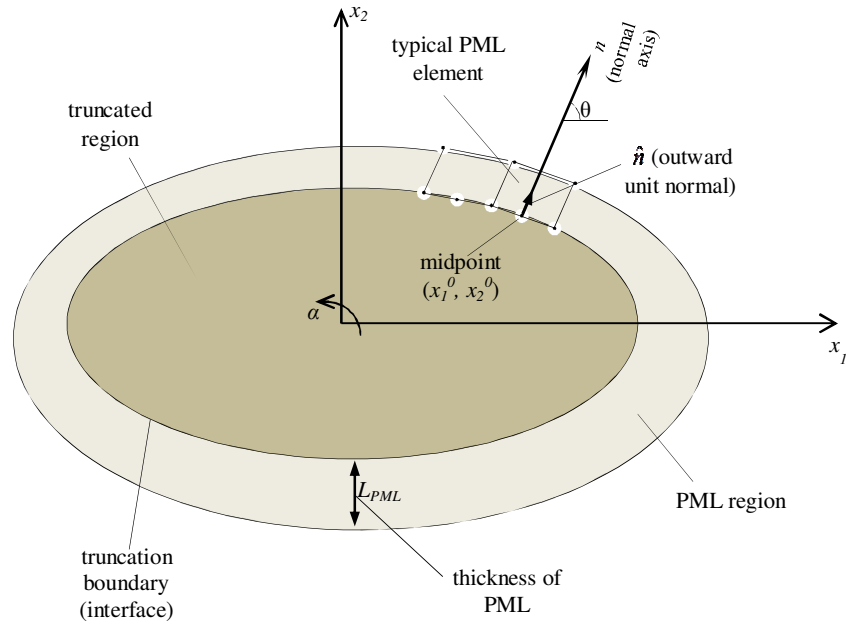
(a)
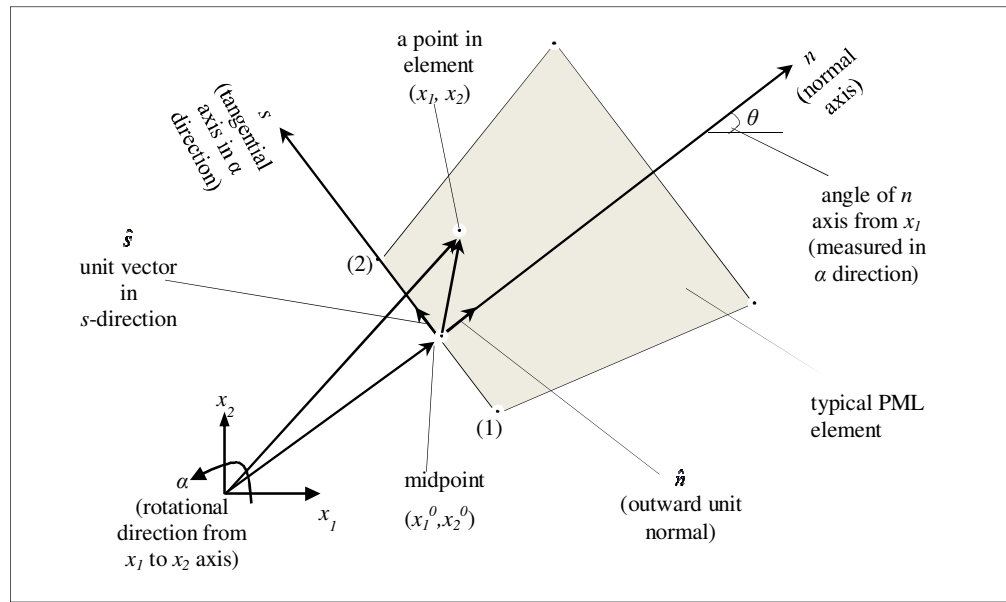
(b)

Figure C.1: (a) Discretization of PML region of arbitrary geometry (b) typical PML element (*s* is in *α* direction as the PML element is viewed from interior (truncated) region; $\overline{\mathbf{12}}$ is directed in s direction).

151
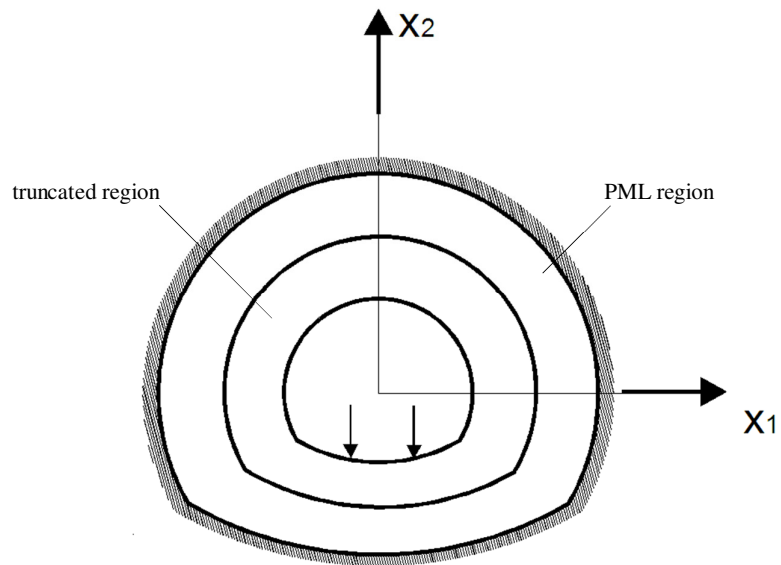
(a)
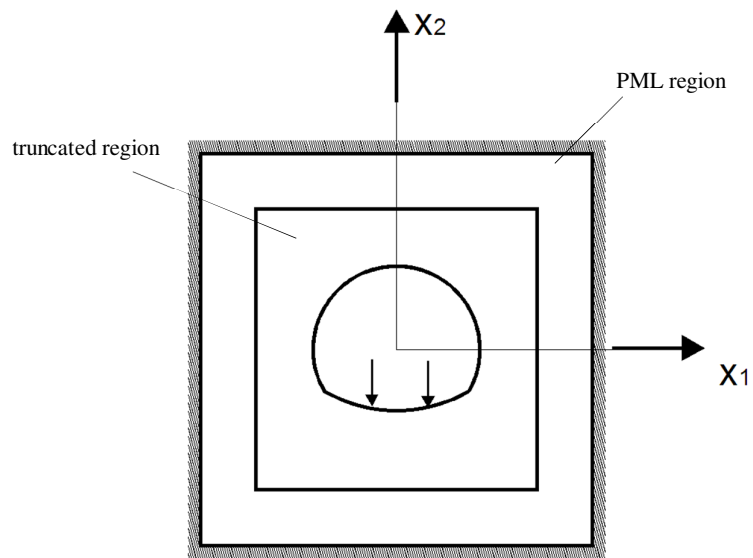
(b)

Figure C.2: PML modeling of a tunnel problem (a) when the geometry of PML is chosen as fitted to the shape of tunnel, (b) when it is selected as parallel as to coordinate axes.

Figure C.3: (a) Trapezoidal strip foundation under vertical, horizontal and rocking vibrations, (b) its PML modeling when the interface is fitted to the shape of the foundation, (c) when it is chosen as parallel to coordinate axes.

Figure C.4: (a) An impedance problem and its PML modeling with the interface chosen (b) as circle (c) as parallel to coordinate axes.

COMPLEX DOMAIN APPROACH IN PML ANALYSIS

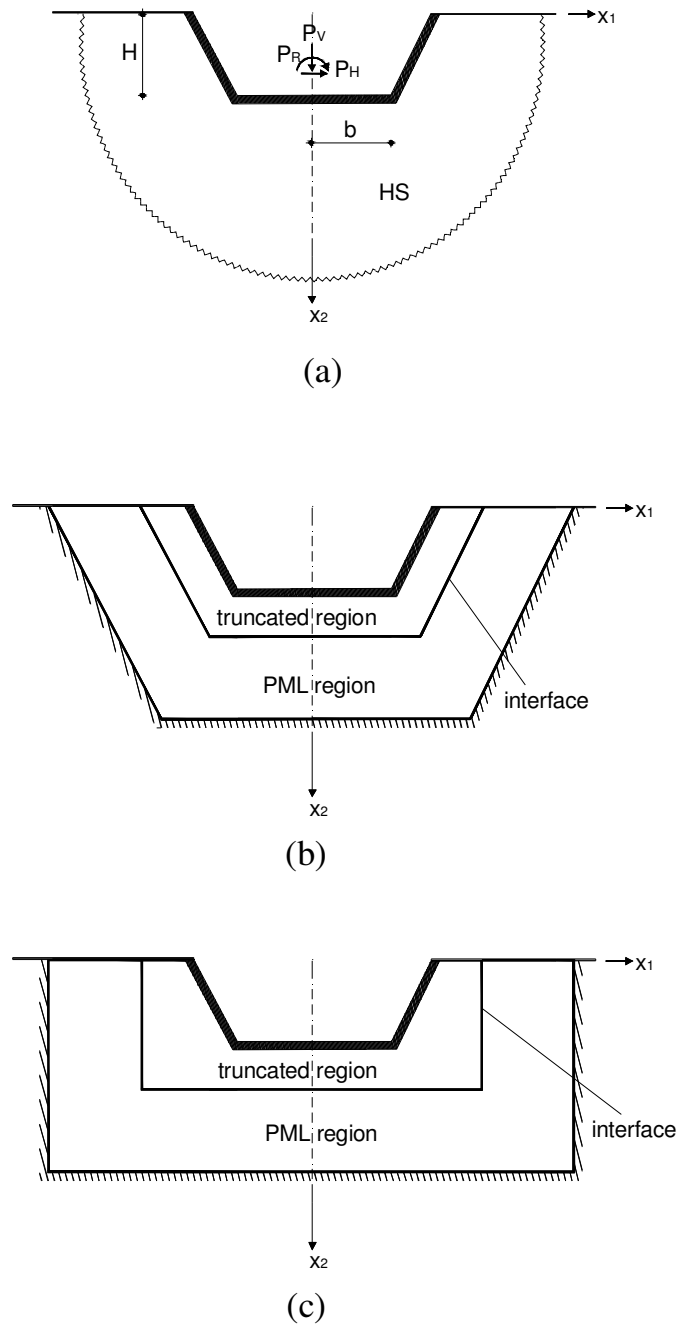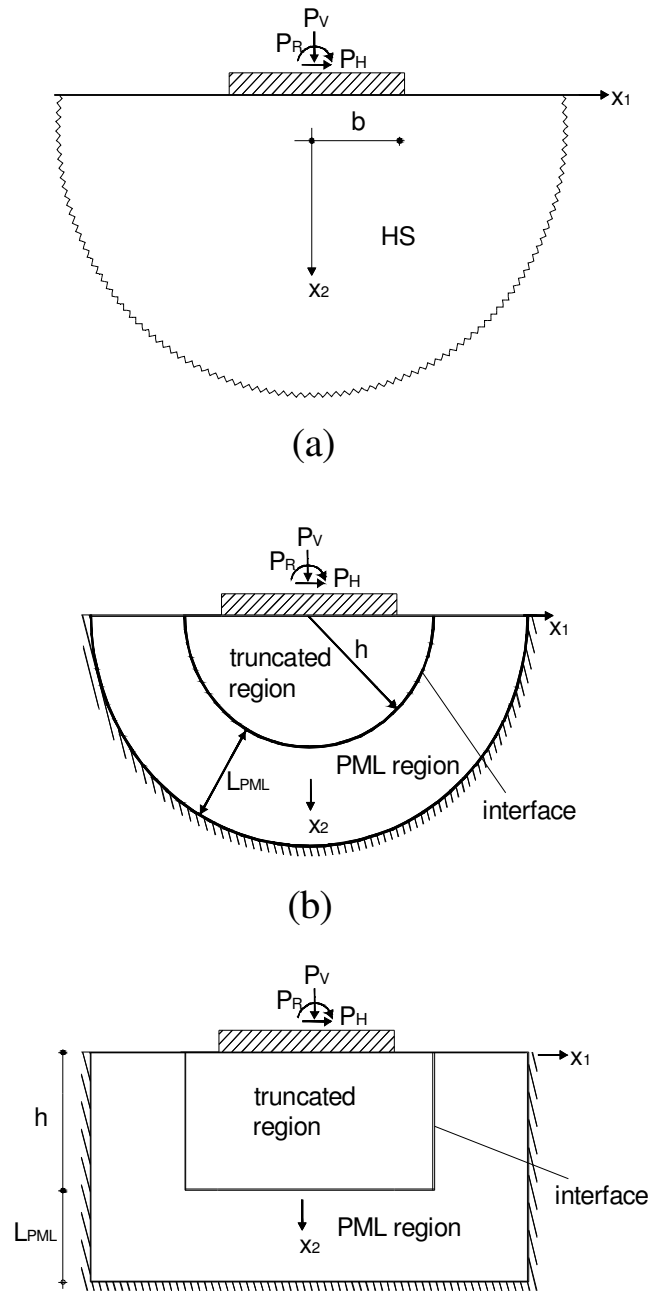The purpose of this approach is to perform the PML analysis directly in complex domain, instead of, in real domain. The main advantage of this approach would be: PML analysis can be carried out in a homogenous complex domain by keeping the original form of the governing equations together with their symmetry properties. It is to be noted that performing PML analysis in real domain requires modifying the form of governing equations and integrating them in real, but, inhomogeneous and anisotropic domain.

It goes without saying that the proposed approach could be used only in frequency space. The discussions below are presented for 2D case and it is assumed that the spacewise integrations are performed by GFDM.

To explain the complex domain approach, Figure D.1 will be referred to; where the first figure (a) shows the description of a point P in PML. In view of this figure, it is obvious that the coordinates x_j of P are given by

$$x_j = x_j^0 + r\hat{n}_j \qquad (j = 1, 2) \qquad\qquad (D.1)$$

where x_j^0 are coordinates of a point P_0 on the interface Γ, $\hat{n}$ is unit normal of Γ at P_0 and r is the distance of point P from P_0.

The unit normal $\hat{n}$ of point P_0 can be determined in terms the parametric equations of the interface Γ.

$$x_j^0 = x_j^0(\alpha) \qquad (j=1,2) \tag{D.2}$$

where α is the line parameter. In view of discussions in Appendix C, for $\hat{n}$ one can write

$$\begin{aligned}\hat{n}_1 &= \hat{s}_2 \\ \hat{n}_2 &= -\hat{s}_1\end{aligned} \tag{D.3}$$

where $\hat{s}$ is unit tangent vector at P_0, which can be determined as, using the parametric equations of Γ,

$$\hat{s}_j = \frac{1}{\sqrt{\left(\dfrac{dx_1^0}{d\alpha}\right)^2 + \left(\dfrac{dx_2^0}{d\alpha}\right)^2}} \frac{dx_j^0}{d\alpha} \qquad (j=1,2) \tag{D.4}$$

It should be noted that, in view of Equation C.3, $\hat{s}$ can also be determined approximately by

$$\hat{s}_j = \frac{\overset{(2)}{x_j^0} - \overset{(1)}{x_j^0}}{L} \qquad (j=1,2) \tag{D.5}$$

where $\overset{(1)}{x_j^0}$ and $\overset{(2)}{x_j^0}$ are two points along Γ enclosing point P_0 closely and L is the length of the distance between these points, that is,

$$L = \sqrt{\left(\overset{(2)}{x_1^0} - \overset{(1)}{x_1^0}\right)^2 + \left(\overset{(2)}{x_2^0} - \overset{(1)}{x_2^0}\right)^2} \tag{D.6}$$

The stretching coordinates of point P in Equation D.1 is given by

$$x_j^0 = x_j^0 + \tilde{r}\hat{n}_j \qquad (j = 1, 2) \tag{D.7}$$

where $\tilde{r}$ is given by, when the simplest form of the stretching function in Equation 3.3 is used,

$$\tilde{r} = \frac{F(r)}{i\omega} \tag{D.8}$$

with $F(r)$ being defined by

$$F(r) = \int_0^r f(\alpha)\, d\alpha \tag{D.9}$$

If the attenuation function f is assumed to have the form given in Equation 3.16, that is,

$$f(r) = f_0 \left(\frac{r}{L_{PML}} \right)^m \tag{D.10}$$

then, for $F(r)$ in Equation D.9, one has

$$F(r) = f_0 \left(\frac{L_{PML}}{m+1} \right) \left(\frac{r}{L_{PML}} \right)^{m+1} \tag{D.11}$$

Equation D.7 maps a point P in actual (real) PML region to a point $\tilde{P}$ in complex PML region.

The complex domain approach proposes performing PML analysis directly in complex PML region and has the following steps when the spacewise integrations are carried out by GFDM.

1) Select some points P_0^i (i=1,2,...) along the interface Γ of PML with truncated region (see Figure D.1 (b)).

157

2) Associated with each P_0^i generate some points along its normal $\hat{n}^i$ using Equation D.1; these points constitute the nodal points in PML region to be used in GFDM.

3) Using Equation D.7, determine the complex stretching coordinates of the nodal points generated in PML region.

4) Write the governing equations at nodal points in terms of their stretching coordinates; it is to be noted that the form of governing equations in terms of stretching coordinates in PML region would be the same as that of the original equations. For example, for the plane strain problem whose actual governing equations are given in Equations 4.11-13, PML equations in terms of stretching coordinates would be the same formwise with these equations, that is, they would be

stress equations of motion:

$$\frac{\partial \sigma_{xx}}{\partial \tilde{x}} + \frac{\partial \tau_{xy}}{\partial \tilde{y}} + \rho \omega^2 u = 0$$

$$\frac{\partial \tau_{yx}}{\partial \tilde{x}} + \frac{\partial \sigma_{yy}}{\partial \tilde{y}} + \rho \omega^2 v = 0$$

stress-strain relation:

$$\sigma = D\varepsilon$$

strain displacement relations:

$$\varepsilon_{xx} = \frac{\partial u}{\partial \tilde{x}}$$

$$\varepsilon_{yy} = \frac{\partial v}{\partial \tilde{y}}$$

$$\varepsilon_{xy} = \frac{1}{2}\left[\frac{\partial u}{\partial \tilde{y}} + \frac{\partial v}{\partial \tilde{x}}\right]$$

5) Express the derivative values (with respect to stretching coordinates) at a nodal point in terms of function values at some points around that nodal (star) point using the star equation of GFDM. The TS2 star equation in terms of stretching coordinates can be obtained through a modification of Equation 2.6 (which was given in terms of real coordinates). It is

$$
\begin{bmatrix}
\sum w_i^2 h_i^2 & \sum w_i^2 h_i k_i & \dfrac{1}{2}\sum w_i^2 h_i^3 & \dfrac{1}{2}\sum w_i^2 h_i k_i^2 & \sum w_i^2 h_i^2 k_i \\[2mm]
\sum w_i^2 h_i k_i & \sum w_i^2 k_i^2 & \dfrac{1}{2}\sum w_i^2 k_i h_i^2 & \dfrac{1}{2}\sum w_i^2 k_i^3 & \sum w_i^2 k_i^2 h_i \\[2mm]
\dfrac{1}{2}\sum w_i^2 h_i^3 & \dfrac{1}{2}\sum w_i^2 k_i h_i^2 & \dfrac{1}{4}\sum w_i^2 h_i^4 & \dfrac{1}{4}\sum w_i^2 h_i^2 k_i^2 & \dfrac{1}{2}\sum w_i^2 h_i^3 k_i \\[2mm]
\dfrac{1}{2}\sum w_i^2 h_i k_i^2 & \dfrac{1}{2}\sum w_i^2 k_i^3 & \dfrac{1}{4}\sum w_i^2 h_i^2 k_i^2 & \dfrac{1}{4}\sum w_i^2 k_i^4 & \dfrac{1}{2}\sum w_i^2 h_i k_i^3 \\[2mm]
\sum w_i^2 h_i^2 k_i & \sum w_i^2 k_i^2 h_i & \dfrac{1}{2}\sum w_i^2 h_i^3 k_i & \dfrac{1}{2}\sum w_i^2 h_i k_i^3 & \sum w_i^2 h_i^2 k_i^2
\end{bmatrix}
\begin{Bmatrix}
\dfrac{\partial f^*}{\partial \tilde{x}} \\[2mm]
\dfrac{\partial f^*}{\partial \tilde{y}} \\[2mm]
\dfrac{\partial^2 f^*}{\partial \tilde{x}^2} \\[2mm]
\dfrac{\partial^2 f^*}{\partial \tilde{y}^2} \\[2mm]
\dfrac{\partial^2 f^*}{\partial \tilde{x} \partial \tilde{y}}
\end{Bmatrix}
$$

$$
=
\begin{pmatrix}
-f^*\sum w_i^2 h_i + \sum f_i w_i^2 h_i \\[2mm]
-f^*\sum w_i^2 k_i + \sum f_i w_i^2 k_i \\[2mm]
-f^*\sum w_i^2 \dfrac{h_i^2}{2} + \sum f_i w_i^2 \dfrac{h_i^2}{2} \\[2mm]
-f^*\sum w_i^2 \dfrac{k_i^2}{2} + \sum f_i w_i^2 \dfrac{k_i^2}{2} \\[2mm]
-f^*\sum w_i^2 h_i k_i + \sum f_i w_i^2 h_i k_i
\end{pmatrix}
\qquad \text{(D.12)}
$$

where w_i is weighting function and

$$
h_i = \tilde{x}_i - \tilde{x}^*, \quad k_i = \tilde{y}_i - \tilde{y}^* \qquad\qquad \text{(D.13)}
$$

with $(\tilde{x}^*, \tilde{y}^*)$ being the star point. In view of discussion presented in Chapter 2, the use of cubic distance weighting function may be suggested in the analysis. In terms of stretching coordinates, this weighting function should modified as

159

$$w_i = \begin{cases} 1/\left(d_i\right)^3 \ with \ d_i = \sqrt{\left|h_i\right|^2 + \left|k_i\right|^2} & for \quad d_i \le dm \\ w_i = 0 \quad for \quad d_i > dm \end{cases} \tag{D.14}$$

where dm is the radius of circle of influence; it should be a real value and positive, and satisfy

$$dm > \max d_i \quad 1 \le i \le m \tag{D.15}$$

with m being the number of points around the star point.

6) Combine the governing equations written at nodal points and solve them in view of boundary conditions.
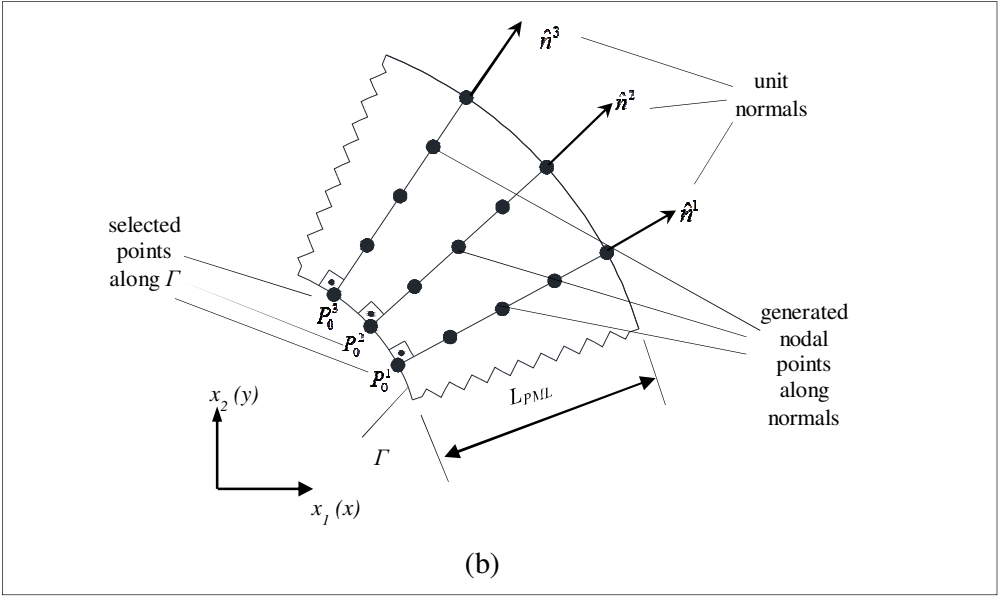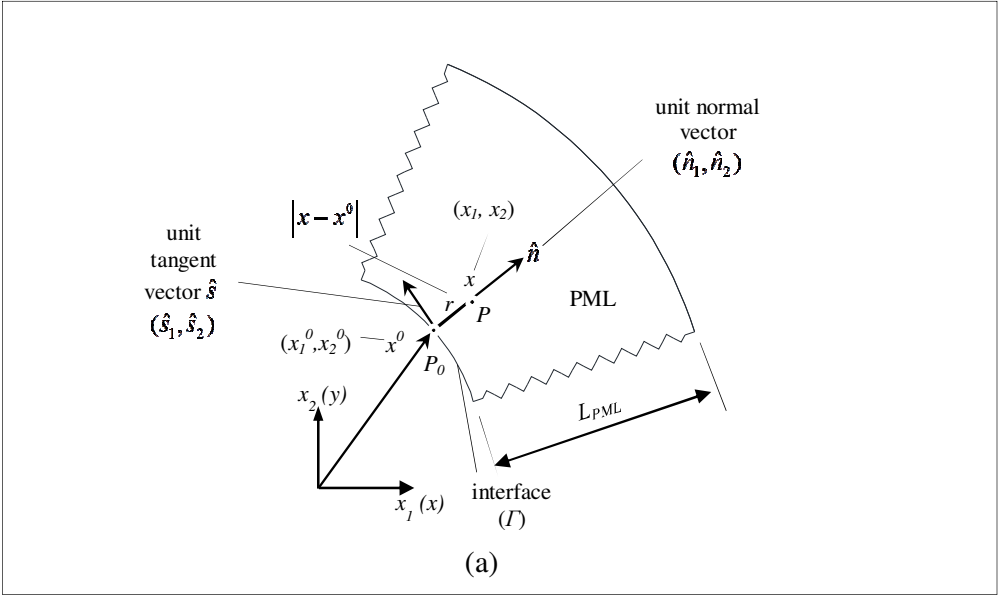
Figure D.1: (a) Description of a point in PML (b) generation of nodal points in PML for GFDM analysis

VITA

Fuat Korkut was born in Bulanık, Muş, Turkey on June 30, 1976, the son of Kadri and Yıldız. He graduated from Diyarbakır Cumhuriyet Science High School. He received the Bachelor of Science degree in Civil Engineering at Gazi University in June 2001. He joined the doctoral program in Department of Engineering Science of the Middle East Technical University in 2004 where he has been working as a research assistant and teaching assistant.

Permanent address: 12.C. 33. S. Özelif Sitesi

               1. Blok No: 55 Demetevler

           06200 Ankara/ Turkey

e-mail: fuatkorkut@gmail.com